Faculty of Science and Engineering

Department of Civil Engineering

Behaviour of CFRP confined reinforced concrete columns with square cross section under eccentric compressive loading

Reza Alishahi

This thesis is presented for the Degree of

Master of Philosophy

Of

Curtin University

April 2018

DECLARATION

To the best of my knowledge and belief this thesis contains no material previously published by any other person except where due acknowledgement has been made.

This thesis contains no material which has been accepted for the award of any other degree or diploma in any university

Signature:

Date: 1/10/2018

ABSTRACT

Application of Fiber Reinforced Polymer (FRP) has been extensively adopted over the past two decades by the industry for the purpose of strengthening and repair of structural elements. Among many classes of FRP, CFRP (Carbon Fiber Reinforced Polymer) is being used extensively due to its high strength and superior durability properties. Also behaviour of columns with various cross sections confined with FRP under concentric static loading has been studied extensively in the literature. However studies on the behaviour of CFRP confined columns under eccentric loading, especially columns with rectangular/square cross sections are scarce. The purpose of this research is to study the mechanical behaviour of such columns both from an experimental perspective as well as theoretical perspective.

Initially a thorough literature review has been carried out both on the constitutive models available for FRP confined concrete as well as experimental studies. Then models are classified and out of the most relevant four are chosen for further investigations.

In the experimental phase of this research, twenty RC columns with square cross sections with side dimension of 175x175mm, height of 800mm, and corner radius of 20mm were cast. These columns had the same exact internal steel reinforcements. Five of these columns remained unconfined and served as reference specimens whereas the rest fifteen columns were divided into groups of five and were confined with one, two, and three wraps of CFRP correspondingly. Out of these twenty columns, eighteen were tested under eccentricities of 0mm, 25mm, 35mm, 50mm and eventually pure flexure (three point beam tests). The behaviour of columns in terms of the axial force-deflection response, axial force vs hoop strains and lateral deflection as well as their ductility and ultimate strength are presented, compared, and discussed. Also the load-moment (P-M) interaction diagram of the confined columns are presented and compared to each other.

In the theoretical stage of the thesis four of the most relevant and latest analytical constitutive models for FRP confined concrete are selected and their applicability in prediction of CFRP confined square columns under various eccentricities are examined.

Keywords: CFRP confined reinforced concrete column, square cross section, eccentric loading, analytical modeling.

ACKNOWLEDGMENT

Initially I would like to thank my mighty and merciful God, for giving me the ability and power to finish my thesis throughout this journey despite of all the hardships I have experienced in these past few years.

I want to thank my supervisor Dr. Faiz U.A Shaikh for guiding me throughout different stages of this research and always supporting me from the very beginning of this journey to the very end. I also would like to extend my gratitude towards my co-supervisor Dr. Prabir Sarker for his consultation and guidance through a number of stages of this research project.

I would like to thank my friends Mr Hassan Malekzehtab and Mr Yashar Safaei for helping me in the casting stage of my research project. Also I am really thankful to all the concrete laboratory staff including Mr Mick Elliss, Mr Luke English, Mr Ashley Hughes, and Mr Arne Bredin for their contribution and cooperation during the experimental phase of this research despite all the hardships caused by new construction and developments in the Civil Engineering Laboratory area.

Most Importantly I would like express my deep sense of gratitude to my beloved parents, my brother and his wife who all supported me both financially and emotionally at the hardest times in which I needed them the most.

PUBLICATION LIST

Faiz, U.A., Alishahi, R., Sarker P. K. (2018) "Behaviour of CFRP confined RC Square Columns Under Eccentric Compressive Loading." 9th International Conference on Fibre-Reinforced Polymer Composites in Civil Engineering, Paris, France (Accepted).

0 Table of Contents

Page

LIST OF FIGURES

LIST OF TABLES

1 Introduction

1.1 Overview

The use of fibre reinforced polymer (FRP) for strengthening and rehabilitation of reinforced concrete (RC) structures is a common practice in the construction industry. Among various structural members, the strengthening and rehabilitation of columns by wrapping with FRP fabric is most effective as the FRP does not debond prematurely and under increasing compression load the confinement efficiency of FRP is significantly increased (Mirmiran and Shahawy (1996), Mirmiran and Shahawy (1997), Saadatmanesh et al. (1994)). For circular columns, the confining pressure occurs around the entire perimeter due to the curvature of the FRP wrap produce uniform confining stress as shown in Figure 1.1-1-(a) below. FRP-confined rectangular columns behave in a significantly different manner due to the nonuniform distribution of hoop strains and stress concentration at the corners (Lam and Teng (2003b), Mirmiran et al. (1998), Parvin and Wang (2002), Rochette and Labossiere (2000)) as shown in Figure 1.1-1-(b). With the application of concentric loading, the FRP wrap goes into tension but the confining forces are only generated at the convex corners in rectangular/square columns.

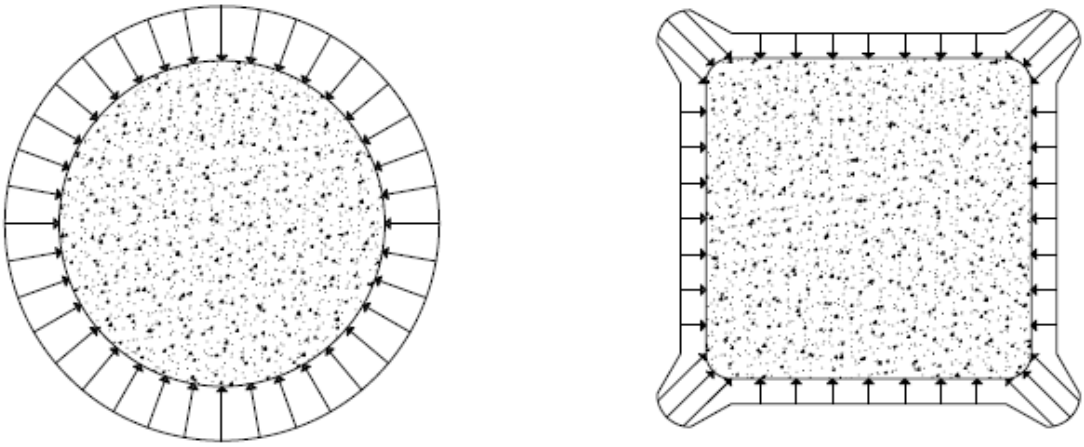

(a) (b)

Figure 1.1-1 Confinement stress distribution around circular vs rectangular columns

The behaviour of FRP confined concrete columns with different cross sections under concentric loading have been studied extensively (Fardis and Khalili (1982), Karbhari and Gao (1997), Samaan et al.(1998), Miyauchi et al. (1999), Saafi et al. (1999), Spoelstra and Monti (1999), Toutanji (1999), Xiao and Wu (2000), Lam and Teng(2003a, 2003b)). However in real world practice due to various reasons such as unsymmetrical loading, construction errors etc. the column undergoes a state of combined flexural and compression stresses, which has not been investigated thoroughly specifically for columns with square/rectangular cross sections (Chaallal and Shahawy (2000), Lignola et al. (2007), Sadeghian et al. (2010), Lei et al. (2012), Widiarsa and Hadi (2013)).

Many researchers have proposed analytical as well as numerical models to predict the behaviour of FRP confined columns with various cross sections under concentric static loading (Eid and Paultre (2008, 2017), Fam et al. (2003), Faustino et al. (2014), Lam and Teng (2002, 2003a, 2003b), Legeron and Paultre (2003), Mirmiran (1996), Samaan et al (1998), Youssef et al (2007), Yu et al (2010a, 2010b), Xiao et al (2010)). However the potential of these constitutive models in predicting the load-moment (P-M) interaction diagrams of the FRP-confined columns with square/rectangular cross sections have not been examined. Motivation of the current study was to first conduct an experimental program to further investigate the behaviour of CFRP confined RC columns with square cross sections under state of combined flexure and compression and secondly to investigate the potential of proposed analytical constitutive Equations in the literature for prediction of the P-M interaction diagrams of such columns.

1.2 Significance

Several studies have been conducted on FRP confined or strengthened RC columns under concentric loads. However, in real situation most columns experience combination of axial compression load and bending moment (i.e. eccentric compression loading) due to construction error, unbalanced moments at the corners of frames or slabs, etc. Therefore, there is a need to understand the behaviour of FRP strengthened columns under eccentric loading. Some research has been conducted on FRP confined columns under eccentric loading. In a study performed by Parvin and Wang (2001), small-scale square concrete columns (i.e. 108 mm × 108 mm × 305 mm) were strengthened with varying layers of carbon FRP (CFRP) composites and subjected to axial load at different eccentricities. The results showed that the increase in eccentricity resulted in a reduction in strength capacity of the column, and the use of CFRP increased the load capacity of the column with respect to unstrengthened columns. Fam et al. (2003) performed an experimental program and proposed an analytical model to describe the behaviour of concrete filled FRP tubes subjected to combined axial compression loads and bending moments. Li and Hadi (2003), Hadi and Li (2004), and Hadi (2006a,b; 2007a,b) tested several FRP-strengthened concrete columns with circular section under eccentric loading at different conditions. The effects of concrete strength, internal steel reinforcement, wrap type, fiber orientation, and eccentricity were studied. The eccentric load was applied through a circular plate at each end of the specimens. The experimental results clearly demonstrated that the FRP wrapping can enhance strength, ductility, and energy absorption of circular as well as rectangular concrete columns under eccentric loading.

This enhancement in strength and ductility is due to the confinement pressure around the column hoop provided by FRP jacket which prevents the concrete rupture as well as buckling of longitudinal rebars at levels of stress in unstrengthened columns. In a study performed by Chaallal and Shahawy (2000), an experimental investigation was conducted on rectangular RC columns strengthened with bidirectional CFRP composites and different eccentricities. The overall length of the two haunched-head specimens was 3.6 m (200 mm wide and 350 mm high in test section). The results indicated that the strength capacity of columns improved significantly as a result of the combined action of the longitudinal and the transverse fibers of the bidirectional composite fabrics. Lignola et al. (2007) have mainly focused their attention on square hollow columns strengthened with CFRP composites (height of 3020 mm, width of 360 mm, and wall thicknesses of 60 mm). The outcomes highlighted that composite wrapping can enhance the structural performance of concrete columns under eccentric loading in terms of strength and especially in terms of ductility. The strength improvement was more pronounced in the case of specimens loaded with smaller eccentricity, while the ductility improvement was more significant in the case of larger eccentricity. Hatami et al. (2013) and Sadeghian et al. (2010) in their studies evaluated the effectiveness of CFRP wrapped rectangular RC columns (200x300mm) of 1.5m long under eccentric compression loading. Lei et al. (2012) and Widiarsa and Hadi (2013) studied the effectiveness of CFRP strengthened RC columns of square cross-section under eccentric loading and reported that the CFRP wrapping enhanced the load carrying capacity and ductility of the square RC columns under eccentric loading. In most of the above studies the columns were either circular, hollow square section or rectangular cross-section. Only few studies reported the behaviour of FRP wrapped square RC columns under eccentric loading. On the other hand there is large library of analytical as well as numerical plasticity based constitutive stress-strain models available in the literature. Potential of these Equations in developing load-moment (P-M) interaction diagrams has not been investigated thoroughly.

1.3 Scope and Objective

The aim of this study is to evaluate the effect of number of CFRP layers and various increasing eccentrics on the behaviour of CFRP wrapped RC square columns under combined flexure and compression and secondly to investigate the potential of existing analytical constitutive models in predicting the P-M interaction diagrams of such columns.

In this study a total of twenty RC square columns are fabricated with same dimensions and reinforcement configuration. Five specimens remain unwrapped and served as reference while fifteen other columns are wrapped with one, two, and three layers of CFRP fabrics. Out of these twenty specimens, eighteen columns are tested (two columns were excluded due to loading limitation of equipment) under eccentricities of 0, 25, 35, and 50 mm as well as infinity (three-point beam tests).

Four analytical models are chosen based the extensiveness of their adoption like Teng et al. (2003) model, or their relevance and/or being the latest developed such as models by Youssef et al. (2007),

Faustino et al. (2014), and Eid and Paultre (2017). These models are then used to develop P-M interaction diagrams and compared to the experimental data.

1.4 Thesis Outline

The current chapter serves as an introduction and presents a brief overview, and states the significance and objectives of this research study.

Chapter 2 provides an extensive literature review on the mechanics of steel and FRP confined concrete. A large library of the proposed constitutive models for FRP-encased concrete are reviewed and classified. The chosen analytical models are presented and discussed and eventually a brief review of experimental studies conducted in the literature is presented

Chapter 3 presents the material properties (concrete, reinforcement, FRP etc.), specimen fabrication, test setup (the testing machine, loading heads, knife edges) and instrumentation (position and number of strain gauges and LVDTs).

Chapter 4 discusses the test results. In this chapter the performance of eccentrically loaded columns as well as beams are discussed in terms of their failure modes and patterns, deformability, yield load, ultimate load, axial force-deflection behaviour and ductility.

Chapter 5 presents the four analytical models adopted for generating the P-M diagrams and detailed algorithms and flow charts for development of such diagrams based on each model. Also a summary of notations used for each model is given in each section of the chapter to avoid confusion. Eventually this chapter discusses the performance of these models by comparing them to the experimental results.

Chapter 6 presents the conclusion and final remarks based on the findings of chapters 4 and 5. In this chapter the recommendations for possible future research are given.

The appendix presents the spreadsheet sample procedures as well as the VBA macro code used to calculate the interaction diagrams for columns with 1 layer of CFRP wrap

2 Literature review

2.1 Introduction

In this chapter the confinement mechanism and mechanical behaviour of steel confined concrete as well as FRP confined concrete and their differences are discussed. Based on extensive review of literature on FRP-confined columns, categories of models presented for such columns are presented. Four of the proposed analytical constitutive models for FRP-confined concrete are chosen and presented two of which are lately developed. Eventually a brief review of the experimental studies that are conducted in the literature is presented.

2.2 Steel-Confined Concrete

In concrete columns confined with transverse reinforcement whether they are stirrups or spirals, the cover concrete strength is always neglected in calculating the strength of the column and would be ineffective when the concrete reaches its unconfined strength limit. On the other hand the core concrete continues to bear stresses and strains that are beyond ultimate state of unconfined concrete due to confinement effect of transverse reinforcement. There were some early studies on the behaviour of concrete confined under active hydrostatic stress which led to the following Equations (Richart et al. (1928) & (1929)) for stress and strain at ultimate state:

$$f'_{cc} = f'_{co} + k_1 f_l \tag{2.2.1}$$

$$\varepsilon_{cc} = \varepsilon_{co}\left(1 + k_2 \frac{f_l}{f'_{co}}\right) \tag{2.2.2}$$

Researchers such as Richard et al.(1928) and Balmer (1944) were among the researchers who conducted early studies for finding the average value for k_1 and k_2 (coefficients which are function of concrete mix as well as lateral pressure). Richard et al. found an average value of $k_1 = 4.1$ and $k_2 = 5k_1$. They also concluded that the strength predicted by their Equations for concrete confined with hydrostatic pressure could be applied to passively confined concrete with densely spaced spirals. Experimental studies by other researchers including Mander et al. (1984) concluded that strength of steel confined concrete could be increased subject to the following conditions:

- Transverse reinforcement is densely spaced.
- Supplementary hoops and cross ties with multiple legs are included.
- Proper distribution of longitudinal reinforcement across the section.
- Either the volumetric ratio of transverse reinforcement to the core concrete or the yield strength of the transverse reinforcement is increased.
- Usage of circular transverse reinforcement instead of rectangular hoops and supplementary cross ties.

There are many studies on steel confined concrete. The stress-strain model that was developed by Mander et al. (1984) is adopted by ACI for prediction of behaviour of steel confined concrete. They developed a stress strain model based on Popovics Equations which is applied to both concrete confined by spirals as well as circular and rectangular stirrups. Under quasi-static loading the following Equation applies:

$$f_c = \frac{f'_{cc} x r}{r - 1 + x^r} \tag{2.2.3}$$

The parameters x and r can be defined by Equations 2.2.4 through 2.2.8:

$$x = \frac{\varepsilon_c}{\varepsilon_{cc}} \tag{2.2.4}$$

$$\varepsilon_{cc} = \varepsilon_{co}\left[1 + \left(\frac{f'_{cc}}{f'_{co}} - 1\right)\right] \tag{2.2.5}$$

$$r = \frac{E_c}{E_c - E_{\text{sec}}} \tag{2.2.6}$$

$$E_c = 5000\sqrt{f'_{co}} \tag{2.2.7}$$

$$E_{sec} = \frac{f'_{cc}}{\varepsilon_{cc}} \tag{2.2.8}$$

In these Equations f'_{cc} and ε_{cc} are ultimate confined concrete strength and strain accordingly, f'_{co} and ε_{co} are unconfined concrete strength and the corresponding strain for which $\varepsilon_{co} = 0.002$ is assumed. E_c is the tangent modulus of elasticity and E_{sec} is secant modulus of elasticity.

They developed the Equation for calculation of ultimate confined concrete strength by utilization of the five-parameter multi axial failure surface developed by William and Warnke. (1975) as well as ultimate strength surface developed by Schickert and Winkler (1977). For the case of concrete confined subjected to triaxial stress state that has equal lateral confinement stresses f'_l from transverse reinforcement the ultimate confined concrete strength is defined by Equation 2.2.9.

$$f'_{cc} = f'_{co}\left(-1.254 + 2.254\sqrt{1 + \frac{7.94 f'_l}{f'_{co}}} - 2\frac{f'_l}{f'_c}\right) \tag{2.2.9}$$

In order to define the lateral confinement stress authors proposed the concept of confinement effectiveness. Confinement stresses develop a stress field in the core concrete that has a the shape of an arch between the

levels of transverse reinforcement for both circular and rectangular hoops as well as across the cross section for rectangular shaped hoops only. These stress fields are illustrated in Figures 2.2-1 and 2.2-2. This action is called arching action and according to the concept of confinement effectiveness only this portion of the core concrete that can be assumed to be effectively confined. Thus, they defined f_l' in Equation 2.2.9 to be:

$$f_l' = f_l k_e \tag{2.2.10}$$

In which the confinement effectiveness coefficient k_e is defined by Equation 2.2.11.

$$k_e = \frac{A_e}{A_{cc}} \tag{2.2.11}$$

A_e is the area of effective area which can be found by subtracting the area of parabola that includes the area of ineffectively confined concrete. The area within the centerlines of the perimeter spiral or hoop A_{cc} is defined by Equation 2.2.12.

$$A_{cc} = A_c(1 - \rho_{cc}) \tag{2.2.12}$$

In Equation 2.2.12 A_c is the area of the core section enclosed with the transverse reinforcement and ρ_{cc} is the ratio of longitudinal reinforcement area to area of the core concrete. In concrete columns with circular cross sections the confinement coefficient for concrete confined with circular hoops and circular spirals can be calculated by Equations 2.2.13 and 2.2.14 accordingly.

$$k_e = \frac{\left(1 - \frac{s'}{2d_s}\right)^2}{1 - \rho_{cc}} \tag{2.2.13}$$

$$k_e = \frac{\left(1 - \frac{s'}{2d_s}\right)}{1 - \rho_{cc}} \tag{2.2.14}$$

In these Equations s' is the clear vertical spacing between spiral or hoop bars and d_s is the diameter of the spirals or circular hoops between the bar centrelines as illustrated in Figure 2.2-1. In the case concrete columns with rectangular cross sections the confinement coefficient shall be calculated by Equation 2.2.15.

$$k_e = \frac{\left(1 - \sum_{i=1}^{n} \frac{(w_i')^2}{6b_c d_c}\right)\left(1 - \frac{s'}{2b_c}\right)\left(1 - \frac{s'}{2d_c}\right)}{(1 - \rho_{cc})} \tag{2.2.15}$$

In which W_i' is the ith clear distance between adjacent longitudinal bars, b_c and d_c are the core dimensions to centreline of the perimeter hoop in x and y directions as illustrated in Figure 2.2-2.

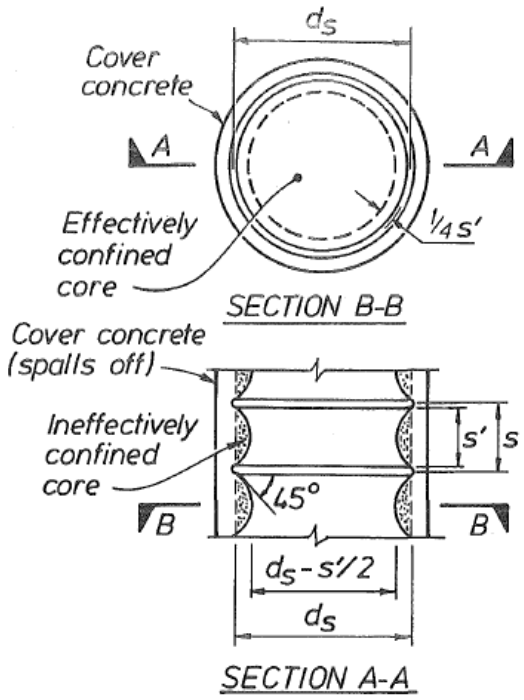

Figure 2.2-1 Stress field shape in the core concrete of circular sections (Mander et al. (1984))

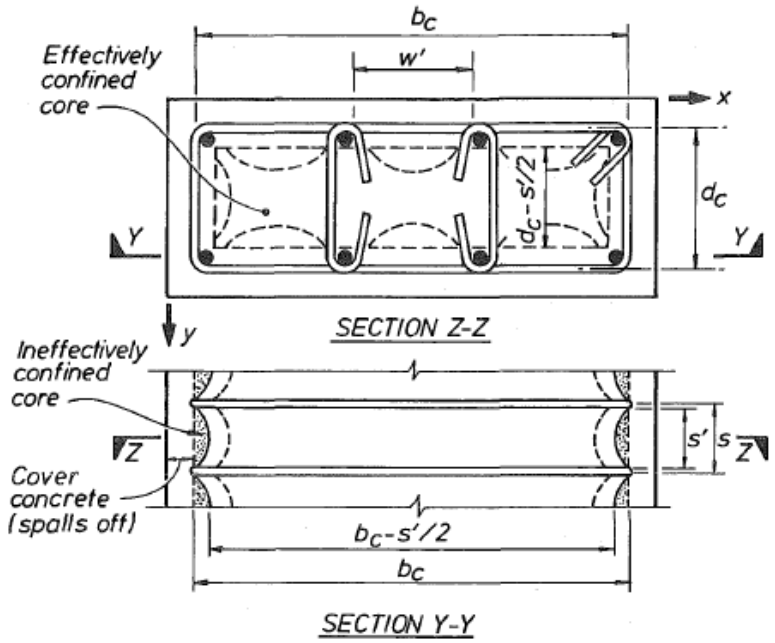

Figure 2.2-2 Stress field shape in the core concrete of rectangular sections (Mander et al. (1984))

2.3 Mechanics of FRP-confined concrete

In contrast with concrete confined with transverse steel reinforcement or tubes, typical FRP-encased concrete stress strain behaviour can be characterized as an approximate bilinear curve in which there is no descending branches as illustrated in Figure 2.3-1. The stress strain curve of a FRP-encased concrete is comprised of three regions; In the first portion of the curve the behaviour is completely similar to that of plain concrete, afterwards with creation and enhancement of microcracks the curve enters a transition zone in which FRP tube or wrap exerts some pressure on the concrete to restrain the microcracks from growing, in the third portion the FRP jacket is completely activated and the curves follows a linear path for which the slope is dependent on the stiffness of the FRP jacket.

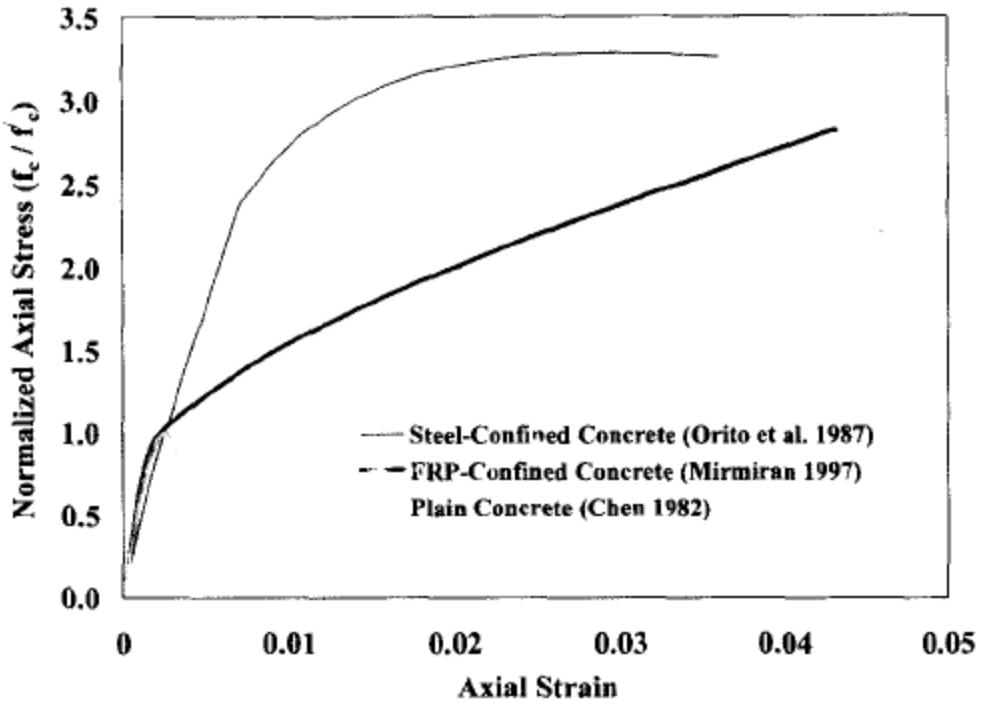

Figure 2.3-1 Axial stress-strain behaviour of FRP confined concrete vs steel confined concrete (Samaan et al. (1998))

2.3.1 Dilation behaviour of FRP-confined concrete

There are fundamental differences in dilation characteristics of steel-encased concrete versus the FRP-confined concrete. Evaluation of volumetric strain response contributes to a better understanding of the roots of these deviations. Volumetric strain ε_v or dilation as it is called is defined as the volume change per unit volume and can be calculated using Equation 2.3.1.1. in which ε_l is the axial strain and ε_r is the lateral strain.

$$\varepsilon_v = \varepsilon_l + 2\varepsilon_r \ (1) \qquad (2.3.1.1)$$

With regards to both plain concrete as well as steel-encased concrete, the concrete goes through a volumetric reduction until it reaches the stress of $0.90f_c'$. After that point an inelastic volumetric expansion occurs until concrete reaches stress of f_c' after which the dilatancy becomes unstable until the point of failure of the concrete. In the case of FRP-confined concrete however if sufficiently confined, the volume expansion of the concrete can be restrained or even reversed. This happens due to increased lateral pressure exerted by the FRP jacket with the hoop expansion of the core concrete. Dilation behaviour of frp-confined concrete is compared to that of unconfined concrete in Figure 2.3.1-1 Mirmiran and Shahawy (1997).

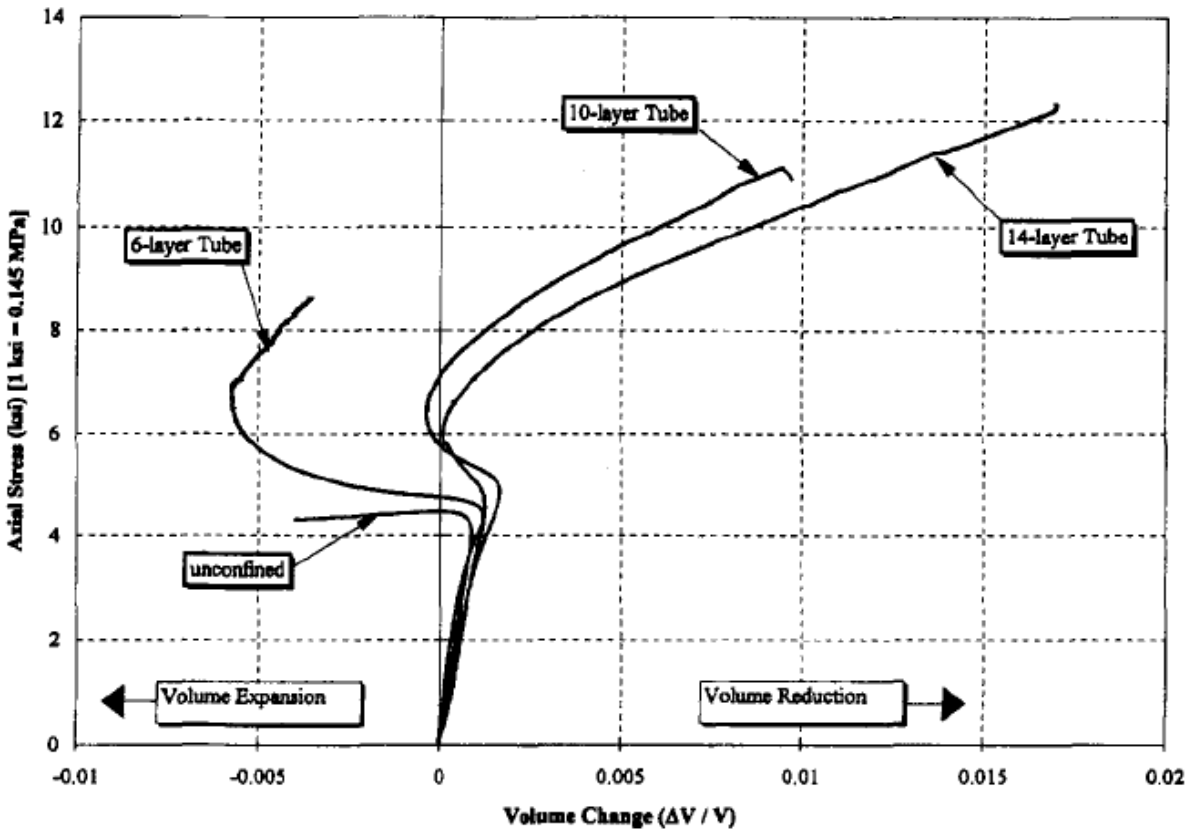

Figure 2.3.1-1 Dilation behaviour of FRP confined concrete vs unconfined concrete (Mirmiran and Shahawy (1997))

If the first derivative of Equation 2.3.1.1 is taken it yields the following Equation:

$$\frac{d\varepsilon_v}{d\varepsilon_l} = 1 + 2\frac{d\varepsilon_r}{d\varepsilon_l} = 1 + 2\mu \qquad (2.3.1.2)$$

In Equation 2.3.1.2, μ is the dilation rate which is the rate of change of lateral strains relative to the axial strains. Mirmiran and Shahawy (1997) studied the dilation rate of unconfined concrete versus FRP-confined concrete. As it is illustrated in the Figure 2.3.1-2 the dilation rate of FRP-encased concrete consists of three regions; in the initial region the dilation rate matches the Poisson's ration of the unconfined concrete and is constant since the concrete is in the elastic range. In the second region with creation of major cracks the dilation rate increases and in the case of unconfined concrete the rate increases at an exponential rate which indicates the instability of crack growth whereas in the case of FRP-encased concrete the rate increases until it arrives at the peak value μ_{max}. The stiffer the FRP jacket is the smaller μ_{max} is going to be. Eventually in the third region the dilation rate begins decreasing until it is stabilized at a constant rate of μ_u which is the ultimate dilation rate.

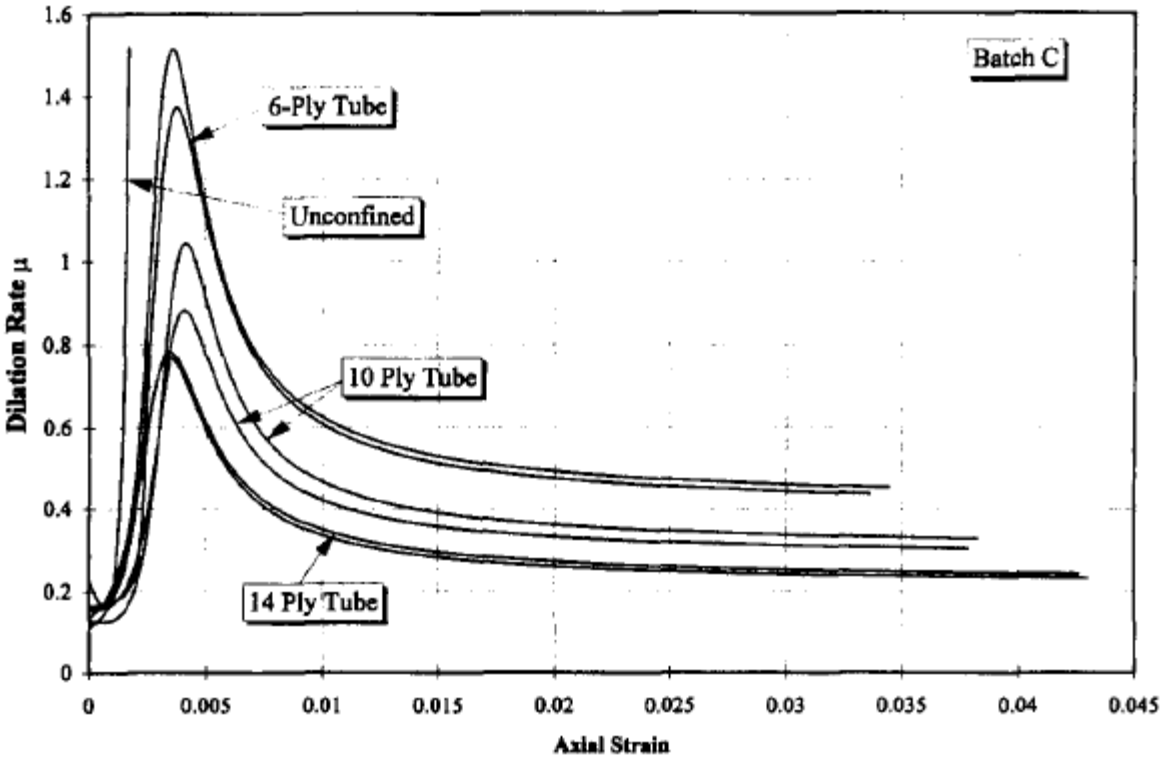

Figure 2.3.1-2 Dilation rate of FRP confined and unconfined concrete (Mirmiran and Shahawy (1997))

As mentioned previously the first important factor in determination of the peak and ultimate dilation rates is the stiffness of the FRP jacket and the second factor is the concrete strength. The following Equations are developed based on regression analysis of an experimental study Mirmiran (1996).

$$\mu_{max} = -0.7611\ ln\left(\frac{2E_j t_j}{f'_{co} D}\right) + 4.0167 \tag{2.3.1.3}$$

$$\mu_u = -0.1375\ ln\left(\frac{2E_j t_j}{f'_{co} D}\right) + 0.8646 \tag{2.3.1.4}$$

In these Equations E_j stands for elasticity modulus of the jacket, t_j is jacket thickness, D is the core concrete diameter and f'_{co} is the unconfined concrete strength.

2.3.2 Failure Criterion

In order to develop a model for FRP-encased concrete two major factors should be taken into account; first the dilation tendency of concrete and secondly the radial stiffness of the confining jacket that is preventing the core concrete from dilation. When addressing these factors, the following criteria should be met; first the strain compatibility between the FRP jacket and the core concrete. Secondly the equilibrium of forces in the free body diagram, created by passing a plane through the middle of the cross section of the member, should be satisfied.

The model developed by Mander et al. for steel-encased concrete is based on an energy balance approach. In this approach it is assumed that compared to plain concrete the additional ductility in concreted confined by steel reinforcement is due to the energy stored in the transverse reinforcement. Based on this assumption Mander et al. (1988) proposed the following equation in order to calculate ultimate strain of confined concrete (ε_{cu}):

$$U_{sh} = U_{cc} + U_{sc} - U_{co} \tag{2.3.2.1}$$

Considering the stress strain curves of plain and steel confined concrete in Figure 2.3.2-1 the strain energy can be defined as the area under the stress strain curve. In Equation 2.3.2.1, U_{sh} is the stored strain energy in transverse steel reinforcement per unit volume of core concrete which is equal to the difference in the area under stress strain curve of confined concrete (U_{cc}) and unconfined concrete (U_{co}), plus the yield energy of longitudinal steel in compression (U_{sc}).

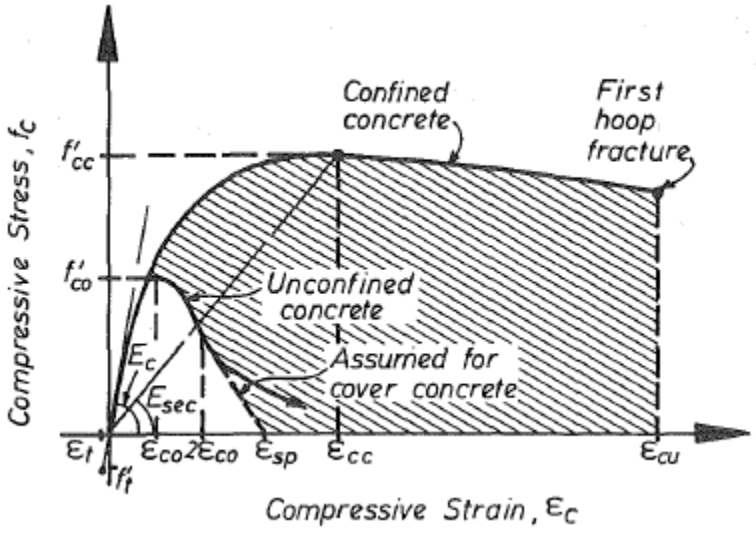

Figure 2.3.2-1 Axial stress-strain curve of steel confined concrete and unconfined concrete

By substitution Equation 2.3.2.2 yields (Mander et al. (1988)):

$$\rho_s A_{cc} \cdot \int_0^{\varepsilon_{sf}} f_s d\varepsilon_s = A_{cc} \cdot \int_0^{\varepsilon_{cu}} f_c d\varepsilon_c + \rho_{cc} A_{cc} \cdot \int_0^{\varepsilon_{cu}} f_{sl} d\varepsilon_c - A_{cc} \cdot \int_0^{\varepsilon_{sp}} f_c d\varepsilon_c \qquad (2.3.2.2)$$

In Equation 2.3.2.2, ρ_s is the volumetric ratio of transverse reinforcement to core concrete, A_{cc} is the area of the core concrete, ε_{sf} is the fracture strain of transverse reinforcement, f_c and ε_c are longitudinal stress and strain of concrete correspondingly, ε_{cu} is the ultimate strain of confined concrete, ρ_{cc} is the ratio of volume of longitudinal reinforcement to volume of core concrete, f_{sl} is the stress in longitudinal rebars, and ε_{sp} is the spalling strain of unconfined concrete. Mander et al. (1984) have proven that the value of the term "$\int_0^{\varepsilon_{sf}} f_s d\varepsilon_s$" is independent of bar size and yield strength and can be estimated as 110 MJ/m^3 with an acceptable error and also the spalling strain of steel ranges from 0.24 to 0.29. They also proved that third term on the right hand side of Equation 2.3.2.2 can be using equation 2.3.2.3:

$$\int_0^{\varepsilon_{sp}} f_c d\varepsilon_c = 0.017\sqrt{f'_{co}}\, MJ/m^3 \qquad (2.3.2.3)$$

By substitution the following Equation yields (Mander et al (1988)):

$$110\rho_s = \int_0^{\varepsilon_{cu}} f_c d\varepsilon_c + \int_0^{\varepsilon_{cu}} f_{sl} d\varepsilon_c - 0.017\sqrt{f'_{co}}\,\frac{MJ}{m^3} \qquad (2.3.2.4)$$

In Equation 2.3.2.4, by substitution of f_c and f_{sl} with their respective relations and numerical solution of integral equation one can find the first hoop fracture strain or the ultimate strain of confined concrete (ε_{cu}). This approach however is not satisfying the strain compatibility criteria and is insensitive to variability of concrete Poisson's ratio. Comparison of experimental studies conducted by Saadatmanesh et al. (1994) and Mirmiran and Shahawy (1996) with the Mander model indicates that the model underestimates the strength of FRP-encased concrete and therefore due to this reason as well as the differences in confinement mechanics laid out previously, is not suitable for such application.

2.4 Design oriented models for FRP-encased concrete

Models developed for prediction of stress strain behaviour of FRP-confined concrete can be divided into two broad categories; namely design-oriented models and analysis-oriented models. In the case of design-oriented models closed form Equations are developed based on statistical analysis of experimental data to predict the ultimate strain, ultimate compressive strength and stress strain behaviour of the confined concrete. These models can be categorized into three main groups based on the geometry of their curve (Ozbakkaloglu. T., Lim. J. C., Vincent. T. (2013)):

- Type I: for which the curve has a parabolic shape
- Type II: in which the stress strain curve is bilinear
- Type III: the curve is a combination of parabolic and linear curves. This category can be subdivided into Type IIIa, IIIb and IIIc based on the method that researchers utilized for the development of the curves.

2.4.1 Model Type I

In the early stages due to scarcity of experimental data various researchers employed the Equations that were originally developed to predict the behaviour of either actively confined concrete or steel-confined concrete. As illustrated in Figure 2.4.1-1 these models have a parabolic curve. Due to the reasons mentioned in previous sections these models are unable to capture the confinement characteristics of the FRP-encased concrete and thus they fail to predict their stress strain curves with accuracy.

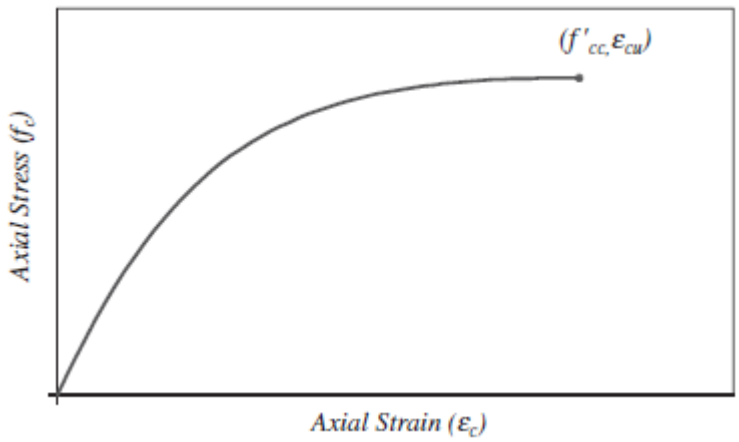

Figure 2.4.1-1 Axial stress-strain curve of model type I(Ozbakkaloglu et al. 2013))

2.4.2 Model Type II

As illustrated in Figure 2.4.2-1 these models are based on a bilinear stress strain curve. In Type II models there are two critical points that define the stress strain model and for each branch of the curve the linear Equation is developed based on those points. First critical point is the transition point which happens at $(f'_{c1}, \varepsilon_{c1})$ .Some studies have considered no enhancement of transition stress and strain compared to the unconfined concrete therefore in these cases the transition point is defined as $(f'_{co}, \varepsilon_{co})$. The second critical point is the ultimate state for confined concrete which is defined by $(f'_{cc}, \varepsilon_{cu})$ in which f'_{cu} and ε_{cu} are calculated using empirical Equations.

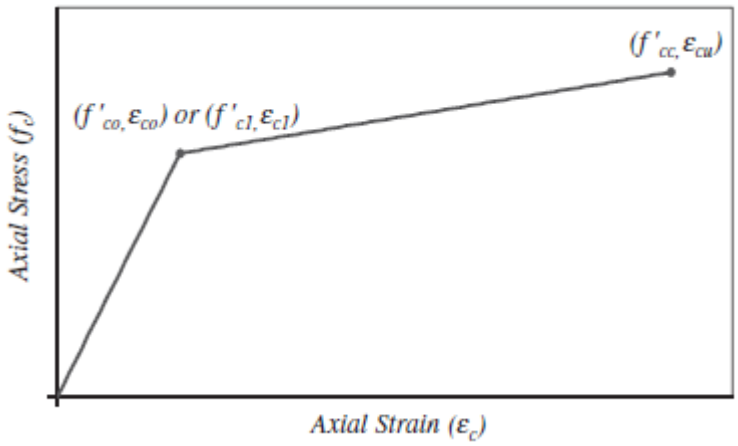

Figure 2.4.2-1 Axial stress-strain curve of model type II(Ozbakkaloglu et al. (2013))

2.4.3 Model Type III

In model Type III the first ascending branch of the stress strain curve was refined and has a parabolic shape and the second branch of the stress-strain curve is approximately linear. Based on the methods different studies adopted to determine the curve, this type is further divided in three subcategories.

Model Type IIIa: In this model Hongnestad's parabola (1951) has been employed to create the first ascending branch and the stress strain can be obtained by Equation 2.4.3.1 for this portion. The second branch is created by connecting the first peak, either $(f'_{co}, \varepsilon_{co})$ or $(f'_{c1}, \varepsilon_{c1})$, to the ultimate condition $(f'_{cc}, \varepsilon_{cu})$ with a straight line defined by Equation 2.4.3.2. The shape of the curve is shown in Figure 2.4.3-1.

$$f_c = f'_{c1}\left[2\left(\frac{\varepsilon_c}{\varepsilon_{c1}}\right) - \left(\frac{\varepsilon_c}{\varepsilon_{c1}}\right)^2\right] \quad for \;\; \varepsilon_c \leq \varepsilon_{c1} \tag{2.4.3.1}$$

$$f_c = f'_{c1} + E_{c2}(\varepsilon_c - \varepsilon_{c1}) \;\; for \;\; \varepsilon_c > \varepsilon_{c1} \tag{2.4.3.2}$$

$$E_{c2} = \frac{f'_{cc} - f'_{c1}}{\varepsilon_{cu} - \varepsilon_{c1}} \tag{2.4.3.3}$$

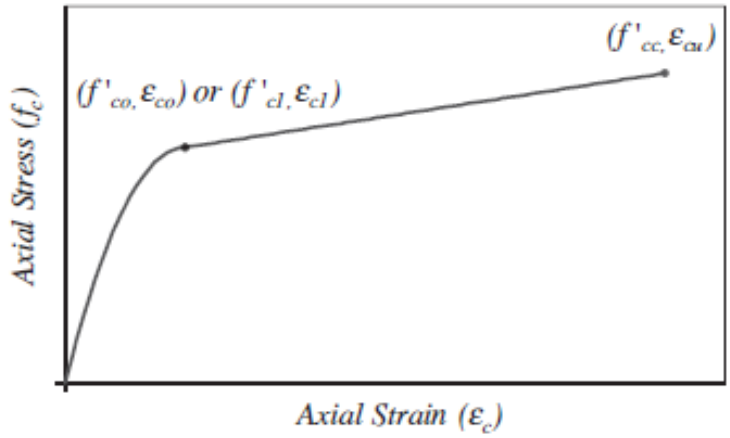

Figure 2.4.3-1 Axial stress-strain curve of model type IIIa(Ozbakkaloglu et al. (2013))

Model Type IIIb: A group of models are based on the curve developed by Richard and Abbott (1975) which is illustrated in Figure 2.4.3-2. In the original formation the stress strain curve is described by 2.4.3.4 in which E_{c1} and E_{c2} are correspondingly the slope of the elastic ascending portion and the post-peak branch of the curve for which different studies have proposed different Equations. As shown in the figure, f_o can be obtained by intersection of the tangent line to the post peak branch and the axial stress axis. Polynomial constant "n" is defined by 2.4.3.6 which creates the smooth transition zone between two branches of the curve.

$$f_c = \frac{(E_{c1} - E_{c2})\varepsilon_c}{\left\{1 + \left[\frac{(E_{c1} - E_{c2})\varepsilon_c}{f_o}\right]^n\right\}^{\frac{1}{n}}} + E_{c2}\varepsilon_c \tag{2.4.3.4}$$

$$f_o = f'_{cc} - E_{c2}\varepsilon_{cu} \tag{2.4.3.5}$$

$$n = 1 + \frac{1}{\frac{E_{c1}}{E_{c2}} - 1} \tag{2.4.3.6}$$

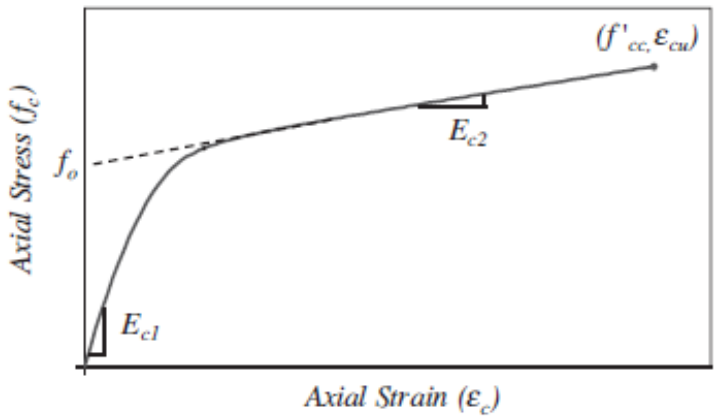

Figure 2.4.3-2 Axial stress-strain curve of model type IIIb(Ozbakkaloglu et al. (2013))

Model Type IIIc: This group of models are based on the general expression developed by Sargin (1971) Equation 2.4.3.7. Some researchers adopted the expression developed by Toutanji (1999), Equation 2.4.3.8 which is the modified version of Equation 2.4.3.7, to express the behaviour of FRP-confined concrete. As shown in Figure 2.4.3-3 E_{c1} and E'_{c2} are the slope of initial ascending branch and second branch respectively. The variables f'_{c1} and ε_{c1} are the initial peak stress and strain. The post-peak slope (E'_{c2}) is the tangential slope of the curve taken immediately after the initial peak point on the curve.

$$\frac{f_c}{f'_{co}} = \frac{A_i\left(\frac{\varepsilon_c}{\varepsilon_{co}}\right) + (D_i - 1)\left(\frac{\varepsilon_c}{\varepsilon_{co}}\right)^2}{1 + (A_i - 2)\left(\frac{\varepsilon_c}{\varepsilon_{co}}\right) + D_i\left(\frac{\varepsilon_c}{\varepsilon_{co}}\right)^2} \tag{2.4.3.7}$$

$$f_c = \frac{A_j \varepsilon_c}{1 + C_j \varepsilon_c + D_j \varepsilon_c^2} \tag{2.4.3.8}$$

$$C_j = \frac{E_{c1}}{f'_{c1}} - \frac{2}{\varepsilon_{c1}} + \frac{E_{c1}E'_{c2}\varepsilon_{c1}}{{f'_{c1}}^2} \tag{2.4.3.9}$$

$$D_j = \frac{1}{\varepsilon_{c1}^2} - \frac{E_{c1}E'_{c2}}{{f'_{c1}}^2} \tag{2.4.3.10}$$

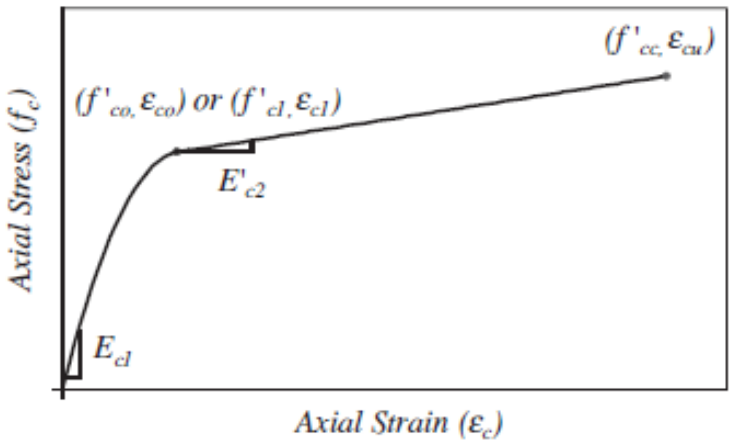

Figure 2.4.3-3 Axial stress-strain curve of model type IIIc (Ozbakkaloglu et al. (2013))

2.5 Analysis oriented models for FRP-encased concrete

Analysis oriented models consider the stress and strain compatibility between the confining jacket and the core concrete and can be incorporated in numerical iterative procedures and finite element models. The early models were based on the assumption that the axial stress-strain behaviour of FRP-encased concrete are the same as actively confined concrete and thus are independent of the stress path. Experimental studies have demonstrated that this assumption is not accurate for FRP-confined concrete (Xiao et al (2010)).There are other models based on advanced theories of strength of materials like plasticity and damage-plasticity based models (Yu et al. (2010a, 2010b)). Analysis oriented models are more generic and powerful than the design based models in a sense that if the appropriate constitutive model is used they can predict behaviour of concrete confined by any material. They can also predict the stress strain behaviour of sufficiently confined concrete with ascending post-peak branch as well as weakly confined concrete with a strain softening post-peak branch with a descending slope. However, our focus in this research is not going to be on the analysis oriented models.

2.6 Lam and Teng model

The most widely used model which is also adopted by ACI 440 guideline is the design oriented model developed by Lam and Teng (2003a). This model is based on the following assumptions:

- Axial stress strain curve of the model is comprised of two portions. The first portion has a parabolic form and the second portion has a linear shape.
- The initial slope of the parabolic portion is equal to the unconfined concrete modulus of elasticity.
- FRP jacket affects the nonlinear part of the first portion of the curve.
- The transition of slope between the first parabolic branch to the second linear branch happens smoothly.
- The linear branch of the curve ends at the ultimate failure point at which both ultimate compressive strength and axial strain have been reached.

The parabolic portion of the curve is based on Hongnestad's parabola with some modifications. The stress strain model is given by Equations 2.6.1 and 2.6.2 and the curve has been illustrated in Figure 2.6-1.

$$\sigma_c = E_c\varepsilon_c - \frac{(E_c - E_2)^2}{4f_o}(\varepsilon_c)^2 \; for \;\; 0 \le \varepsilon_c \le \varepsilon_t \tag{2.6.1}$$

$$\sigma_c = f_o + \; E_2\varepsilon_c \;\; for \;\; \varepsilon_t \le \varepsilon_c \le \varepsilon_{cu} \tag{2.6.2}$$

In which E_c is the elasticity modulus of unconfined concrete, f_o as shown in the figure is the intersection of the extension of the second linear branch and the stress axis. Based on experimental data Lam and Teng suggested that $f_o = f'_{co}$ be used. The transition strain can be obtained by the following Equation:

$$\varepsilon_t = \frac{2f_o}{E_c - E_2} \tag{2.6.3}$$

In Equation 2.6.3, E_2 is the slope of the linear portion and can be calculated using Equation 2.6.4.

$$E_2 = \frac{f'_{cc} - f_o}{\varepsilon_{cu}} \tag{2.6.4}$$

In Equation 2.6.4 f'_{cc} is the strength of confined concrete. In another study Lam and Teng (2002) have demonstrated that the ultimate strength of confined concrete can be obtained by Equation 2.6.5 in which $f_{l,a}$ is the actual maximum confinement pressure and can be calculated by Equation 2.6.6. The authors demonstrated that the actual rupture strain $\varepsilon_{h,rup}$ of the FRP is lower than the ultimate strain which is obtained by standard coupon tests. The major reasons for this phenomenon are reported to be first due to the localized cracking and deformation which results in uneven stress distribution in the FRP shell and thus the premature failure. The second major cause is arising from adverse effect of the curvature on the ultimate tensile rupture of the FRP. For CFRP authors recommended that $\varepsilon_{h,rup}$ is 0.586 of the ultimate strain by coupon tests ε_u.

$$\frac{f'_{cc}}{f'_{co}} = 1 + 3.3\frac{f_{l,a}}{f'_{co}} \tag{2.6.5}$$

$$f_{l,a} = \frac{2E_{frp}t\varepsilon_{h,rup}}{d} \tag{2.6.6}$$

For calculation of the ultimate strain the authors developed the following Equation based on the trends of the test data:

$$\frac{\varepsilon_{cu}}{\varepsilon_{co}} = 1.75 + 12\left(\frac{f_{l,a}}{f'_{co}}\right)\left(\frac{\varepsilon_{h,rup}}{\varepsilon_{co}}\right)^{0.45} \quad (2.6.7)$$

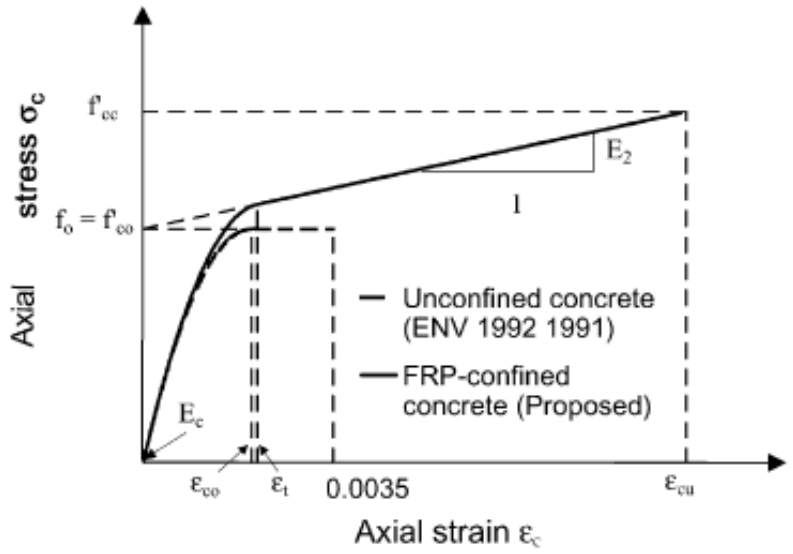

Figure 2.6-1 Axial stress-strain curve of Lam & Teng model (Lam and Teng (2003a))

2.7 Youssef et al. Model

In their study Youssef et al. (2007) developed a generic model that captures the behaviour of columns with both circular as well as rectangular cross sections, the model also accounts for both the strain hardening as well as the strain softening curve after the first peak stress is reached. Researchers in this study divided the stress strain curve into two areas:

- $0 \leq \varepsilon_c \leq \varepsilon_t$: In this portion of the curve based on the experimental observations the stress strain behaviour of confined concrete matches that of unconfined concrete
- $\varepsilon_t \leq \varepsilon_c \leq \varepsilon_{cu}$: In this region of the curve two scenarios can happen, in the case of sufficiently confined circular and rectangular columns the slope of the post-peak portion is ascending, in the case of the majority of rectangular columns and insufficiently confined circular columns the post-peak portion has a descending slope.

For the first portion of the curve they adopted the same approach as Hoshikuma et al. (1997) and used the polynomial in Equation 2.7.1 to develop the stress strain model. In order to define the constants C_1, C_2, C_3 and n in this Equation two scenarios are considered and for each scenario stress strain Equation was obtained by placing the appropriate boundary conditions.

$$f_c = C_1\varepsilon_c^n + C_2\varepsilon_c + C_3 \tag{2.7.1}$$

In the first scenario in which the post-peak slope is ascending ($E_2 > 0$), we have the following boundary conditions:

$$f_c = 0 \ @ \ \varepsilon_c = 0 \tag{2.7.2}$$

$$\frac{df_c}{d\varepsilon_c} = E_c \ @ \ \varepsilon_c = 0 \tag{2.7.3}$$

$$\frac{df_c}{d\varepsilon_c} = E_2 \ @ \ \varepsilon_c = \varepsilon_t \tag{2.7.4}$$

$$f_c = f_t \ @ \ \varepsilon_c = \varepsilon_t \tag{2.7.5}$$

By substitution of the boundary conditions 2.7.2 to 2.7.5 into Equation 2.7.1 the stress strain model is obtained as following:

$$f_c = E_c\varepsilon_c\left[1 - \frac{1}{n}\left(1 - \frac{E_2}{E_c}\right)\left(\frac{\varepsilon_c}{\varepsilon_t}\right)^{n-1}\right] \tag{2.7.6}$$

$$n = \frac{(E_c - E_2)\varepsilon_t}{E_c\varepsilon_t - f_t} \tag{2.7.7}$$

In the second scenario in which the post-peak slope is descending ($E_2 < 0$) the slope of the tangent at first peak stress becomes zero and the boundary condition in 2.7.4 is substituted by 2.7.8 and thus the stress strain curve can be obtained using Equations 2.7.9 and 2.7.10.

$$\frac{df_c}{d\varepsilon_c} = 0 \ @ \ \varepsilon_c = \varepsilon_t \tag{2.7.8}$$

$$f_c = E_c\varepsilon_c\left[1 - \frac{1}{n}\left(\frac{\varepsilon_c}{\varepsilon_t}\right)^{n-1}\right] \tag{2.7.9}$$

$$n = \frac{(E_c)\varepsilon_t}{E_c\varepsilon_t - f_t} \tag{2.7.10}$$

For the post-peak region ($\varepsilon_t \leq \varepsilon_c \leq \varepsilon_{cu}$) the linear Equation 2.7.11 is used which covers both ascending and descending post-peak slope scenarios. By substitution of boundary conditions 2.7.12 and 2.7.13 in Equation 2.7.11, the stress strain relationship is obtained as Equation 2.7.14.

$$f_c = a\varepsilon_c + b \tag{2.7.11}$$

$$f_c = f_t \ @ \ \varepsilon_c = \varepsilon_t \tag{2.7.12}$$

‘

$$f_c = f'_{cu} \ @ \ \varepsilon_c = \varepsilon_{cu} \tag{2.7.13}$$

$$f_c = f_t + E_2(\varepsilon_c - \varepsilon_t) \tag{2.7.14}$$

In the calculation of stress-strain curve using this model there are four critical variables which should be calculated initially, namely the transition (f_t, ε_t) and ultimate (f'_{cu}, ε_{cu}) stress and strain. The authors developed empirical Equations 2.7.15 to 2.7.18 based on rigorous regression analysis of experimental data to estimate these variables. The following Equations have a generic form and their respective shape factors including $\alpha, \beta, \gamma, \lambda, \eta, \mu$ and ψ are summarized in Table 2.7-1 for the case of circular as well as rectangular sections independently.

$$\frac{f'_{cu}}{f'_c} = \left[\alpha + \beta\left(\frac{f'_{lu}}{f'_c}\right)^{\gamma}\right] \tag{2.7.15}$$

$$\varepsilon_{cu} = \left[\lambda + 0.260\left(\frac{f'_{lu}}{f'_c}\right)\left(\frac{f_{ju}}{E_j}\right)^{\frac{1}{2}}\right] \tag{2.7.16}$$

$$\frac{f_t}{f'_c} = \left[1 + \eta\left(\frac{\rho_j E_j \varepsilon_{jt}}{f'_c}\right)^{\frac{5}{4}}\right] \tag{2.7.17}$$

$$\varepsilon_t = \left[\mu + \psi\left(\frac{\rho_j E_j \varepsilon_{jt}}{f'_c}\right)^{\frac{6}{7}}\left(\frac{f_{ju}}{E_j}\right)^{\frac{1}{2}}\right] \tag{2.7.18}$$

Table 2.7-1 Proposed general model shape factors (Youssef et al. (2007))

Shape Factors	α	β	γ	λ	η	μ	ψ
Circular	1	2.25	1.25	0.00337	3	0.00274	0.117
Rectangular	0.5	1.225	0.6	0.00433	1.135	0.0020	0.078

In Equations 2.7.15 to 2.7.18 ρ_j, E_j, f_{ju} and ε_{jt} are volume ratio, modulus of elasticity, tensile strength and transition strain of the jacket respectively. The effective lateral confining stress (f'_{lu}) in Equations above can be calculated by multiplying the confinement effectiveness coefficient (k_e) and the lateral confining stress of the jacket at ultimate condition in Equation 2.7.19. The confinement coefficient for circular column is taken as 1 while for rectangular columns it can be calculated using Equation 2.7.21. in which b is width of rectangular section, h is the width of the section, r_c is the corner radius of the section and ρ_l is the area ratio of the longitudinal reinforcement.

$$f'_{lu} = k_e f_{lu} \tag{2.7.19}$$

.

$$f_{lu} = \frac{1}{2}\rho_j f_{ju} \tag{2.7.20}$$

$$k_e = \frac{1 - \left[\frac{(b-2r_c)^2 + (h-2r_c)^2}{3hb}\right] - \rho_l}{1-\rho_l} \tag{2.7.21}$$

2.8 Faustino et al. Model

This analytical model was developed based on extensive experimental database of large scale squared shaped CFRP confined RC columns (Faustino et al. (2014)). This database considers variety of parameters which include corner ratios (R/B) ranging between 0.033 to 0.247, cross sections with side dimensions (B) from 150 to 914 mm, various longitudinal reinforcement ratios (ρ_L) ranging between 1 to 1.5%, transverse reinforcement volumetric ratios (ρ_v) ranging from 0.11 to 0.45% and CFRP volumetric ratios (ρ_f) from 0.21 to 0.94%. As demonstrated in Figure 2.8-1 the axial stress-strain curve consists of two linear branches that have a smooth transition zone. The model takes both strain hardening curves with an ascending post-peak branch as well as strain hardening curves with a descending post peak branch into account. The stress strain curve can be obtained by Equation 2.8.1 which is based on the curve developed by Richard and Abbott (Type IIIb curve) except for the fact that all the parameters are calibrated for RC columns with square cross sections.

$$f_c = \frac{(E_1 - E_2)\varepsilon_c}{\left[1 + \left(\frac{(E_1 - E_2)\varepsilon_c}{f_0}\right)^n\right]^{\frac{1}{n}}} + E_2\varepsilon_c \leq f_{cc} \tag{2.8.1}$$

$$\begin{cases} E_1 = 3950\sqrt{f_{c0}} & (a) \\ E_2 = 510\left(\frac{2R}{B}f_{lu}\right)^{0.04} f_{c0}^{0.95} - 440 f_{c0} & (b) \\ f_0 = f_{c0} + 0.5\left(\frac{2R}{B}\right)f_{lu} & (c) \end{cases} \tag{2.8.2}$$

In the Equations above the lateral confinement stress (f_{lu}) and the confined concrete stress (f_{cc}) can be calculated by Equations 2.8.3 and 2.8.4. In Equation 2.8.1 for square sections n = 3 can be assumed. In this model the contribution of transverse reinforcement to the total confinement stress (f_{lu}) has been taken into account by adding the term f_{shu} to lateral stress caused by FRP jacket (f_{ju}) in Equation 2.8.3. In Equations 2.8.4 to 2.8.11 the variables are as follows:

- Variables R and B are corner radius and diameter of an equivalent circular cross section respectively.
- The coefficient in Equation 2.8.4 is taken as $k_1 = 3.7$.
- The parameters t, E_f and ε_{lu} in Equation 2.8.5 are thickness, modulus of elasticity and the lateral ultimate strain of the CFRP jacket correspondingly.
- In Equation 2.8.6, variables A_{sw}, f_{sw} and s are transverse reinforcement area, tensile strength and spacing between the hoops respectively. The diameter of the transverse reinforcement (d_w) is calculated the same way as the dimension B.
- The coefficient in Equation 2.8.10 is taken as $k_2 = 18.89$ for CFRP confined columns with square cross section.

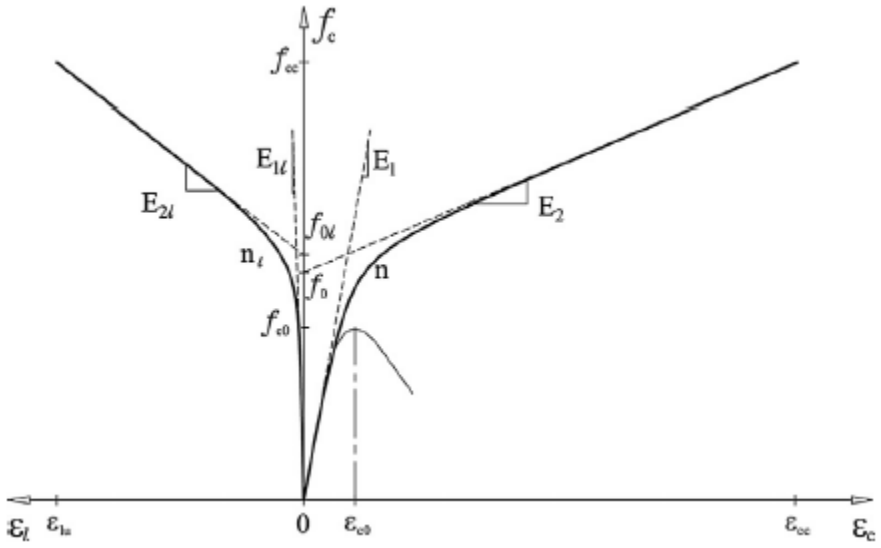

Figure 2.8-1 Axial stress-strain curve of Faustino et al model (Faustino et al. (2014))

$$f_{lu} = f_{ju} + f_{shu} \tag{2.8.3}$$

$$f_{cc} = f_{c0} + k_1 \left(\frac{2R}{B}\right) f_{lu} \tag{2.8.4}$$

$$f_{ju} = \frac{2t}{B} E_f \varepsilon_{lu} \tag{2.8.5}$$

$$f_{shu} = \frac{2A_{sw}}{d_w s} f_{sw} \tag{2.8.6}$$

$$f_{sw} = \begin{cases} E_s \times \dfrac{d_w}{B} \varepsilon_{lu} \;\; for \;\; \varepsilon_{lu} < \dfrac{B}{d_w} \varepsilon_y \\ f_y \qquad\qquad for \;\; \varepsilon_{lu} \geq \dfrac{B}{d_w} \varepsilon_y \end{cases} \tag{2.8.7}$$

$$\varepsilon_{lu} = 0.7 \left(\frac{2R}{B}\right)^{0.23} \varepsilon_{fu} \tag{2.8.8}$$

$$\varepsilon_{cc} = k_2 \varepsilon_{c0} \left(\frac{f_{lu}}{f_{c0}}\right) \tag{2.8.9}$$

$$\varepsilon_{c0} = \frac{0.7}{1000} (f_{c0})^{0.31} \tag{2.8.10}$$

2.9 Eid and Paultre Model

This model is one of the latest unified stress-strain models that can predict the behaviour of columns with either circular or square/rectangular cross sections and concrete types in the range of normal to high strength (20 to 140 MPa) with transverse reinforcement with normal to high strength (300 to 1400 Mpa) (Eid and Paultre (2017)). This model also takes the interaction between transverse steel with FRP jacket into account. As illustrated in Figure 2.9-1 the curve is comprised of three regions; for the first region strain is below confined concrete first peak strain ($\epsilon_c \leq \epsilon'_{cc}$), has a nonlinear form. The second region of the curve is the post-peak zone in which the axial strain is between the confined concrete first peak and FRP rupture strain ($\epsilon_{cu} \geq \epsilon_c > \epsilon'_{cc}$) which is nonlinear in the transition zone and becomes approximately linear with either an ascending or descending curve depending on the amount of confinement provided. The third zone belongs to axial strains beyond the point of FRP rupture ($\epsilon_c > \epsilon_{cu}$) in which the transverse steel is still providing

confinement until fails. In this final portion the curve stays on the approximate linear path with the same slope as the end of the second zone.

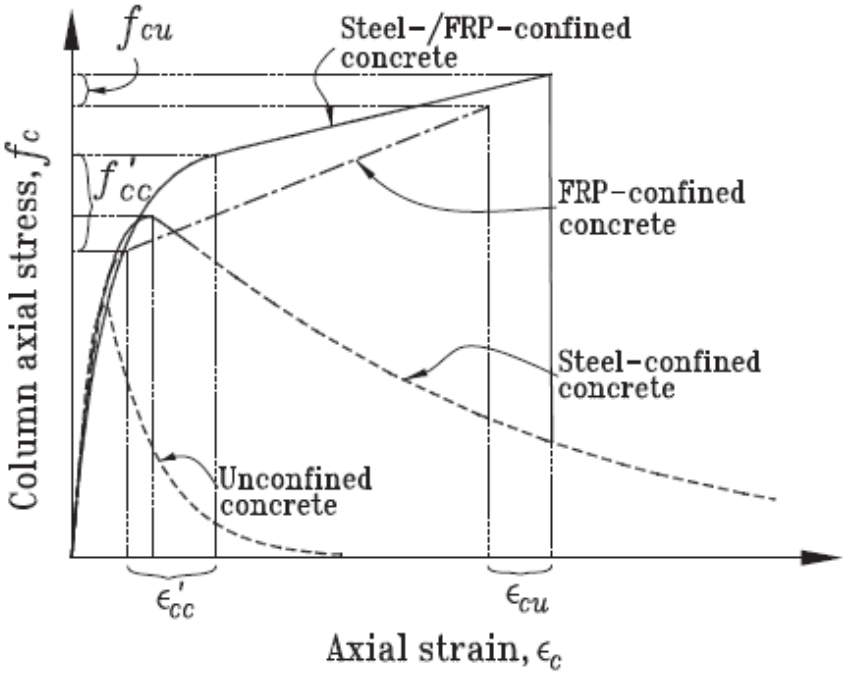

Figure 2.9-1 Axial stress-strain curve of Eid & Paultre model(Eid and Paultre (2017))

In the pre-peak branch the stress strain curve is calculated by Equation 2.9.1 which is based on Popovics Equation in which the coefficients a, b and z are the parameters that dictate the curvature and slope of this branch and will be obtained by applying the boundary conditions 2.9.2 in Equation 2.9.1. In Equations 2.9.3, E_{ct} is the tangent modulus of elasticity of concrete, E_{cu} is the post-peak slope of the curve, f'_{cc} and ϵ'_{cc} are the confined concrete strength and strain at the first peak respectively which can be obtained by Equations 2.9.4 and 2.9.5. In Equations 2.9.4 and 2.9.5, parameter $I'_e = \frac{f'_{le}}{f'_c}$ is the effective confinement index evaluated at concrete peak stress.

$$f_c = \frac{a\epsilon_c}{1 + b\epsilon_c + z\epsilon_c^2} \quad for\ \epsilon_c \le \epsilon'_{cc} \tag{2.9.1}$$

$$\left(\frac{df_c}{d\epsilon_c}\right)_{\epsilon_c=0} = E_{ct}, \qquad (f_c)_{\epsilon_c=\epsilon'_{cc}} = f'_{cc}, \qquad \left(\frac{df_c}{d\epsilon_c}\right)_{\epsilon_c=\epsilon'_{cc}} = E_{cu} \tag{2.9.2}$$

$$a = E_{ct}, \qquad b = \frac{E_{ct}}{f'_{cc}} - \frac{2}{\epsilon'_{cc}} + \frac{E_{ct}E_{cu}\epsilon'_{cc}}{{f'_{cc}}^2}, \qquad z = \frac{1}{{\epsilon'_{cc}}^2} - \frac{E_{ct}E_{cu}}{{f'_{cc}}^2} \tag{2.9.3}$$

$$\frac{f'_{cc}}{f'_c} = 1 + 2.4(I'_e)^{0.7} \tag{2.9.4}$$

$$\frac{\epsilon'_{cc}}{\epsilon'_c} = 1 + 35(I'_e)^{1.2} \tag{2.9.5}$$

As shown in Figure 2.9-2 the confinement mechanism of FRP-Steel confined concrete can be illustrated by a cut half cross section. The transverse reinforcement is replaced by a uniform equivalent steel envelope with a thickness of e that exerts the lateral pressure of $\frac{2ef'_h}{D_c}$ at the peak stress. In Equation 2.9.6, f'_{lf} is the confinement pressure exerted by the FRP and Δp is the pressure developed due to the action of transverse steel reinforcement as illustrated in Figure 2.9-2 (c). This pressure is negligible in the columns with regular cover (In the range of $c/D \leq 0.1$).

$$f'_{le} = \frac{2ef'_h}{D_c} + f'_{lf} - \Delta p = \rho_{sey} f'_h + E_{fl}\epsilon'_f - \Delta p \tag{2.9.6}$$

In the elastic range and especially for columns with small cover thickness the tangential FRP strain ϵ_f can be taken equal to the tangential strain of the transverse steel ϵ_h. With this assumption and using the strain compatibility, Equation 2.9.7 yields at the first peak. In this Equation ν'_{cc} and E'_{ccl} are concrete's secant Poisson's ratio and secant modulus of elasticity respectively.

$$\epsilon'_h = \nu'_{cc}\epsilon'_{cc} - \frac{(1-\nu'_{cc})f'_{le}}{E'_{ccl}} \tag{2.9.7}$$

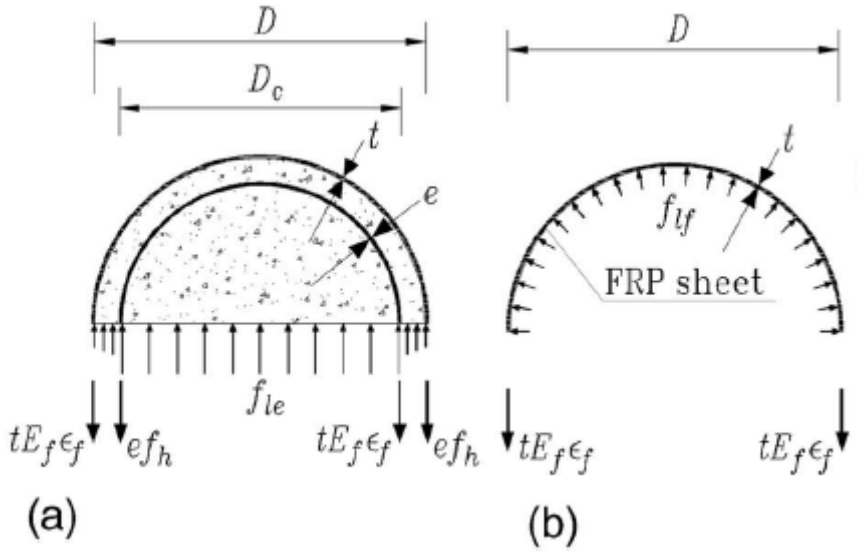

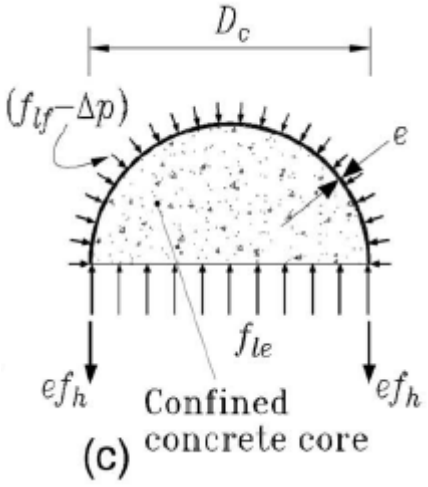

Figure 2.9-2 Lateral confinement pressure by internal reinforcement and FRP (Eid and Paultre (2008))

It is assumed that $E'_{ccl} = \alpha f'_{cc}/\epsilon'_{cc}$ and $\alpha \geq 1$. If Equations 2.9.4 and 2.9.5 are substituted in Equation 2.9.7 and the resultant Equation is divided by ϵ'_{cc} the following Equation yields which relates the lateral strain to the axial strain of the concrete at the first peak:

$$\frac{\epsilon'_h}{\epsilon'_c} = [1 + 35(I'_e)^{1.2}]\left[\nu'_{cc} - \frac{1-\nu'_{cc}}{\alpha}\frac{I'_e}{1+2.4(I'_e)^{0.7}}\right] \tag{2.9.8}$$

For concrete confined with transverse steel Legeron and Paultre (2003) have suggested $\alpha = 1.1$ and $\nu'_{cc} = 0.43$. Several experimental studies (Xiao and Wu 2003; Mirmiran and Shahawy 1997) demonstrated that due to the high lateral modulus of FRP the value of secant Poisson's ratio can be much lower than 0.43. The Equation 2.9.9 is proposed by Xiao and Wu (2003) for estimating ν'_{cc} in FRP-confined concrete. In order to take the effect of transverse reinforcement in evaluating ν'_{cc}, Equation 2.9.10 is adopted by Legeron and Paultre (2003). In Equations 2.9.9 to 2.9.16 the parameters are defined as following :

- ν_{c0} is the initial secant Poisson's ratio of the concrete which can be taken as 0.15.
- $\gamma_{sf} = \epsilon_{hy}/\epsilon_{fu}$.
- E_{fl} is the lateral modulus of FRP which can be obtained using Equation 2.9.11.
- ρ_{se} is the effective sectional ratio of confinement reinforcement which can be calculated by Equation 2.9.12.
- K_f is the geometric coefficient of confinement effectiveness for square/rectangular columns which is calculated using Equation 2.9.13.
- K_e is the arching geometrical effectiveness coefficient of transverse reinforcement confinement which can be calculated by Equation 2.9.14.
- K_v is the vertical arching geometrical effectiveness coefficient of transverse reinforcement which is calculated by Equation 2.9.15.

- K_h is the horizontal arching geometrical effectiveness coefficient of transverse reinforcement which is calculated by Equation 2.9.16.
- c_x and c_y are the dimensions of the rectangular column core in x and y directions respectively.
- A_{sh} is the total cross section area of transverse reinforcement within tie spacing s in circular columns. In columns with square/rectangular cross sections A_{shx} and A_{shy} are the total transverse reinforcement area within spacing s that are perpendicular to x and y directions respectively.
- D is the full column diameter and c is the core concrete diameter.
- Dimensions b and h are the column cross section dimensions ($b \leq$ h). Dimension r_c is the corner radius of square/rectangular columns.
- A_g is the area of the gross section of the column.
- Parameter ρ_g is the ratio of area of longitudinal reinforcement to that of the cross section of the column. Parameter ρ_{cc} is the ratio of longitudinal reinforcement area to that of the core section.
- In Equation 2.9.14, parameter n is equal to 1 for columns confined by spirals and 2 for columns confined with ties and hoops.
- Parameter s is center to center transverse reinforcement spacing and s' is the clear spacing of transverse reinforcement.
- Parameter w_i is the clear horizontal spacing between two adjacent laterally supported longitudinal bars.

$$v'_{cc} = 10\left[\frac{f'_c}{E_{fl}}\right]^{0.9} \tag{2.9.9}$$

$$v_{c0} \leq v'_{cc} = 10\left[\frac{f'_c}{E_{fl} + \rho_{se}E_s\gamma_{sf}}\right]^{0.9} \leq 0.5 \tag{2.9.10}$$

$$E_{fl} = \begin{cases} \dfrac{2tE_f}{D} & for\ circular\ columns \\ 2K_fE_f\left(\dfrac{2t}{c_x + c_y}\right) & for\ square/rectangular\ columns \end{cases} \tag{2.9.11}$$

$$\rho_{se} = \begin{cases} \dfrac{K_eA_{sh}}{sc} & for\ circular\ columns \\ \dfrac{K_e}{s}\left(\dfrac{A_{shx} + A_{shy}}{c_x + c_y}\right) & for\ Square/Rectangular\ columns \end{cases} \tag{2.9.12}$$

$$K_f = \frac{1 - \frac{\left[\left(\frac{b}{h}\right)(h-2r_c)^2 + \left(\frac{h}{b}\right)(b-2r_c)^2\right]}{3A_g} - \rho_g}{(1-\rho_g)} \geq 0 \tag{2.9.13}$$

$$K_e = \begin{cases} \frac{\left(1-\frac{s'}{2c}\right)^n}{(1-\rho_{cc})} \geq 0 & for\ circular\ columns \\ K_h K_v \geq 0 & for\ square/rectangular\ columns \end{cases} \tag{2.9.14}$$

$$K_v = \frac{\left(1-\frac{s'}{2c_x}\right)\left(1-\frac{s'}{2c_y}\right)}{(1-\rho_{cc})} \geq 0 \tag{2.9.15}$$

$$K_h = 1 - \frac{\sum w_i^2}{6c_x c_y} \tag{2.9.16}$$

On the basis of Equation 2.9.8 as well as experimental observations the following simpler relationship is developed:

$$\frac{\epsilon_h'}{\epsilon_c'} = \nu_{cc}' + \eta I_e' \tag{2.9.17}$$

In Equation 2.9.17 the parameter η is defined as follows:

$$\eta = 29.8\nu_{cc}' - 3.56 \tag{2.9.18}$$

On the other hand if the force equilibrium of the half cross section of the column is considered for an arbitrary point in pre-peak portion of stress strain curve and if Δp is neglected, the effective confinement index I_e can be developed as following:

$$I_e = \frac{\rho_{sey} f_h}{f_c'} + \frac{E_{fl}\epsilon_f}{f_c'} \tag{2.9.19}$$

In Equation 2.9.19, f_h is considered a function of ϵ_h/ϵ_c' and as a result I_e will be a function of ϵ_h/ϵ_c'. On the other hand Equation 2.9.17 can be rearranged in a way that I_e' is a function of ϵ_h'/ϵ_c'. In order to find the peak point, Equations 2.9.17 and 2.9.19 have to be satisfied simultaneously which means the intersection of two Equations should be determined. As illustrated in Figure 2.9-3 three situations might happen regarding the intersection of 2.9.17 and 2.9.19 that yields the peak stress; in the first situation the peak stress occurs when the lateral strain of the column is within the elastic strain range of TSR ($\epsilon_h < \epsilon_{hy}$) (group C in Figure 2.9-3). In the second situation the lateral strain is larger than the TSR yield strain but smaller than the FRP rupture strain ($\epsilon_{hy} \leq \epsilon_h < \epsilon_{fu,a}$) (group A in Figure 2.9-3). In the final situation the peak stress occurs at a point for which the lateral strain is equal to the actual FRP rupture strain $\epsilon_{fu,a}$. In the final case (group B in Figure 2.9-3) peak happens at a strain so low that the curves have no intersection and peak confinement index reaches its maximum value as in Equation 2.9.20. In this Equation ϵ_{fu} is the ultimate FRP strain achieved in coupon tests and $\xi = \epsilon_{fu,a}/\epsilon_{fu}$ is the efficiency factor.

$$I_{e,max} = \frac{\rho_{sey} f_{hy}}{f_c'} + \frac{E_{fl}\epsilon_{fu}\xi}{f_c'} \tag{2.9.20}$$

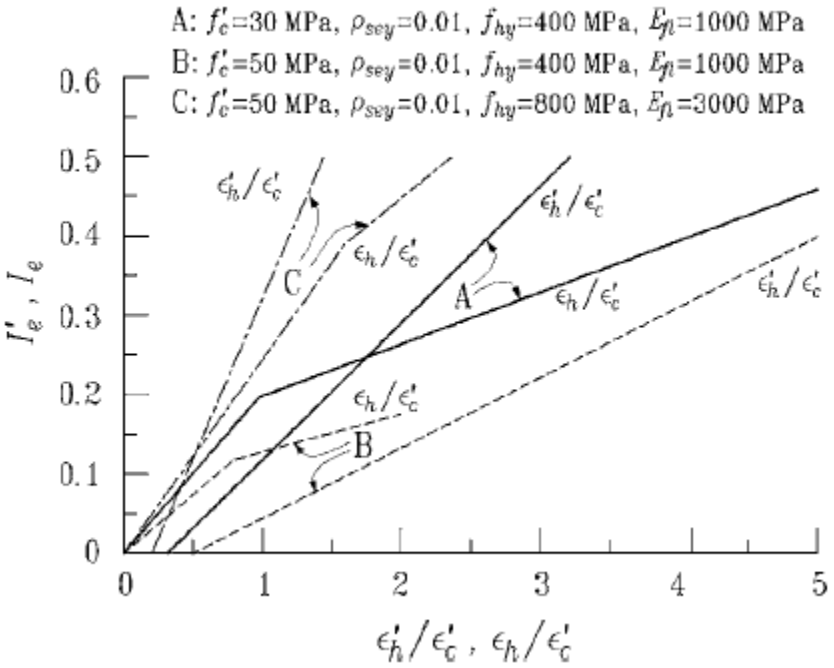

Figure 2.9-3 $\frac{\epsilon_h'}{\epsilon_c'}$ vs $\frac{\epsilon_h}{\epsilon_c'}$ for groups A, B, and C (Eid and Paultre (2008))

In the final case since FRP is ruptured at peak stress, the post-peak behaviour of the column is mainly controlled by the confining stresses exerted by the TSR. On the contrary in the first two cases the FRP also contributes in the post-peak confinement and axial stresses might reach values that are higher than the first peak stress. Equation 2.9.21 is obtained by simultaneous solution of 2.9.17 and 2.9.19.

$$I'_e = \begin{cases} I'_{e1} = \dfrac{v'_{cc}}{\kappa_1 - \eta} \le I'_{e2} & if\ \kappa_1 > \eta\ \ (\kappa_2 \gg \eta) \\ I'_{e2} = \dfrac{v'_{cc} f'_c + \kappa_2 \rho_{se} f_{hy}}{f'_c(\kappa_2 - \eta)} \le I_{e,max} & if\ \kappa_1 \le \eta\ and\ (\kappa_2 > \eta) \\ I_{e,max} = \dfrac{\rho_{se} f_{hy}}{f'_c} + \dfrac{E_{fl}\epsilon_{fu}\xi}{f'_c} & if\ \kappa_1 \le \eta\ and\ (\kappa_2 \ll \eta) \end{cases} \quad (2.9.21)$$

In Equation 2.9.21 κ_1 and κ_2 are defined as follows:

$$\kappa_1 = \frac{f'_c}{\rho_{se} E_s \epsilon'_c + E_{fl}\epsilon'_c} = \frac{E'_c}{E_{sl} + E_{fl}} \quad (2.9.22)$$

$$\kappa_2 = \frac{f'_c}{E_{fl}\epsilon'_c} = \frac{E'_c}{E_{fl}} \quad (2.9.23)$$

In Equations 2.9.22 and 2.9.23, $E'_c = f'_c/\epsilon'_c$ is the secant modulus of concrete at peak stress and $E_{sl} = \rho_{se} E_s$ is the lateral stiffness of TSR.

The post peak branch of the stress strain curve is obtained using Equation 2.9.24. In this Equation E_{cu} is the slope of the post-peak curve of the confined concrete which is given by Equation 2.9.25. Parameters f_{cu} and ϵ_{cu} are the ultimate concrete stress and strain given by Equations 2.9.26 and 2.9.27 respectively. k_1 and k_2 are the parameters controlling the shape of the post-peak curve which can be obtained by Equations 2.9.28 and 2.9.29.

$$f_c = \begin{cases} f'_{cc} \exp\left(k_1 (\epsilon_c - \epsilon'_{cc})^{k_2}\right) + E_{cu}(\epsilon_c - \epsilon'_{cc}) & for\ \epsilon_{cu} \ge \epsilon_c > \epsilon'_{cc} \\ f'_{cc,s} \exp\left(k_{1,s}\left(\epsilon_c - \epsilon'_{cc,s}\right)^{k_{2,s}}\right) & for\ \epsilon_c > \epsilon_{cu} \end{cases} \quad (2.9.24)$$

$$E_{cu} = \frac{f_{cu} - f'_{cc}}{\epsilon_{cu} - \epsilon'_{cc}} \le \frac{f_{cu} - f'_{cc}}{\epsilon_{cu}} \qquad (and\ E_{cu} \ge 0) \quad (2.9.25)$$

$$\frac{f_{cu}}{f'_c} = 1 + 3.3\left(\frac{b}{h}\right)^2 \left(\frac{\rho_{se} f_{hy}}{f'_c} + \frac{E_{fl}\epsilon_{fu}}{f'_c}.\xi\right) \ge \frac{f'_{cc}}{f'_c} \quad (2.9.26)$$

$$\frac{\epsilon_{cu}}{\epsilon'_c} = 1.56 + 12\left(\frac{\rho_{se} f_{hy}}{f'_c K_h^2} + \frac{E_{fl}\epsilon_{fu}}{f'_c}.\xi\right)\left(\frac{\epsilon_{fu,a}}{\epsilon'_c}\right)^{0.45} \quad (2.9.27)$$

$$k_1 = \frac{\ln(0.5)}{(\epsilon_{cc50} - \epsilon'_{cc})^{k_2}} \tag{2.9.28}$$

$$k_2 = 1 + 25(I_{e50})^2 \tag{2.9.29}$$

In Equation 2.9.28, ϵ_{cc50} is the post-peak strain that corresponds to the stress level that is 50% of the confined concrete peak stress which can be calculated by Equation. 2.9.30 for normal strength concrete and 2.9.31 for HSC ($f'_c \geq 60\ MPa$).

$$\frac{\epsilon_{cc50}}{\epsilon_{c50}} = 1 + 60I_{e50} \tag{2.9.30}$$

$$\epsilon_{cc50} = \epsilon_{c50} + 0.15(I_{e50})^{1.1} \tag{2.9.31}$$

In these relations I_{e50} is the effective confinement index corresponding to ϵ_{cc50} which can be calculated by the following Equation:

$$I_{e50} = \frac{\rho_{sey} f_{hy}}{f'_c} + \frac{E_{fl}\epsilon_{fu}}{f'_c} \tag{2.9.32}$$

In Equation 2.9.24, after the rupture of the FRP the linear term of the Equation is removed since the only confining member is the TSR and parameters $f'_{cc,s}$, $k_{1,s}$, $\epsilon'_{cc,s}$ and $k_{2,s}$ are calculated by consideration of the effect of TSR alone in the subsequent Equations. For calculation of $f'_{cc,s}$ and $\epsilon'_{cc,s}$ the same Equations are used (Eqs 2.9.4 and 2.9.5) with the exception that instead of I'_e, $I'_{e,s}$ will be used. $I'_{e,s} = \rho_{sey} f'_h / f'_c$ and f'_h can be calculated by the following Equation:

$$f'_h = \begin{cases} f_{hy} & if\ \kappa \leq 10 \\ \dfrac{0.25 f'_c}{\rho_{sey}(\kappa - 10)} \geq 0.43\varepsilon'_c E_s \nsucc f_{hy} & if\ \kappa > 10 \end{cases} \tag{2.9.33}$$

2.10 Review of experimental studies in the literature

Several studies have been conducted on FRP confined and strengthened RC columns under concentric loads. However, it is clear that in real situation most columns experience combination of axial compression load and bending moment (i.e. eccentric compression loading) due to construction error, etc.. Therefore, there is a need to understand the behaviour of FRP strengthened columns under eccentric loading. Some research has been conducted on FRP confined columns under eccentric loading. In a study performed by

Parvin and Wang (2001), small-scale square concrete columns (i.e. 108 mm × 108 mm × 305 mm) were strengthened with varying layers of carbon FRP (CFRP) composites and subjected to axial load at different eccentricities. The results showed that the increase in eccentricity resulted in a decrease in strength capacity of the column, and the use of CFRP increased the load capacity of the column.Fam et al. (2003) performed an experimental program and proposed an analytical model to describe the behaviour of concrete filled GFRP tubes subjected to combined axial compression loads and bending moments. In the experimental study 10 specimens were tested under eccentric loading conditions, two specimens under concentric loading and two specimens under pure bending (beam test). Two different laminate structures were considered for the GFRP tubes. In this study researchers concluded that interaction curves are significantly affected by the structure of the laminates as well as diameter to thickness of the tubes.

In an experimental study by Li and Hadi (2003), they tested RC columns with circular cross sections wrapped by CFRP as well as E-glass fibers. Totally seven high strength circular columns with hunched ends. These columns had a diameter of 235mm at haunched ends and diameter of 150mm in the test region. The clear distance between the haunched ends was 620mm and the overall length of each specimen was 1400mm. Two of these columns were internally reinforced. The internal reinforcement were consisted of

six RW10 bars spaced equally at the circumference of a 110mm diameter helix throughout the whole length of the specimens as well as three RW8 rebars spaced equally at haunched ends all of which were confined by circular ties. In terms of wrapping scheme, five specimens were continually wrapped of which two were wrapped by one layer and three layers of CFRP whereas three specimens were wrapped with one layer, three layers and five layers of E-glass fiber. Of the two remaining internally reinforced specimens one was only wrapped at the ends by three layers of CFRP while the other was wrapped continually with three layers of E-glass. The specimens were tested under eccentric loading 42.5 mm of eccentricity. They concluded that although CFRP wraps improve the strength of the specimens, the improvement is not significant compared to CFRP wrapped columns with normal strength concrete or under concentric loading.

In another study Hadi and Li (2004) investigated the behaviour of circular columns externally reinforced with different materials under concentric as well as eccentric loading. Five cylindrical columns, none of which were internally reinforced, were tested under concentric loading and had diameter of 205mm and height of 910mm. Two columns in this group were continually wrapped with one and three layers of CFRP whereas another two columns were wrapped with one and three layers of Kevlar Fibers. The remaining two columns in this group were reference specimens. Also six cylindrical concrete columns with diameter of 205mm and height 620mm were tested under eccentricity of 50 mm. Three of these columns were wrapped with unidirectional FRP, two were reinforced with steel straps with 20mm width and 0.5mm thickness and final internally reinforced column was used as a reference specimen. They concluded that Kevlar sheet wrapped columns had the maximum improvement in axial load capacity whereas the E-glass confined specimens had the poorest performance. They also concluded that fiber layout and width of the tape rolls had an effect on the performance of the columns.

In another experimental study by Hadi (2006a) six cylindrical columns for which the geometry was similar to that of Li and Hadi (2003) were cast and tested under eccentric loading with eccentricity of 42.5mm. Normal strength concrete was used in this study with a strength of 32 MPa. Two of the specimens were internally reinforced whereas others did not have any internal reinforcement. One of the columns was not wrapped two were wrapped with one layer of CFRP, two columns were wrapped with 3 layers of CFRP and eventually one specimen was wrapped with 5 layers of CFRP. They concluded that CFRP confinement increased the ductility and lateral deformability of the columns in a more significant manner compared to improvement of strength. They also suggested a minimum of three layers of wraps to achieve meaningful structural improvement based on their limited experimental study.

Hadi (2006b) undertook another experimental study in which nine HSC short cylindrical columns with 925mm height and 205mm diameter were created. Three of these columns were internally reinforced whereas six other specimens were made of plain concrete. Three of these six columns were wrapped with CFRP while the other three were wrapped with E-glass. For each group of columns one specimen was tested concentrically, one specimen with 25mm and another specimen with 50mm eccentricity. In this study the researcher used the knife edges to create eccentric loading conditions. The axial and lateral load-deflection of behaviour of tested columns were studied. They concluded that by enhancement of eccentricity significant drop in strength of specimens is observed. They also suggested extent of the lateral deformability of the columns is dependent on the strength of the FRP jacket.

In other studies by Hadi (2007a,b), tested several FRP-strengthened concrete columns (confined with CFRP, GFRP, and E-Glass) with circular section under eccentric loading at different conditions. The effects of concrete strength, internal steel reinforcement, wrap type, fiber orientation, and eccentricity were studied. The eccentric load was applied through a circular plate at each end of the specimens. The experimental results clearly demonstrated that the FRP wrapping can enhance strength, ductility, and energy absorption of circular concrete columns under eccentric loading. In a study performed by Chaallal and Shahawy (2000), an experimental investigation was conducted on rectangular RC columns strengthened with bidirectional CFRP composites and different eccentricities. The overall length of the two haunched-head specimens was 3.6 m (200 mm wide and 350 mm high in test section). The results indicated that the strength capacity of columns improved significantly as a result of the combined action of the longitudinal and the transverse fibers of the bidirectional composite fabrics.Lignola et al. (2007) have mainly focused their attention on square hollow columns strengthened with CFRP composites (height of 3020 mm, width of 360 mm, and wall thicknesses of 60 mm). The outcomes highlighted that composite wrapping can enhance the structural performance of concrete columns under eccentric loading in terms of strength and especially in terms of ductility. The strength improvement was more pronounced in the case of specimens loaded with smaller eccentricity, while the ductility improvement was more significant in the case of larger eccentricity. Sadeghian et al. (2010) in their study evaluated the effectiveness of CFRP wrapped rectangular RC columns (200x300mm) of 1.5m long (2.7m between haunched ends) under eccentric compression loading. In this study total of seven large-scale specimens were tested and the variables in the tests were different FRP thicknesses of two, three, and five layers, fiber orientations of 0˚, 45˚, and 90˚, and finally eccentricities of 200 and 300 mm. They concluded that the axial stiffness and yield of the strengthened columns with CFRP fibers oriented along the longitudinal axis of the columns. Although the curvature capacity of the columns were not significantly improved, specimens with fibers oriented along the axis of the column demonstrated improvements in flexural capacity while transverse fibers had little effect on flexural capacity of the columns failing in the tension controlled region.

Lei et al. (2012) and Widiarsa and Hadi (2013) studied the effectiveness of CFRP strengthened RC columns of square cross-section under eccentric loading and reported that the CFRP wrapping enhanced the load carrying capacity and ductility of the square RC columns under eccentric loading. In the study by Widiarsa and Hadi, researchers test 12 rectangular RC columns under compressive loading with eccentricities of 0, 25, and 50mm. All the columns had side dimensions of 200x200mm and height of 800mm. The internal reinforcement included four 12mm longitudinal rebars (500 MPa tensile strength) as well as 8mm ties spaced at 100 mm (250 MPa tensile strength). These columns were divided in four groups; three columns were unwrapped, three were wrapped with one layer of CFRP, three were wrapped with three layers of CFRP, and the fourth group were wrapped with two layers of horizontal and one vertical strap of CFRP. They concluded that load carrying capacity and ductility of columns are increased for the wrapped specimens and their performance is improved by postponing the rupture of concrete and reinforcement. In the case of the columns under compressive loading with high eccentricity, performance of specimens with

vertical straps were reported to be better in terms of load carrying capacity and ductility. In most of the above studies the columns were either circular, hollow square section or rectangular cross-section. Only few studies reported the behaviour of FRP wrapped square RC columns under eccentric loading. The experimental phase of this study presents the results of a comprehensive experimental program where 18 RC square columns are wrapped with various layers of CFRP fabric and are subjected to increasing eccentricities under pin-pin end conditions in compression. Effects of eccentricities and number of CFRP layers on the ultimate failure load, axial shortening at peak load, hoop strain in CFRP and mid height lateral deflection of all CFRP strengthened columns are also evaluated.

2.11 Summary

In this chapter the mechanical behaviour of FRP-encased columns is reviewed, different types of proposed analytical constitutive models available in the literature are reviewed. Among these models four are chosen (namely Lam & Teng (adopted by ACI 440), Youssef et al, Faustion et al, and Eid & Paultre.) to further investigate their potential and accuracy for development of P-M interaction diagrams of CFRP confined RC square columns. Also a brief review of the experimental studies available in the literature on FRP confined columns under eccentric loading conditions is presented. It is clear from this literature review that behaviour of CFRP confined columns with rectangular/square cross section under eccentric loading is under investigated and thus should be studied.

3 Methodology: Materials, experimental program, casting and testing details.

3.1 Introduction

Last chapter presented a review of the mechanical behaviour of FRP-encased concrete and the constitutional models proposed for prediction of their stress-strain behaviour. In this chapter the specifications of the specimens, their fabrication, curing and wrapping process, material properties, instrumentation and test setup, as well as the experimental program are presented.

3.2 Testing program and specimen specs

Twenty square shaped reinforced concrete columns were fabricated in this study. All square columns had the same cross section dimensions of 175×175 mm and the rounded corners with the radius of 20 mm and they had the same height of 800 mm and the same concrete compressive strength of 47 MPa. The ratio of the cross section dimensions to the height of the columns satisfied the requirements for a short column, therefore, global buckling of the columns was not an issue orin other words stability did not play an important role in the failure load of the column. As illustrated in Figure 3.2-1 all columns were also reinforced with same longitudinal as well as transverse reinforcement with four 12 mm longitudinal reinforcements and eight 6 mm rebars spaced at 100 mm as the transverse reinforcement. Both the longitudinal as well as the transverse reinforcements had the yield strength of 560 MPa.

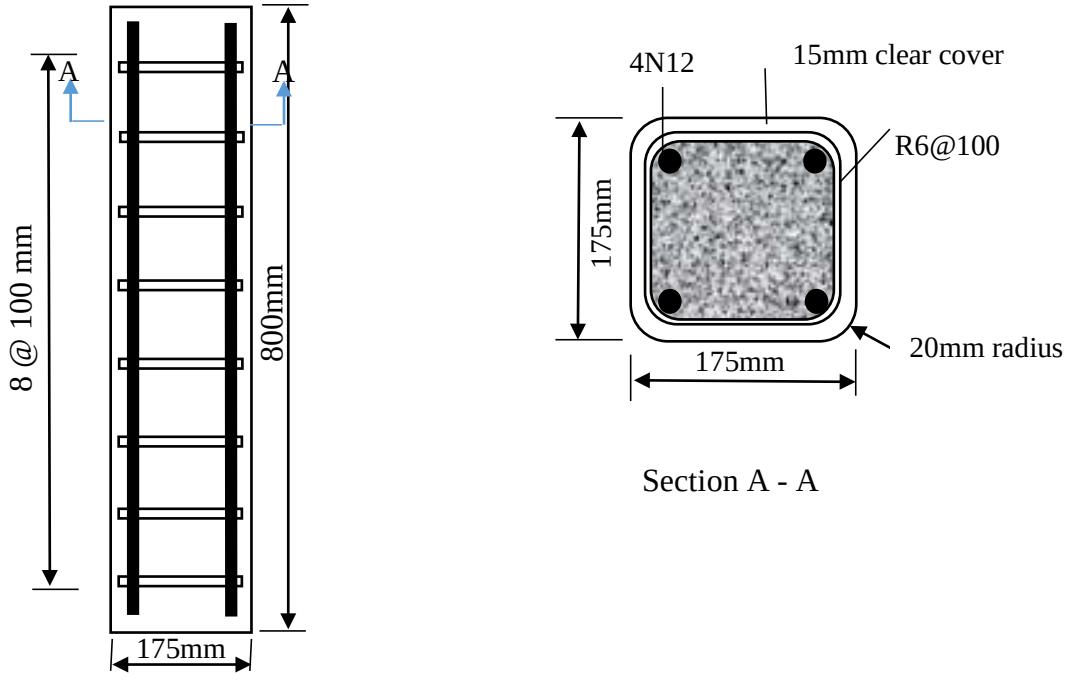

Figure 3.2-1 RC column dimensions and reinforcement configuration

The parameters that were varied in this experimental program were the applied CFRP layers (0, 1, 2 and 3 layers) as well as eccentricities under which the static compressionload was applied (0, 25, 35 and 50 mm). These set of eccentricities were chosen based on the limitation of testing equipment such as universal loading machine as well as the knife edges, also they were chosen to cover a range from pure compression and tension to compression and tension controlled areas of P-M diagram. Furthermore the eccentricity ratios (e/h = 0, 0.14, 0.2, and 0.29) chosen in this study were kept as close as possible to the values chosen in similar studies (Hadi, M. N. S. (2006a), (2006b), (2007a), (2007b), Hadi, M. N. S. and Widiarsa, I. B R. (2012), and Parvin, A., and Wang, W. (2002)). As shown in Table 3.2-1 the specimens were divided in to five groups. The first group of specimens were tested under concentric compression loading (zero eccentricity), while in second, third and fourth groups the specimens were subjected to eccentric compression loading with 25, 35 and 50mm eccentricities, respectively. The specimens in fifth series were subjected to three-point bending test. In the naming code CR stands for the unwrapped reference columns and CF stands for CFRP wrapped columns. The first number after CF indicates the number of CFRP wraps applied to that specimen. The second number after CF as well as the number after the letters CR indicate the eccentricity of the load in which 0, 1, 2 and 3 stand for eccentricities of 0, 25, 35, and 50 mm accordingly. Specimens CF20 and CF30 exceeded the universal testing machine's capacity and hence, the tests were not carried out so a total of 18 specimens were tested.

Group	Specimens	Eccentricity, e	Number of CFRP layers	Longitudinal reinforcement	Transverse reinforcement
First	CR0 CF10 CF20 CF30	Nil	0 1 2 3	4N12	R6@100mm
Second	CR1 CF11 CF21 CF31	25mm	0 1 2 3	4N12	R6@100mm
Third	CR2 CF12 CF22 CF32	35mm	0 1 2 3	4N12	R6@100mm
Fourth	CR3 CF13 CF23 CF33	50mm	0 1 2 3	4N12	R6@100mm
Fifth	CRB CF1B CF2B CF3B	Pure flexure (Beam Test)	0 1 2 3	4N12	R6@100mm

Table 3.2-1 Specimen naming code and properties

3.3 Specimen Fabrication

3.3.1 Concrete and Formwork Fabrication

The formworks were fabricated from plywood and were placed at the metal beds for horizontal fabrication of concrete columns. The joints of the formwork were sealed using plywood to avoid any concrete bleeding and leak of concrete outside the formwork. In order to create the 20mm radius at the corners of the specimens, specially manufacture strips of foam with 20 mm radius were attached at the corner of the formworks.

3.3.2 Steel Cages

Longitudinal rebars as well as stirrups were ordered from ARC (The Australian Reinforcing Company) and arrived as cut and deformed shape. All the steel cages were then woven together using tie wire twister and loop ties. And spacers were placed at three sides of the reinforcement cage for 15mm clear cover spacing.

3.3.3 Concrete pouring and curing

Ready-mixed concrete with maximum aggregate size of 10mm was purchased from Boral which is one of most renowned construction and building material manufacturer and suppliers in Australia. The slump tests were carried out immediately after the arrival of the concrete. The results from the slump tests showed that the concrete had a slump of more than 150 mm. After that the concrete was poured in three equal layers and each layer was compacted using hand vibrator. All specimens were then covered with wet hessian. The specimens were demoulded next day and cured in room temperature for 28 days before they were wrapped with CFRP fabrics.

3.3.4 CFRP wrapping of columns

After the demolding, relatively small voids and superficial damages were spotted on the substrate of some specimens as shown in Figure 3.3.4-1. These damages were first patched with standard cement mortar as the application guideline of SIKA CFRP wraps recommends. After three days of application of patches the surface of the specimens were smoothed on the four sides on which the wraps were going to be applied using concrete grinder. All the dust and loose cement were removed and the substrate of the specimens were completely cleaned and prepared for application of wraps.

The SikaWrap 230C along with Sikadure 330CN adhesive were used for strengthening of the columns. The CFRP fabrics were cut with widths of 500 mm and 150 mm, the 150 mm wide wraps were applied at both ends of each column and the 500 mm wide wraps were applied at the middle portion of the columns (As shown in Figure 3.3.4-2). For application of CFRP wraps the wet layup application was used as recommended by manufacturer guidelines. In this method 2/3 of the expected Sikadure 330CN was applied

onto the concrete surface, afterwards the wraps were applied on this saturated surface while they are being stretched. After application of the wraps the remaining 1/3 of the adhesive is applied on the surface of the wrap and the wraps were saturated by rolling a plastic roller in the direction of fibers (which was provided by the manufacturer) and the excessive air in the adhesive was driven out in this manner. Since application of wraps took place during high temperatures of the summer, for each batch there was only 30 minutes available until the adhesive hardens. According to the recommendation of manufacturer if the next layers of wraps are not applied within the first 60 minutes, at least 12 hours should pass before the next layers could be applied. For this reason, the second and third layers of wraps were applied in consecutive days. Whilst wrapping the specimens 100mm overlap was maintained for all CFRP wraps in accordance with the manufacturer recommendations. After application of CFRP wraps the specimens were left to dry for 14 days as specified by supplier.

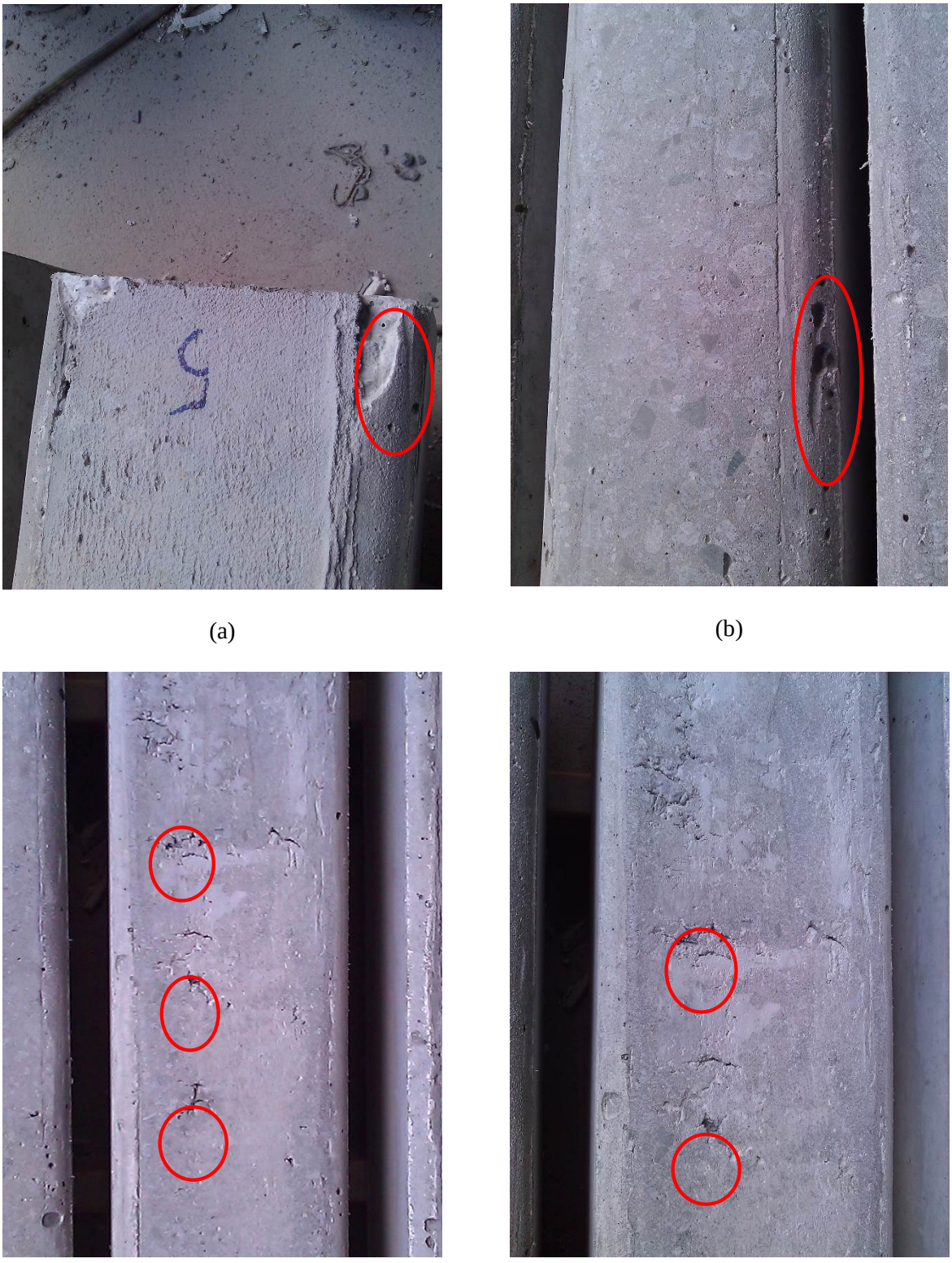

(a) (b)

(c) (d)

Figure 3.3.4-1 Damages and voids on concrete substrate

Figure 3.3.4-2 Wrapped specimens

3.4 Material testing and properties.

Standard 100mm diameter by 200mm height and 150mm diameter by 300mm heightcylindrical samples were cast at the time concrete pouring to measure the compressive and indirect tensile strengths of concrete. After 28 days of curing split tensile as well as compressive strengths were measured in accordance with ASTM C496 (ASTM (2011)) and ASTM C39 (ASTM (2014)), respectively. Standard compressive strength test setup is shown in Figure 3.4-2. The tensile test of rebars was performed in universal machine as shown in Figure 3.4-1. Properties of steel reinforcement as well as concrete are summarized in Table 3.4-1.

The properties of CFRP fabric, epoxy as well as the wrap were obtained from the manufacturer manual and are summarized in Table 3.4-2. The fabric tensile modulus as well as strength are based on the minimum

value while the corresponding values for laminate are based on average values. Laminate properties are used for modelling.

28 days Concrete compressive strength (MPa)	28 days Concrete tensile strength (MPa)	Steel yield strength (MPa)	Steel yield strain	Steel ultimate strength (MPa)	Steel ultimate strain
48	4	570	0.028	690	0.068

Table 3.4-1 Mechanical properties of concrete and longitudinal steel

	Tensile strength (MPa)	Elongation at rupture (%)	Tensile modulus (GPa)	Thickness (mm)
CFRP fabric (Sikawrap 230C)	4300	1.8	234	0.13
Two-part epoxy (Sikadur 330)	30	0.9	4.5	-
Laminate Properties (related to fibre thickness)	3176	1.8	216	0.131

Table 3.4-2 Properties of CFRP fabric, epoxy and laminate.

Figure 3.4-1 Tensile strength test of rebars

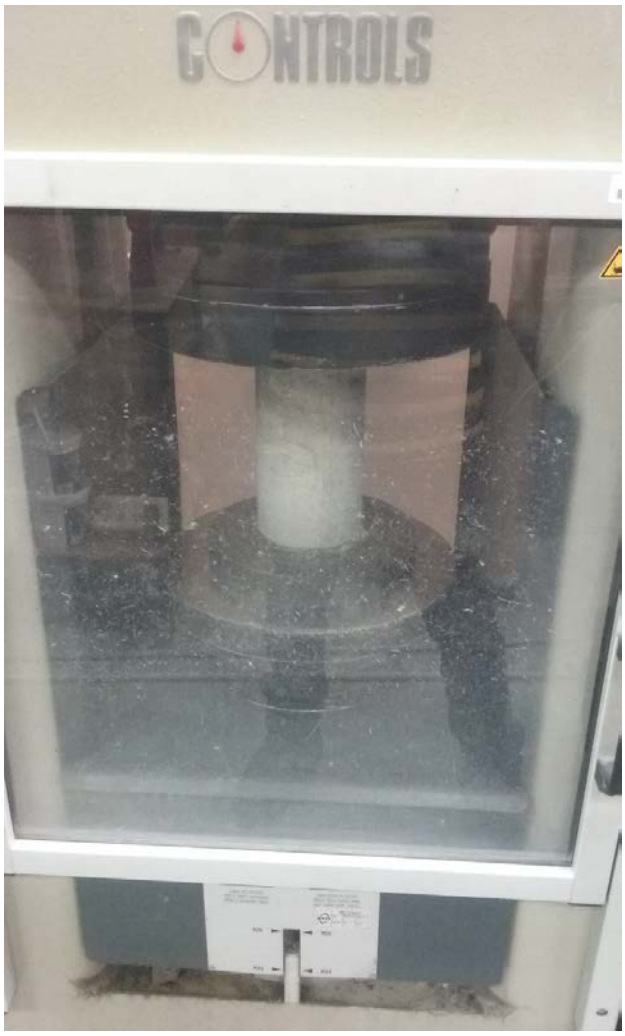

Figure 3.4-2 Standard cylindrical compressive test of concrete

3.5 Test setup, loading apparatus and instrumentation.

For column tests an especially designed loading system was used to apply eccentric loading in the columns. The loading system consists of steel loading head at both ends of the column. The loading head is connected to a thick steel plate which is then attached to a knife edge arrangement to facilitate the pin connection at both ends. These heads are shown in Figure 3.5-1. The thick plate which was connected to loading head, contained adjustable long slots to maintain the required eccentricities in this study. Figure 3.5-2 shows the detail of eccentric load arrangement. All the specimens were capped at both ends using high strength plaster to ensure even distribution of forces. Calibration was carried out to ensure the specimen was placed in the centre. The loading rate for the column tests were maintained at the rate of 70kN/min which ensures 0.16 mm/min displacement rate in the elastic range of the column to simulate static loading conditions.

As shown in Figure 3.5-2, three horizontal LVDTs were attached at 200 mm spacing to measure the lateral deflection of the columns. Also two vertical LVDTs were attached at the opposite corners of the bottom

plate to measure the axial deformation of the columns. In total 8 electrical strain gauges were attached horizontally on CFRP at mid height of each column to measure the hoop strains. Four of those strain gauges were attached at the corners of the columns while four were attached at each side of the column as shown in Figure 3.5-3.

Figure 3.5-1 Knife edge and loading head details

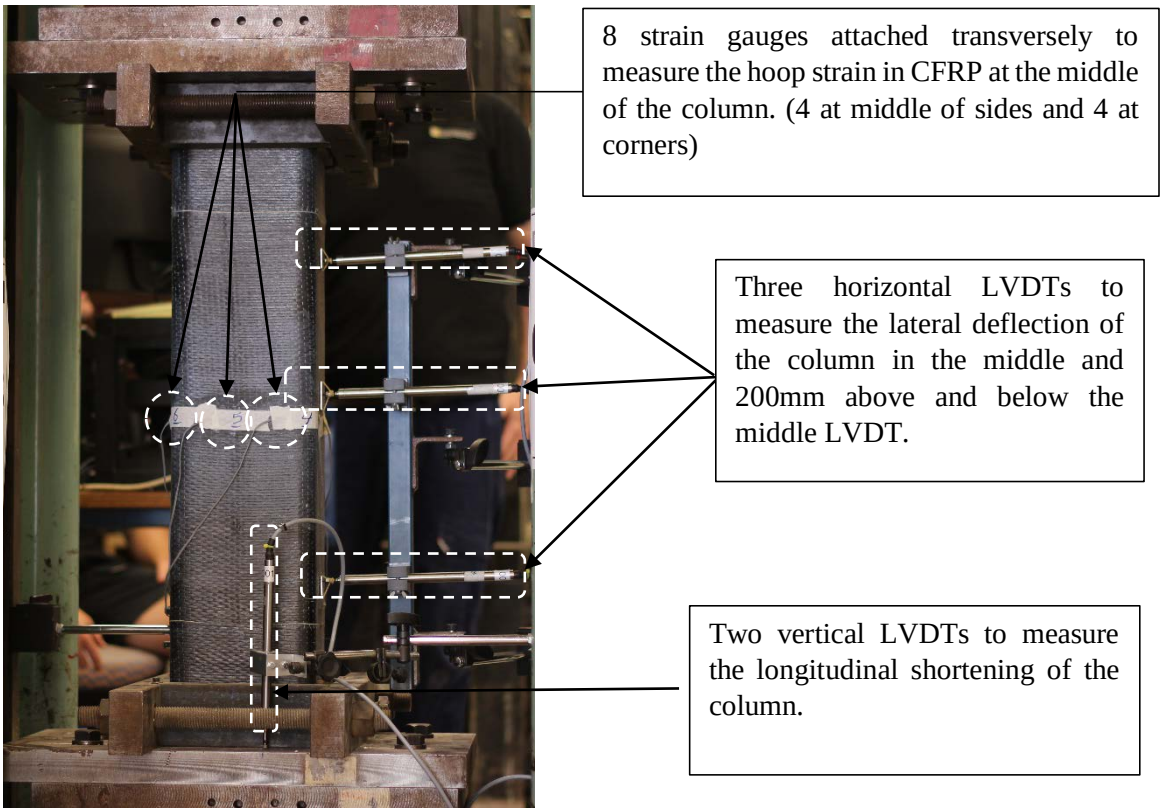

Figure 3.5-2 Loading apparatus and instrumentation

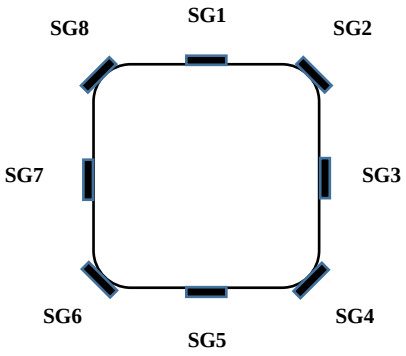

Figure 3.5-3 Strain gauge arrangement around the hoop at mid-height of the column

For the beam tests a three-point bending configuration was chosen. As shown in Figure 3.5-4 the struts are attached to a load cell apply a concentrated load at the middle of the span of the beams. The length of the span is 700 mm and the support to the left is roller and the support to the right is a pin support. The load is being exerted on a v shaped metal plate which is attached to the surface of the specimen using rapid setting

plaster. As shown in Figure 3.5-5 three LVDTs are placed every 200 mm along the length of the beam. In order to simulate the static loading conditions, the rate of 70 kN/min loading was maintained during the tests.

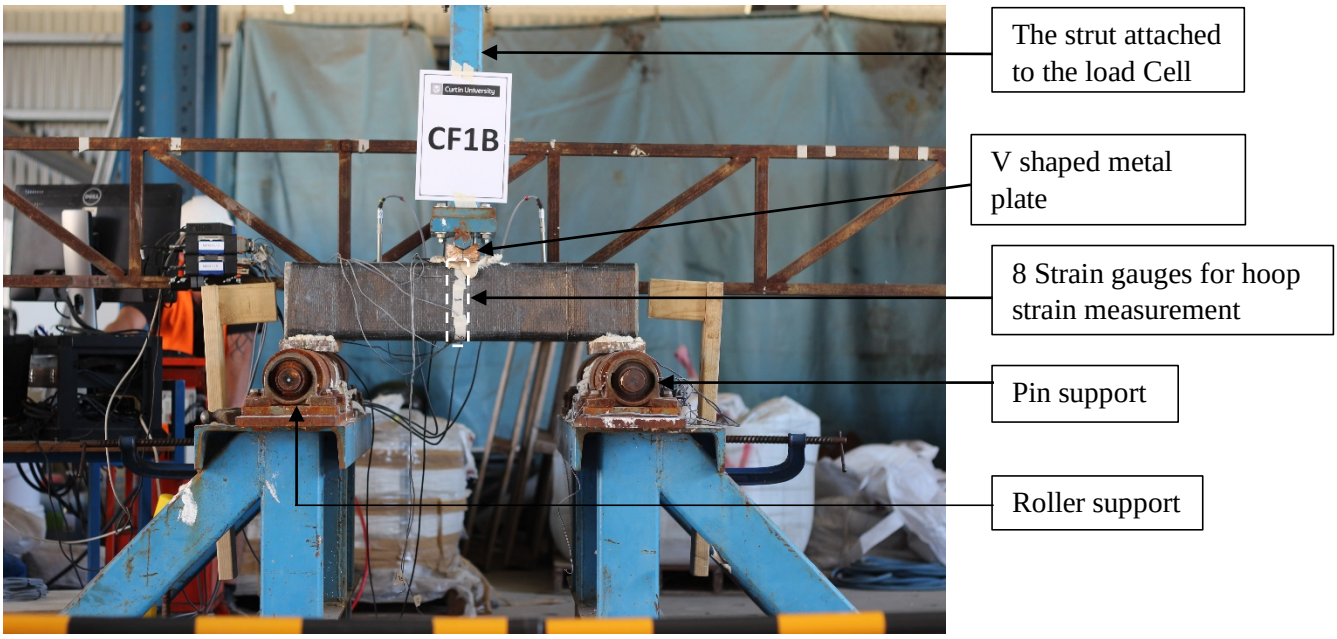

Figure 3.5-4 Beam test apparatus

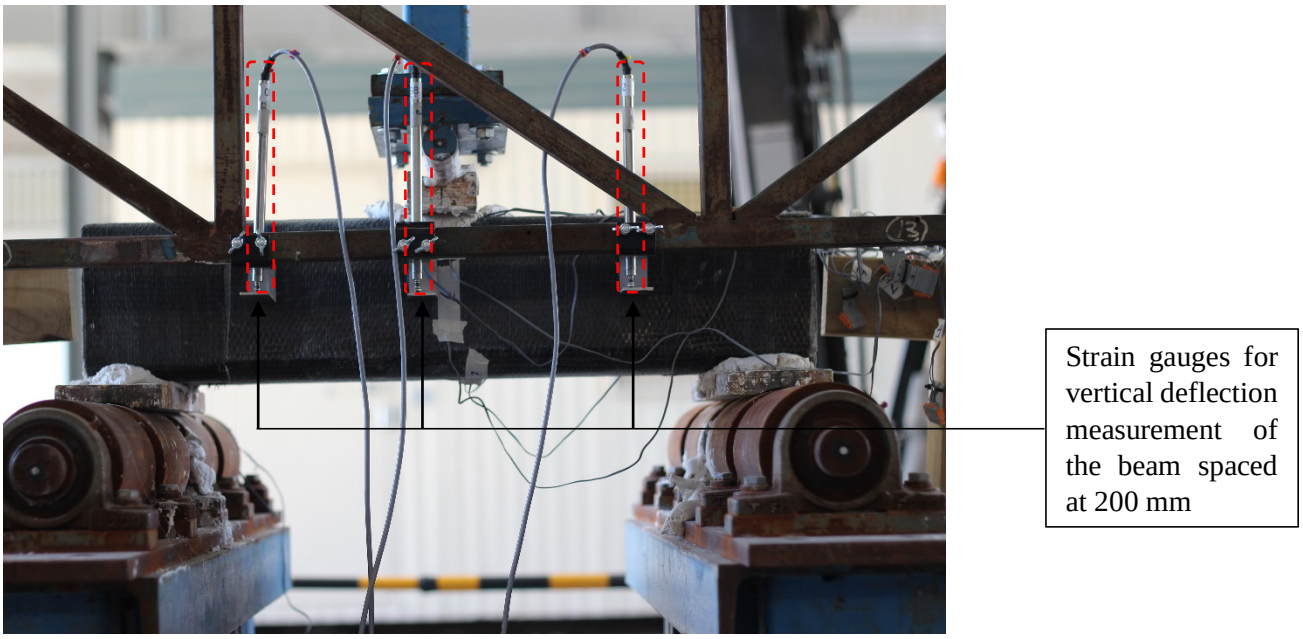

Figure 3.5-5 Beam test instrumentation

3.6 Summary

In this chapter testing program, material properties, specimen preparation, testing apparatus, and instrumentation are discussed. The results of tensile test on the rebars, standard cylindrical compressive test of concrete, as well as properties of CFRP jackets and epoxy agents are presented in this chapter. The test results are presented in the following chapter.

4 Test Results and discussion.

4.1 Introduction.

In this chapter the test results of CFRP confined RC square columns subjected eccentric compression loading are presented. The variables in these test are the various eccentricities as well as number of CFRP wrap layers attached to the specimens. Out of eighteen specimens, thirteen are wrapped and five specimens are unwrapped used as reference specimens. All of the specimens were tested until the point of failure is reached. The values of yield and ultimate load and their corresponding strains as well as the axial stress strain behaviour and mid-height strains of the columns are presented herein. Also for the three-point beam tests the failure characteristics of the specimens are discussed in this chapter.

4.2 Mechanical behaviour of columns with concentric compression loading

4.2.1 Failure characteristics and mechanism

For the concentric loading flat plates were used at both ends of the specimens instead of the knife edges and loading heads. In the case of control column (CR0) micro cracks and damages appeared after the approximate yield load of 696.5 kN and they started to propagate gradually during the process of loading. Once the column was reachedits ultimate peak load of 1550.4 kN the micro cracks started to join and formed macro localized cracks. The post-peak behaviour of the column was relatively brittle accompanied by concrete spalling at top and the middle of the column as well as longitudinal reinforcement buckling at the mid-height of the column as shown in Figures 4.2.1-1 through 4.2.1-3.

In the case of column wrapped by one layer of CFRP fabric (CF10) subjected to concentric compression loading the longitudinal deformations became apparent when the specimen reached its approximate yield load of 710.5 kN. As the column was reaching its peak load of 1784.5 kN the perimeter of the column hoop was expanded significantly as the column was shortening. After the peak load the CFRP wrap was completely engaged in terms of providing confinement pressure as well as resistance for further hoop expansion of the column. As the column was reaching its point of failure sounds of CFRP debonding and concrete cracking was heard and finally the specimen failed in a much more ductile manner compared to control specimen (CR0). As shown in Figures 4.2.1-4 to 4.2.1-7 the failure of CF10 column was accompanied by concrete crushing at the mid-height and the bottom, CFRP rupture at the same locations and reinforcement buckling at the mid-height of the specimen.

Figure 4.2.1-1 Overall view of CR0 failure

Figure 4.2.1-2 Localized macro crack and concrete spalling at the top

Figure 4.2.1-3 Rebar buckling and concrete spalling/crushing at mid-height

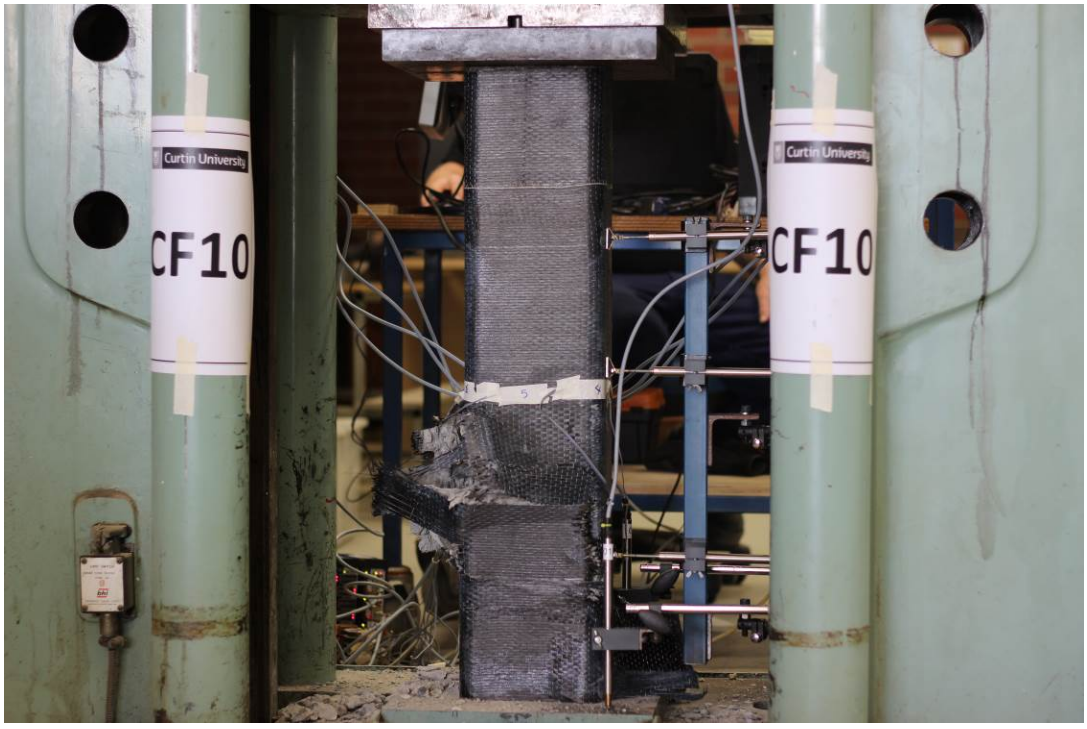

Figure 4.2.1-4 Overall view of CF10 failure

Figure 4.2.1-5 Crushed concrete and reinforcement buckling at mid-height

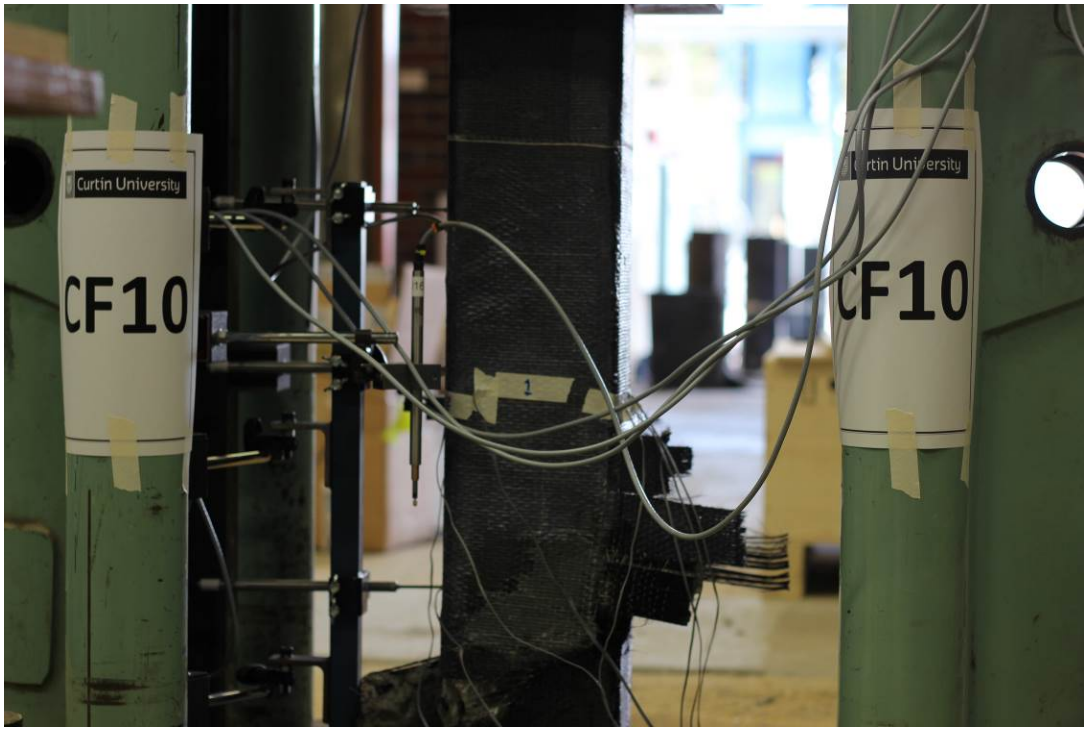

Figure 4.2.1-6 CFRP rupture at the mid-height and the bottom of CF10

Figure 4.2.1-7 Concrete crushing and CFRP rupture at the bottom of specimen

4.2.2 Axial load versus axial and lateral deflection behaviour

The axial load-axial displacement behaviour of control column and column confined with one layer of CFRP is shown in Figure 4.2.2-1. It can be seen that the case of CF10 column, the pre-peak branch of the load-displacement curve exhibits higher slope to that of the control column CR0 meaning the CFRP confinement has increased the stiffness of the confined column. It has been found that the stiffness of control column is increase from 518.7 kN/mm to 584 kN/mm (about 12% increase) due to confinement by one layer of CFRP. This improvement trend is also observed by others e.g. Parvin and Wang (2001) reported an increase of 53.8% and Widiarsa and Hadi (2013) reported an improvement of 1% all for the maximum ultimate axial load of specimens wrapped with one layer of CFRP. One major reason for the variation of this improvement can be attributed to the ratio of strength of CFRP to the compressive strength of the concrete; higher ratios result into more significant improvements in ultimate strength. This ratio in the current study was 89.6 whereas for Parvin and Wang (2001) and Widiarsa and Hadi (2013) the ratios were 177.6 and 10.7 correspondingly. It can also be seen in table 4.2.2-1 that the ultimate load capacity is also increased by about 15% due to confinement by one layer of CFRP. This increase is attributed to the confinement pressure provided by the CFRP jacket which prevents micro crack formations at early stages and also delays the buckling of longitudinal rebars and as a result spalling and crushing of concrete . While the columns confined with two and three layer of CFRP were not possible to test due to limitation of the testing machine's capacity, the tangent post-yield stiffness and ultimate load of these columns are expected to increase due to higher confining effect with increase in CFRP layers, which has been reported by others e.g. in Parvin and Wang (2001) reported 100% increase in maximum ultimate load and 170% increase in post-yield tangent stiffness for specimens with two layers CFRP wrap. Also Widiarsa and Hadi (2013) reported a 10% increase in the maximum ultimate load whereas post-peak tangent stiffness was improved by 50% for specimens with three layers of CFRP wrap. With regard to the post peak behavior it can be seen

that the CF10 column exhibit relatively longer post-peak branch than the control column. The post-peak load at 85% of the ultimate load ($P_{85\%\,u}$) has also increased by 15% from 1317.8 kN to 1516.8 kN as shown in Figure 4.2.2-1.

Ductility is defined in this study as the ratio of the area under the axial load-displacement curve from the beginning until the post-peak load corresponding to 85% of the ultimate peak load to the area under the load-displacement curve from beginning to the yield load (Hadi and Widiarsa (2012)). It can be seen in Table 4.2.2-1 that the ductility of CF10 is significantly increased by 53% compared to CR0.

As seen in Figure 4.2.2-2 there is a 43% increase in the ultimate mean hoop strain of CF10 compared to the unwrapped CR0 specimen. The increase in the mean hoop strain is an indicator of efficiency of the FRP wrap to provide confinement after the yield point has reached. This confinement pressure prevents brittle crushing of the concrete and restrains the longitudinal rebars against buckling until the point of CFRP rupture. The strain gauges that were placed at the corners of the specimen recorded higher levels of strain compared to those placed at the sides of the column. Also at the point of failure the strain gauges near the buckling zones of the longitudinal rebars recorded a sudden jump in hoop strains until the rupture of the CFRP as well as the strain gauges.

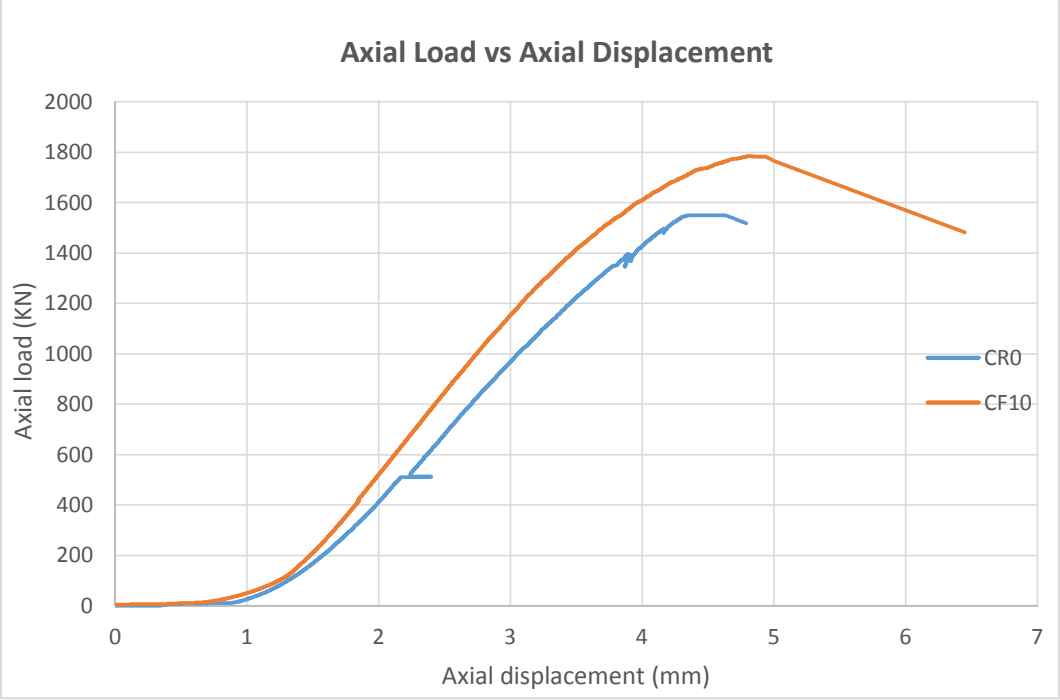

Figure 4.2.2-1 Axial load versus axial displacement behaviour of control column and column containing one layer of CFRP wrap under concentric loading

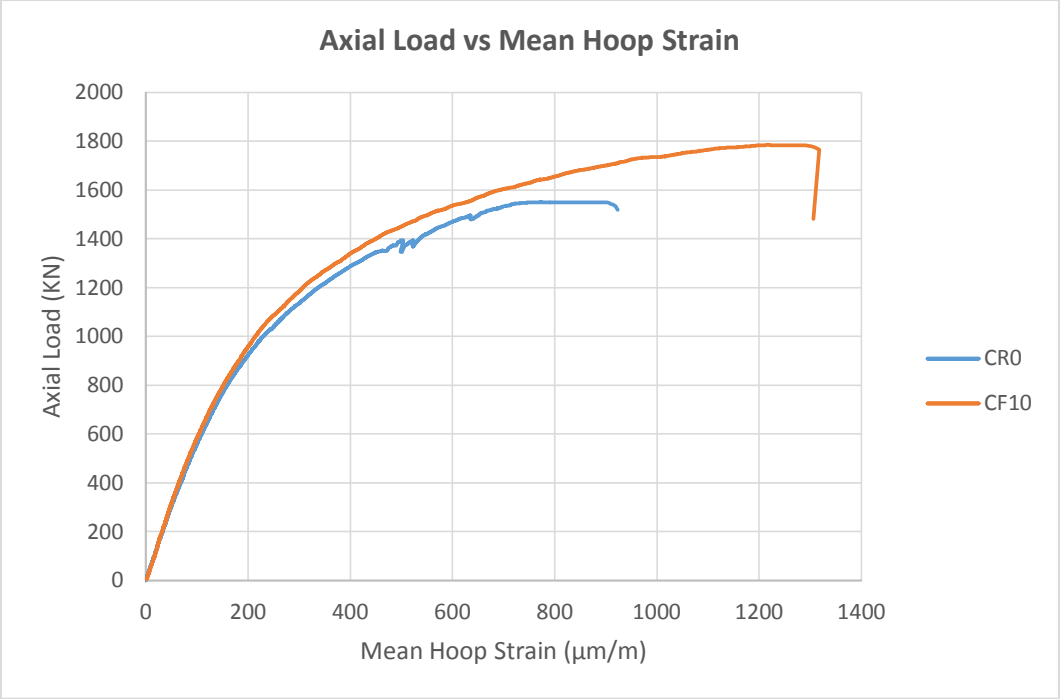

Figure 4.2.2-2 Axial load versus mean hoop train of control column and column containing one layer of CFRP wrap under concentric loading

Column code	CR0	CF10
P_y (kN)	696.47	710.50
P_u (kN)	1550.41	1784.50
$P_{85\%\,u}$ (kN)	1317.85	1516.83
Ductility	1.27	1.93

Table 4.2.2-1 Summary of strength and ductility properties of columns under concentric loading

4.3 Mechanical behaviour of columns subjected to 25 mm eccentric loading

4.3.1 Failure characteristics and mechanism

In the testing of columns under eccentric loading the knife edges were used with various eccentricities in order to simulate the combined state of flexural and axial loading. In the case of CR1 column micro cracks started appearing shortly after reaching the yield load of 728.9 kN. After reaching the ultimate load of 1045.9 kN the micro cracks joined each other to form macro localized cracks in both the compressive as well as in tensile zones of the column and relatively brittle failure of the column was accompanied by spalling and rebar buckling in compressive zone as demonstrated in Figures 4.3.1-1 and 4.3.1-3 as well as development of flexural cracks in the tension zone of the column as shown in Figure 4.3.1-2.

In all of the specimens with CFRP wraps the axial and lateral deformations of the columns became apparent after reaching the yield load. The wrapped columns failed by rupture of CFRP wraps near the zone at the mid-height on the compression side of the columns also they went through noticeable plastic deformation as shown in Figures 4.3.1-4, 4.3.1-8, and 4.3.1-11. In all of the wrapped columns when the specimen was close to its ultimate load the sounds of CFRP rupture was heard. In the case of CF11 column after the peak load the column sustained plastic lateral deformations and the relatively ductile failure of the column was accompanied by concrete crushing, rebar buckling and CFRP rupture in the compressive zone of the column as shown in Figures 4.3.1-5 - 4.3.1-6 as well as CFRP rupture and tearing in the tension zone of the column as demonstrated in Figure 4.3.1-7.

In the case of CF21 column the postpeak behaviour was more ductile compared to CR1 and CF11 columns in a sense that the specimen sustained higher level of loads while undergoing plastic deformations and the failure was accompanied by concrete crushing and CFRP rupture and tearing as shown in Figures 4.3.1-9 - 4.3.1-10. Column CF31 however had the most ductile failure behaviour among the columns of this group meaning it endured higher level of loads whilst undergoing larger plastic deformations. The failure pattern was similar to that of CF11 and CF21 columns and is shown in Figures 4.3.1-12- 4.3.1-13.

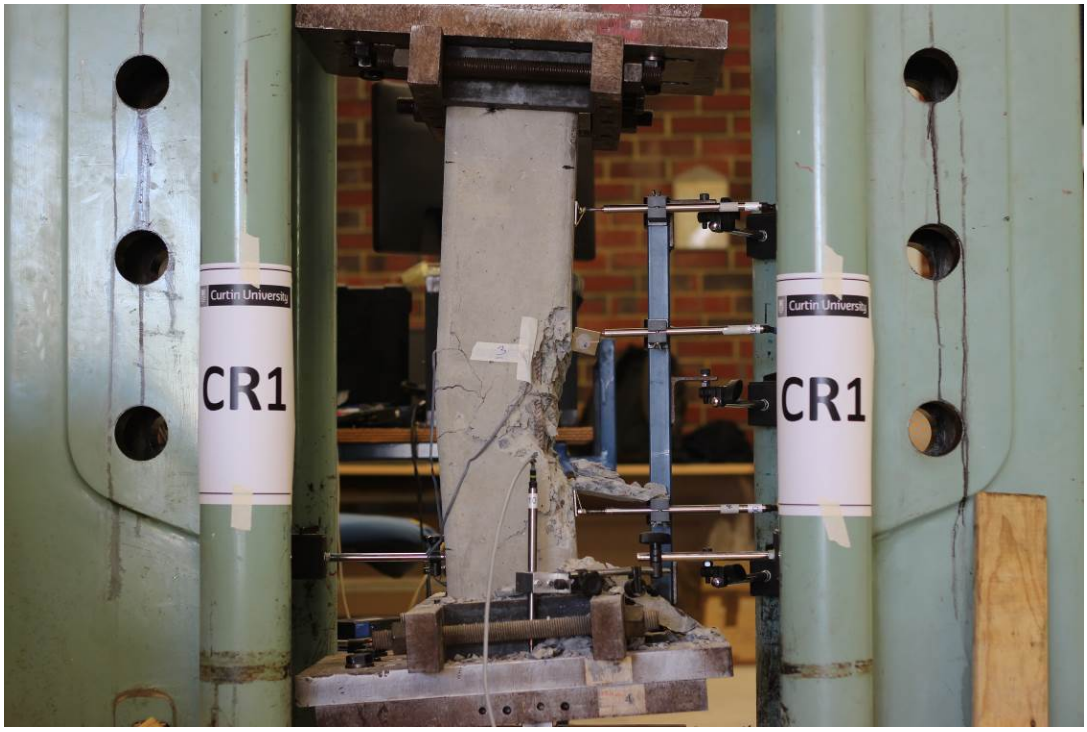

Figure 4.3.1-1 Overal view of CR1

Figure 4.3.1-2 Concrete cracking in the tension zone of CR1

Figure 4.3.1-3 Concrete spalling and rebar buckling in compressive zone of CR1

Figure 4.3.1-4 Overal view of CF11

Figure 4.3.1-5 Concrete crushing in the compressive zone of CF11

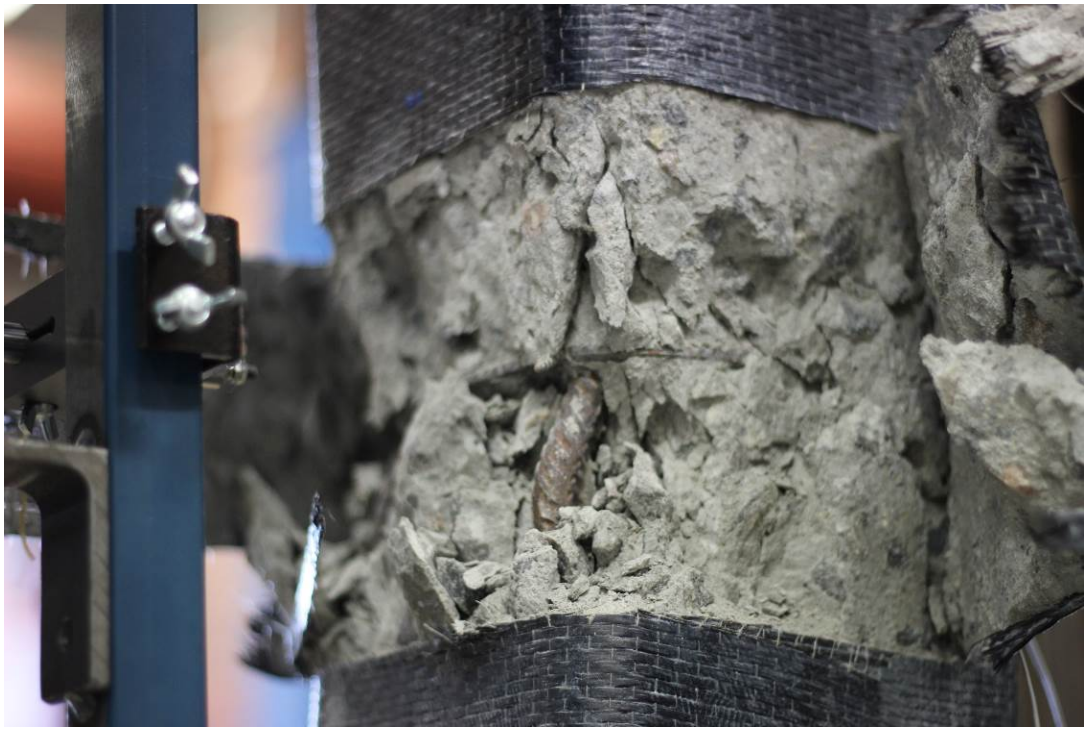

Figure 4.3.1-6 Rebar buckling in the compressive zone of CF11

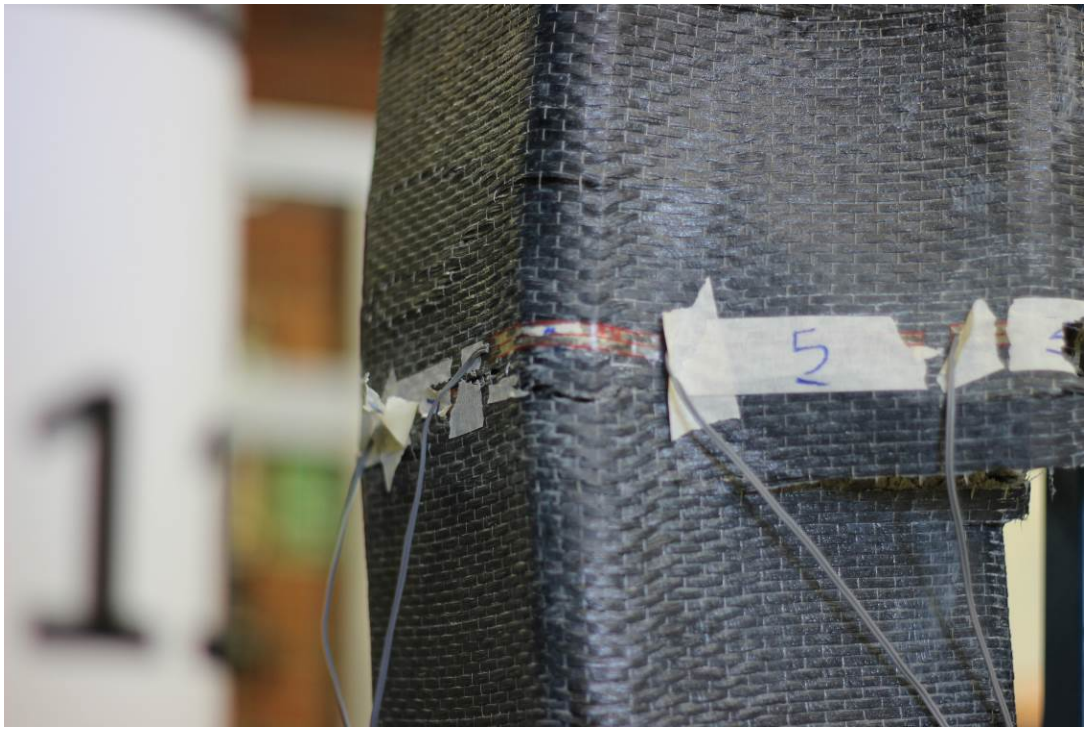

Figure 4.3.1-7 CFRP rupture as well as tears in the tension zone of CF11

Figure 4.3.1-8 Overal view of CF21

Figure 4.3.1-9 Concrete crushing and CFRP rupture in CF21

Figure 4.3.1-10 Torn CFRP wraps in the tension zone of CF21

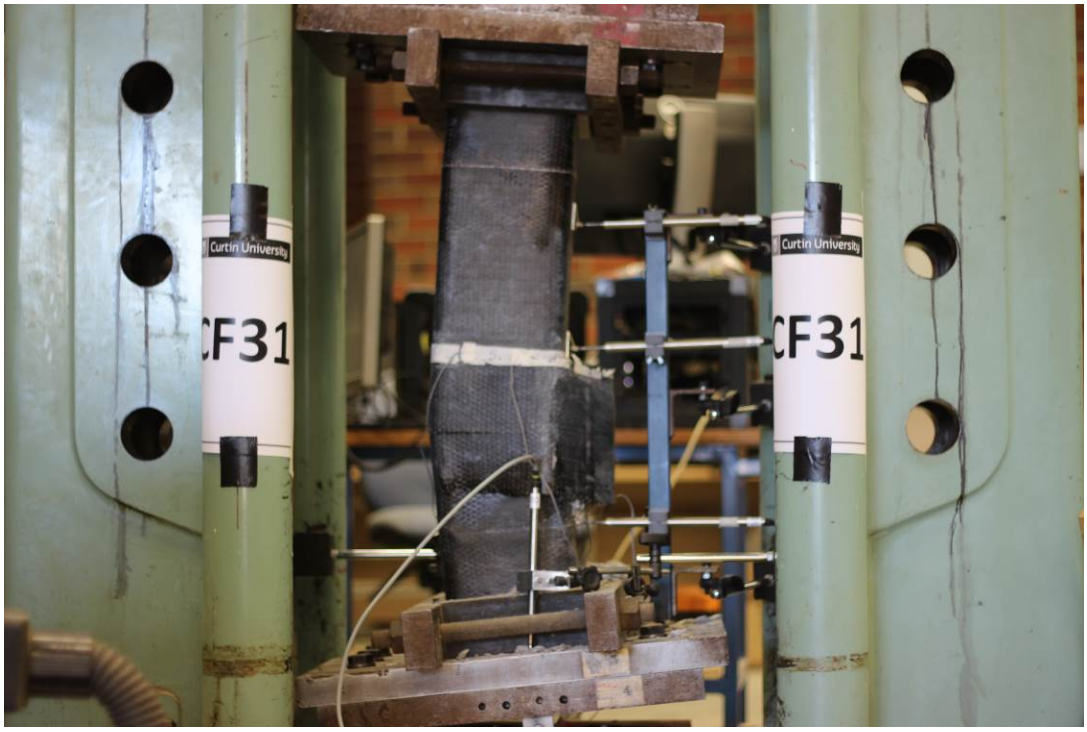

Figure 4.3.1-11 Overal view of CF31

Figure 4.3.1-12 Concrete crushing and rebar buckling in compressive zone of CF31

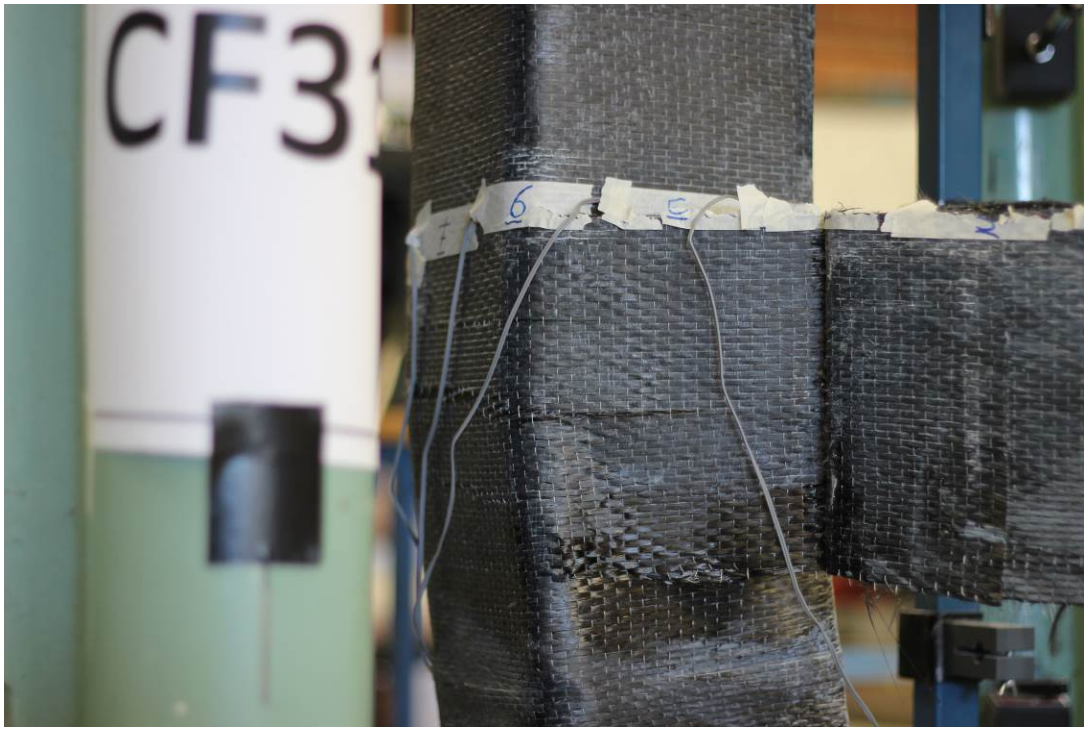

Figure 4.3.1-13 Rupture as well as tearing of CFRP in specimen CF31

4.3.2 Axial load versus axial and lateral deflection behaviour

The axial load vs axial deflection curve in Figure 4.3.2-1 indicates that the CFRP confined columns exhibit imporovements in peak load. The post-peak branch of the curve shows a smoother slope and higher failure load compared to that of the unwrapped specimen. For specimens CF31, CF21, and CF11 improvements in the peak load (P_u) compared to that of CR1 were 17.5% , 26.3%, and 23.6% (from 1045.9 kN to 1229 kN, 1320.1 kN, and 1292.3 kN), respectively. Accordingly there is also increase of 17.5%, 26.2%, and 23.6 , for $P_{85\%\,u}$ (from 889 kN to 1044.9 kN, 1122 kN, and 1098.4 kN). No clear trend for the lateral deflection at the peak load (δ_u) is observed but they are generally lower than the corresponding deflections in the unwrapped columns (-48%, -98%, and -59% for columns CF11, CF21, and CF31 accordingly). The lower deflections at peak load can be attributed to the fact that wrapped columns yield at a higher load and thus are generally stiffer at the peak load. Although there is a slight decrease in P_u and $P_{85\%\,u}$ of CF31 compared to CF21, an increase in the value of failure lateral plastic deformation ($\delta_{85\%\,u}$) and ductility is observed for CF31 relative to CF21. In comparison to CR1, the deflection at 85% of peak load $\delta_{85\%\,u}$ has changed by -30%, -14%, +60% for specimens CF11, CF21, and CF31 (as demonstrated in Figure 4.3.2-3 and Table 4.3.2-1), respectively which is a proof of effectiveness of CFRP wrapping with multiple layers in improvement of column ductility/deformability. The ductility of wrapped columns however show an steady increasing pattern compared to CR1 75%, 86%, and 160% increase for specimens CF11, CF21, and CF31, respectively.

Despite an overall improvement in the value of mean hoop strain of wrapped columns compared to CR1 (refer to Figure 4.3.2-2) with 327%, 483%, 189%, increase for specimens CF11 to CF31 accordingly, no clear patterns are observed. The variability of ultimate mean hoop strains in the confined columns seems to be dependent on the failure zone of the columns. For instance in the case of column CF31 the failure zone

is located further below the location of strain gauges thus the recorded strains have lower values whereas for columns CF11 and CF21 the failure zone is almost at the mid-height of the columns. The precise location of failure zone can be relatively random and is highly dependent on where the buckling of rebars and as a result high localized hoop strains take place.

The moments at the peak load (M_u) as well as moments at postpeak load ($M_{85\%\,u}$) are calculated based on Equation 4.3.2.1 in which "e" is the eccentricity of compressive load (25mm in this series of tests) and δ is the mid-height deflection of the column at peak or post-peak load.

$$M = P \times (e + \delta) \qquad (4.3.2.1)$$

The moment at the peak load (M_u) has improved to the same extent for columns CF11 to CF31 (9%, 8.3%, 12.9%) whereas an increasing trend is observed for post-peak moment ($M_{85\%\,u}$) for the corresponding columns (11.3%, 23.2%, 36%)

In the study by Widiarsa and Hadi (2013), for columns under eccentric loading with 25mm eccentricity researchers reported 6%, and 16% improvement in ultimate peak axial load, 20% and 13% improvement in lateral deflection at ultimate load (δ_u), and 43%, 298% improvement in ductility for columns with one and three layers of CFRP wrap accordingly. Also in the other study by Parving and Wang (2001) for columns under eccentric loading with eccentricity of 15.6mm and approximately the same eccentricity to cross section height ratio (e/h = 0.14) a similar trend is observed. They reported 47.8% and 80.9% improvement in ultimate peak axial load for columns with one and three CFRP wraps accordingly. Although the percentage of improvements vary depending on the jacket to concrete strength ratio, the results in the literature confirm the trend in the tests of the present study.

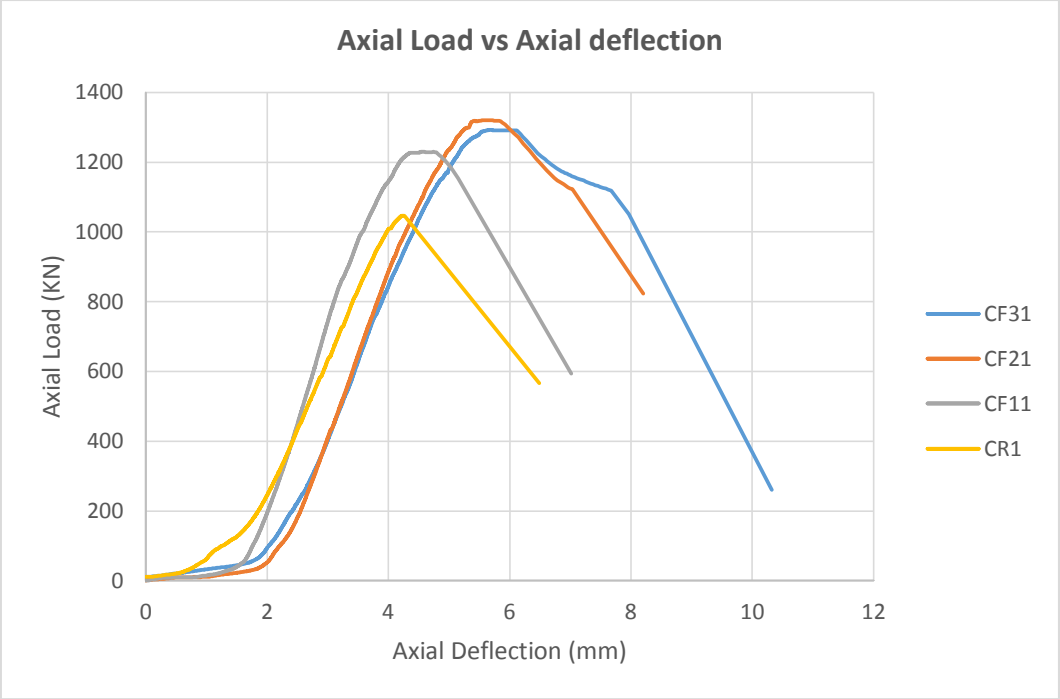

Figure 4.3.2-1 Axial load versus axial displacement behaviour of control column and column containing one, two and three layers of CFRP wrap under ecentric loading of 25mm ecentricity

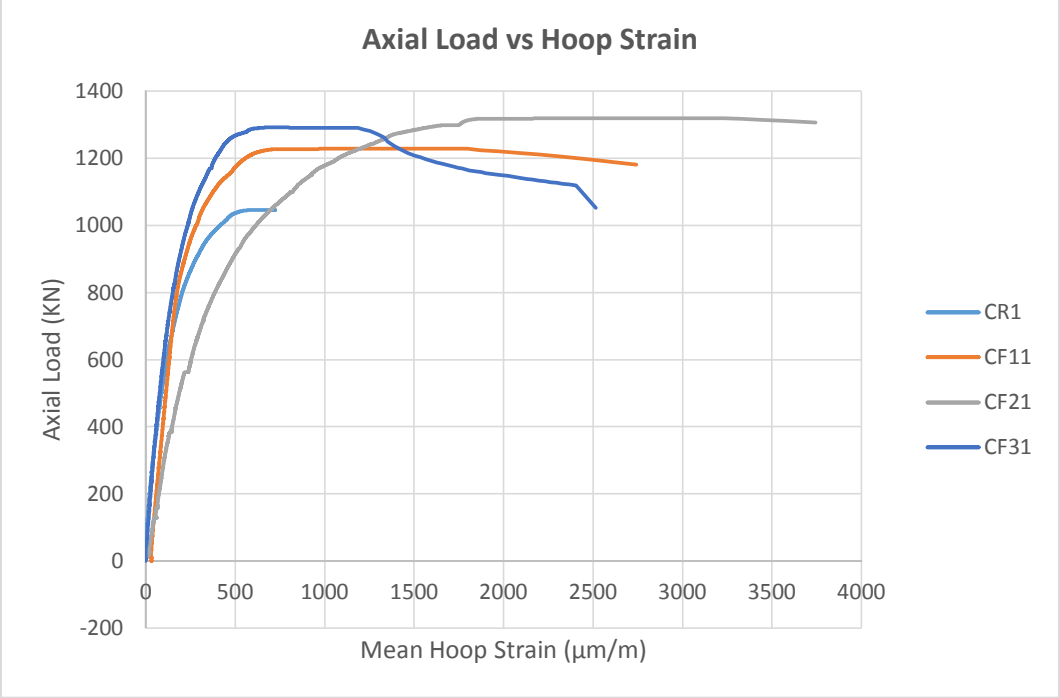

Figure 4.3.2-2 Axial load versus hoop strain of control column and column containing one, two and three layers of CFRP wrap under ecentric loading of 25mm ecentricity

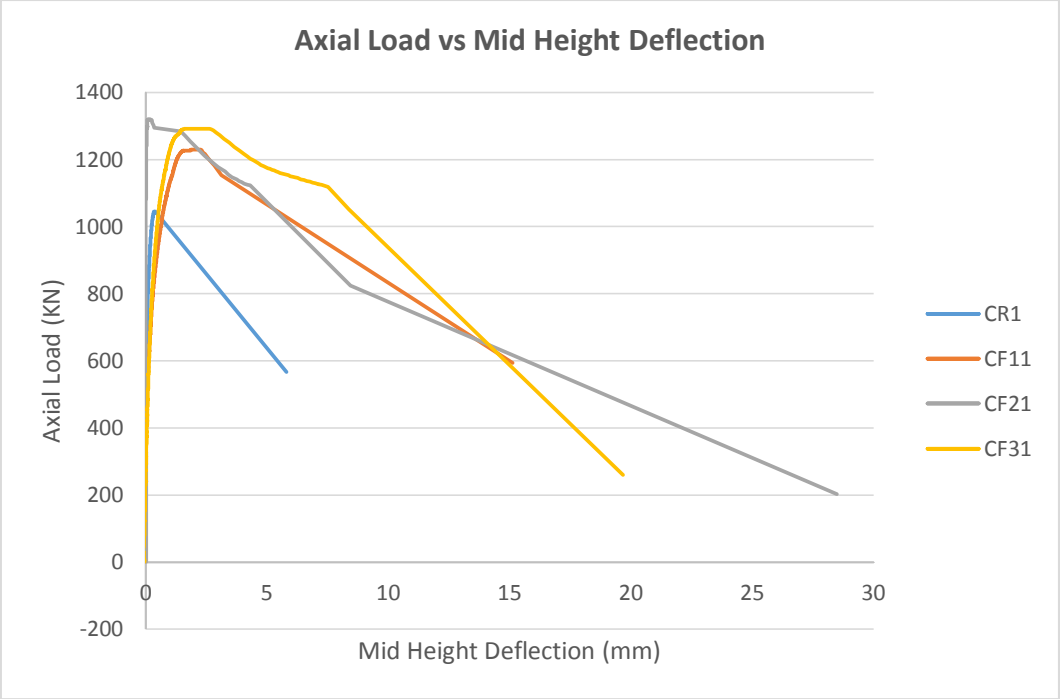

Figure 4.3.2-3 Axial load versus mid-height deflection behaviour of control column and column containing one, two and three layers of CFRP wrap under ecentric loading of 25mm ecentricity

Column code	CR1	CF11	CF21	CF31
P_y (kN)	728.89	866.98	975.33	840.00
P_u (kN)	1045.93	1229.32	1320.07	1292.27
$P_{85\%\,u}$ (kN)	889.04	1044.93	1122.06	1098.43
δ_u (mm)	4.25	2.20	0.10	1.73
$\delta_{85\%\,u}$ (mm)	4.99	3.41	4.28	8.00
M_u (kN.m)	30.59	33.43	33.13	34.55
$M_{85\%\,u}$ (kN.m)	26.66	29.69	32.86	36.25
Ductility	2.24	3.93	4.18	5.82

Table 4.3.2-1 Summary of strength and ductility properties of columns under 25mm eccentric loading

4.4 Mechanical behaviour of columns subjected to 35 mm eccentric loading

4.4.1 Failure characteristics and mechanism

In the case of CR2 column cracks became apparent after reaching the yield load of 680 kN and after the ultimate peak load of 839.8 kN there is a sudden drop in the bearing load of the column and finally the failure of CR2 is accompanied by concrete spalling in the compressive zone and flexural cracking and rupture of the longitudinal rebars in the tension zone of the column as shown in Figures 4.4.1-1 through 4.4.1-3.

In the case of CF12 column longitudinal and lateral deflections became apparent after reaching the yield load of 744.8 kN and at this stage the snapping sound of CFRP laminate micro cracking was heard. After reaching the ultimate load of 1098.8 kN the column sustained plastic deformations and the failure was accompanied by rupture of the CFRP and concrete crushing and rebar buckling in the compressive zone of the column while in the tension zone rebar rupture and CFRP tearing were observed as shown in Figures 4.4.1-4 through 4.4.1-7.

The case CF22 and CF32 columns sustianed higher post-peak loads (compared to CF12) while undergoing plastic deformations.The failure patterns were similar to that of CF12 except the longitudinal steel rupture in the tension zone of the specimens was not observed as shown in Figures 4.4.1-8 through 4.4.1-14.

Figure 4.4.1-1 Overal view of CR2

Figure 4.4.1-2 Concrete cracking as well as rebar rupture in tension zone of CR2

Figure 4.4.1-3 Concrete crushing and spalling in compressive zone of CR2

Figure 4.4.1-4 Overal view of CF12

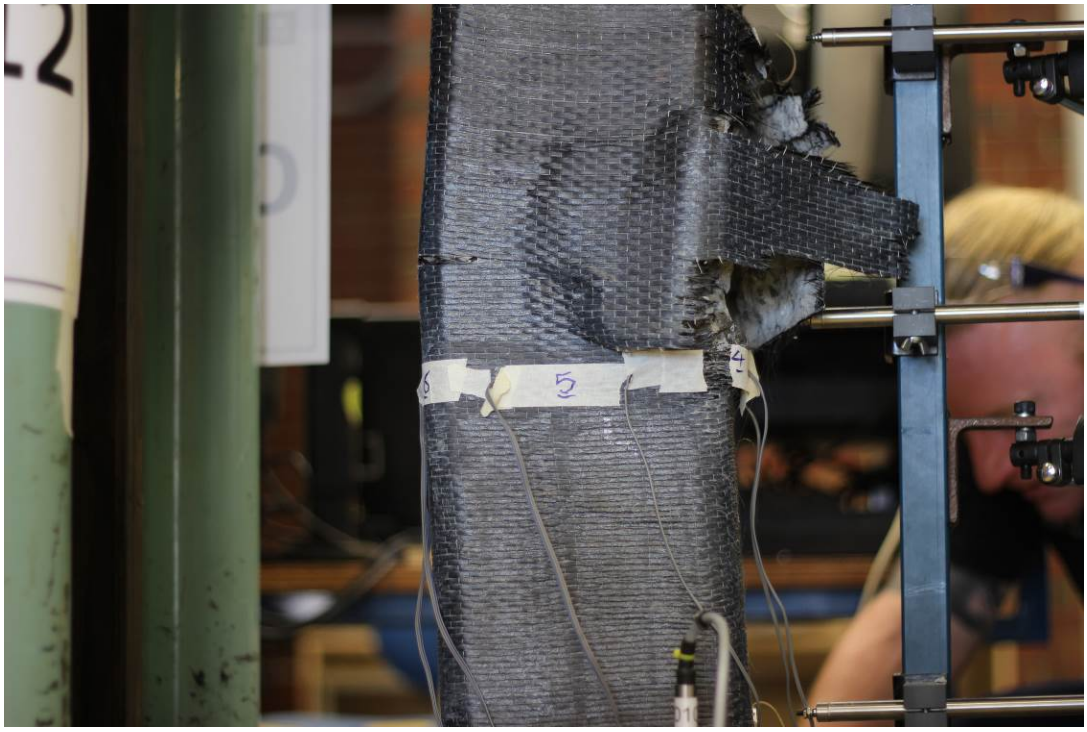

Figure 4.4.1-5 CFRP rupture in specimen CF12

Figure 4.4.1-6 Concrete crushing and rebar buckling in compressive zone of CF12

Figure 4.4.1-7 Torn CFRP in tension zone of CF12

Figure 4.4.1-8 Overal view of CF22

Figure 4.4.1-9 CFRP rupture and tearing in CF22

Figure 4.4.1-10 Concrete crushing and CFRP rupture in CF22

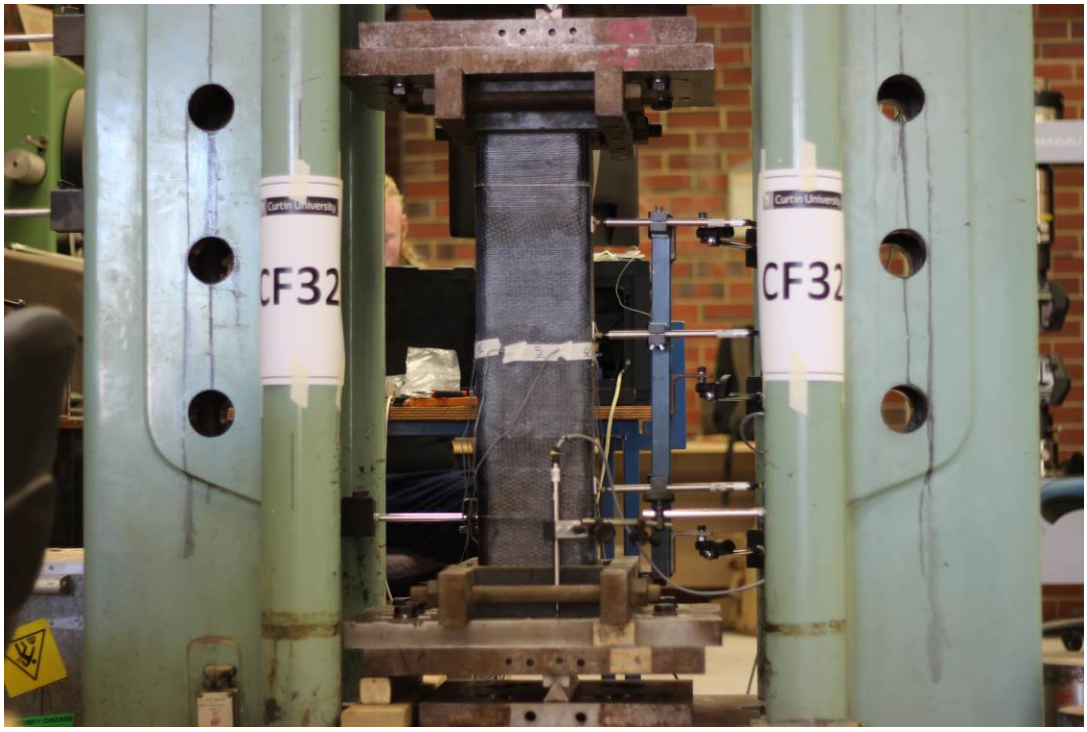

Figure 4.4.1-11 Overal view of CF32

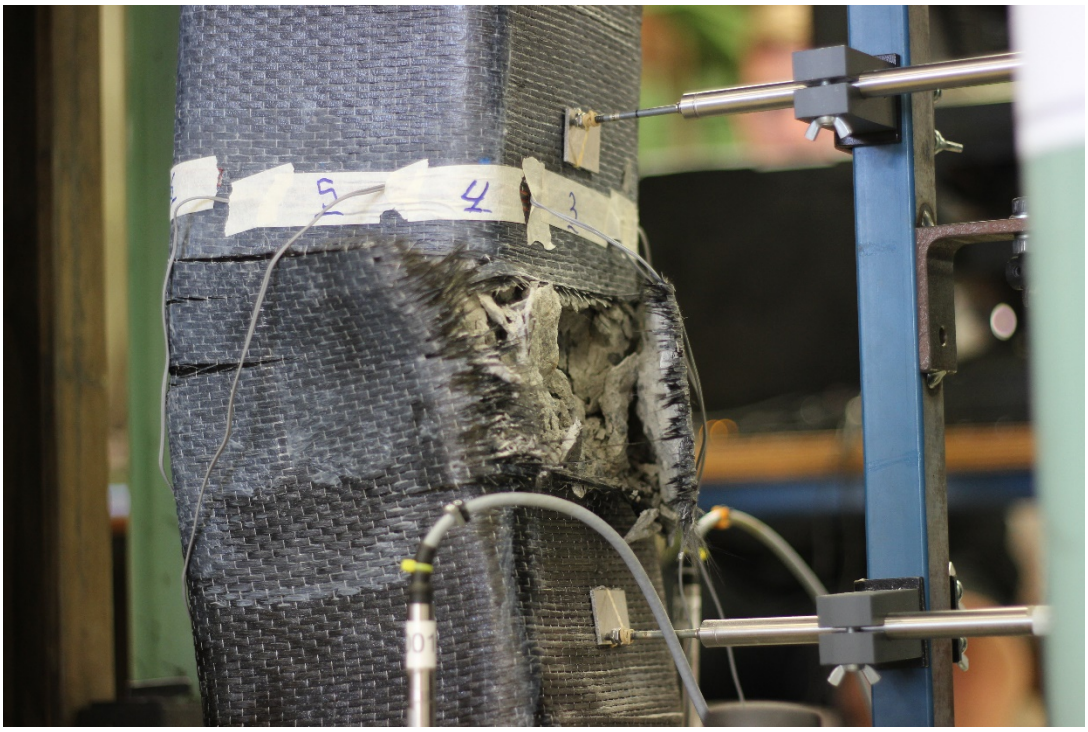

Figure 4.4.1-12 Concrete crushing and CFRP rupture in CF32

Figure 4.4.1-13 Concrete crushing and rebar buckling in compressive zone of CF32

Figure 4.4.1-14 CFRP tearing in specimen CF32

4.4.2 Axial load versus axial and lateral deflection behaviour

As shown in Figure 4.4.2-1 wrapping improved the peak ultimate load of the columns but there was a slight drop in the peak load of CF22 and CF32 compared to that of CF12. Compared to specimen CR2, there was 31%, 21%, and 19% improvement in P_u for columns CF12, CF22, and CF32 (from 840 kN to 1099kN, 1020 kN, and 1000 kN) respectively. Despite this drop in the ultimate peak load the specimens CF22 and CF32 demonstrated higher axial deformations and mean hoop strains while sustaining higher levels of axial load as seen in Figures 4.4.2-1 and 4.4.2-2.

No clear patterns were observed for the lateral deflection at the peak load (δ_u) with -10%, 61%, and -42% difference with respect to unwrapped column (CR2). The improvement in $\delta_{85\%\,u}$ compared to that of CR2 were 40%, 181%, and 120% for columns CF12, CF22, and CF32, respectively. The lower ultimate deflection value of column CF32 compared to CF22 can be attributed to the mode of failure for which CF32 failure is a compression controlled failure accompanied initially by concrete crushing (Figure 4.4.1-12) whereas CF22 failure is a tension controlled failure accompanied initially by yielding of the tensile rebars and tearing of the tensile zone CFRP (Figure 4.4.1-9). A steady increasing pattern was observed for the ductility of the columns compared to CR2. Ductility is improved by 108%, 165%, and 193% for columns CF12, CF22 and CF32, respectively which demonstrates the improvement in energy absorption capability of the CFRP confined columns with increase of number of CFRP layers.

As shown in Figure 4.4.2-3 the mean hoop strains of the specimens at failure load improved as the number of wraps increased. The improvements were 320%, 320%, and 420% for specimens CF12, CF22 and CF32, respectively.

As seen in Table 4.4.2-1, the peak load moment (M_u) has improved by 30%, 28%, and 15% and the post-peak moment ($M_{85\%\ u}$) is improved by 36%, 42%, 33% for columns CF12, CF22, and CF32 accordingly. Although it is evident that wrapping generally improves the flexural capacity of the columns no clear trend is observed for flexural capacity vs number of CFRP layers in these series of tests (35mm eccentricity). The drop post-peak flexural capacity of column CF32 can be attributed to the fact that the failure zone and thus the location at which the maximum lateral deflection occurs is below the mid-height of the column (Figure 4.4.1-12). Therefore the real value of the flexural capacity of the column is actually higher than the recorded value.

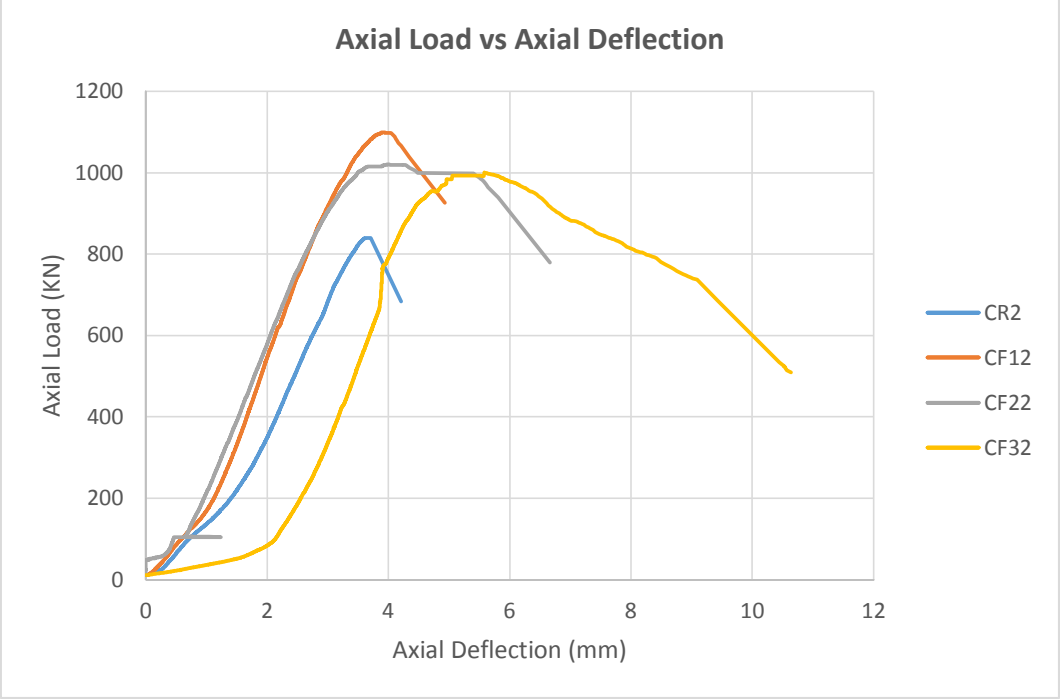

Figure 4.4.2-1 Axial load versus axial displacement behaviour of control column and column containing one, two and three layers of CFRP wrap under ecentric loading of 35mm ecentricity

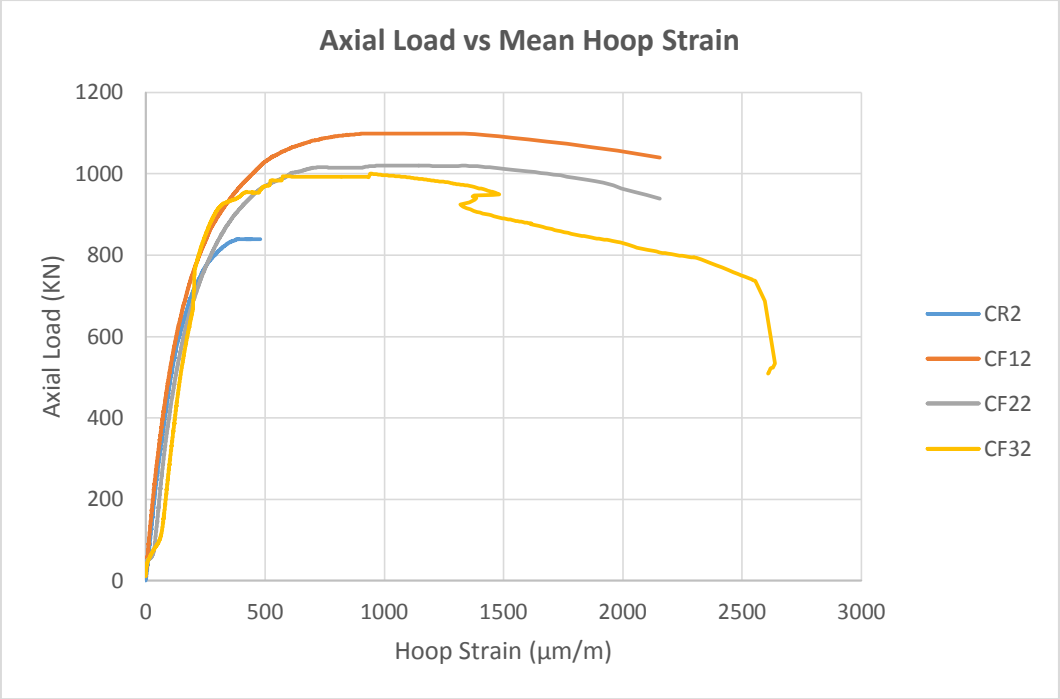

Figure 4.4.2-2 **Axial load versus hoop strain of control column and column containing one, two and three layers of CFRP wrap under ecentric loading of 35mm ecentricity**

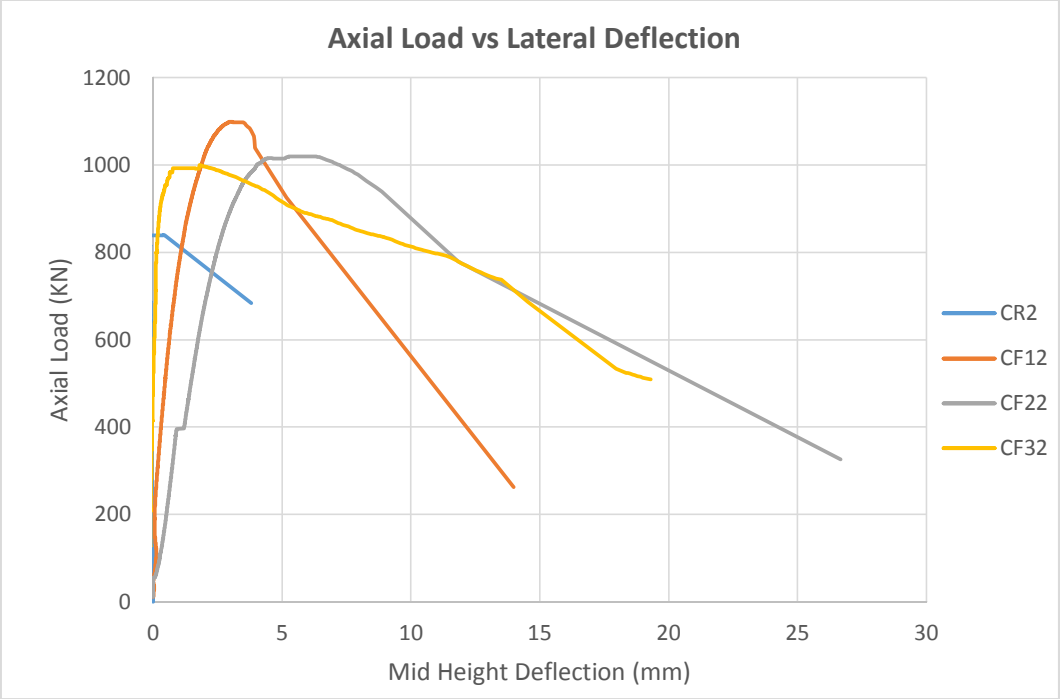

Figure 4.4.2-3 Axial load versus mid-height deflection behaviour of control column and column containing one, two and three layers of CFRP wrap under ecentric loading of 35mm ecentricity

Column code	CR2	CF12	CF22	CF32
P_y (kN)	680.00	744.81	774.50	794.86
P_u (kN)	839.86	1098.79	1020.02	1000.53
$P_{85\%\,u}$ (kN)	713.88	933.98	867.02	850.45
δ_u (mm)	3.33	3.01	5.36	1.94
$\delta_{85\%\,u}$ (mm)	3.69	5.17	10.36	8.10
M_u (kN.m)	32.19	41.77	41.17	36.96
$M_{85\%\,u}$ (kN.m)	27.62	37.52	39.32	36.65
Ductility	1.69	3.51	4.48	4.94

Table 4.4.2-1 Summary of strength and ductility properties of columns under 35mm eccentric loading

4.5 Mechanical behaviour of columns subjected to 50 mm eccentric loading

4.5.1 Failure characteristics and mechanism

In the case of column CR3 after the ultimate peak load of 654.5 kN there was a considerable drop in the load and a brittle mode of failure accompanied by crushing of concrete in the compressive zone of the column at mid height (Figures 4.5.2-1 and 4.5.1-2) and flexural cracking of the concrete in the tension zone (Figure 4.5.1-3).

All the wrapped columns demonstrated improved performance in terms of higher ultimate peak load as well as sustaining higher levels of post-peak load while undergoing plastic deformations. In CF13 column, the failure of the column was accompanied by concrete spalling and CFRP rupture and longitudinal rebar rupture in the tension zone at the bottom of the specimen as shown in the overal view (Figure 4.5.1-4) as well as detailed pictures (Figures 4.5.1-5 and 4.5.1-6).

In the case of both CF23 and CF33, the columns continued to sustain high levels of loads after reaching the peak loads of 844.6 kN and 840.9 kN, respectively. The failure of these columns was accompanied by concrete crushing and rebar buckling as well as CFRP rupture and tearing as shown in Figure 4.5.1-7 to 4.5.1-12

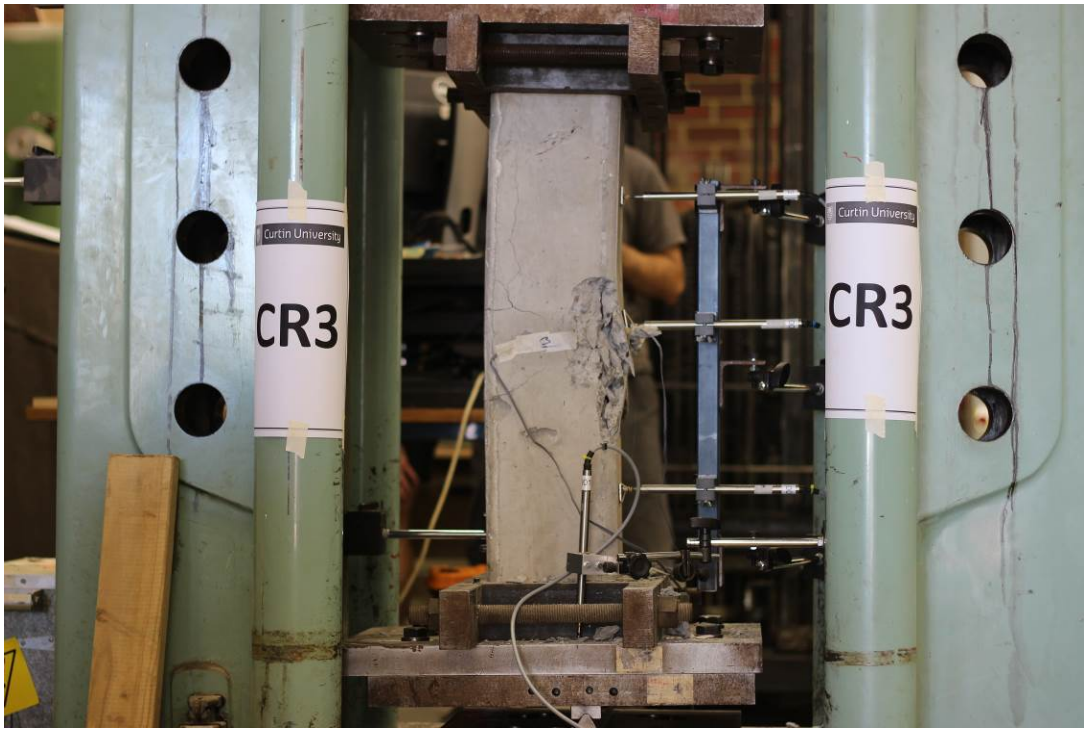

Figure 4.5.1-1 Overal view of CR3

Figure 4.5.1-2 Concrete crushing in compressive zone of CR3

Figure 4.5.1-3 Horizontal tensile cracks in the tension zone of CR3

Figure 4.5.1-4 Overal view of CF13 failure

Figure 4.5.1-5 Concrete spalling and rebar rupture in the tension zone of CF13

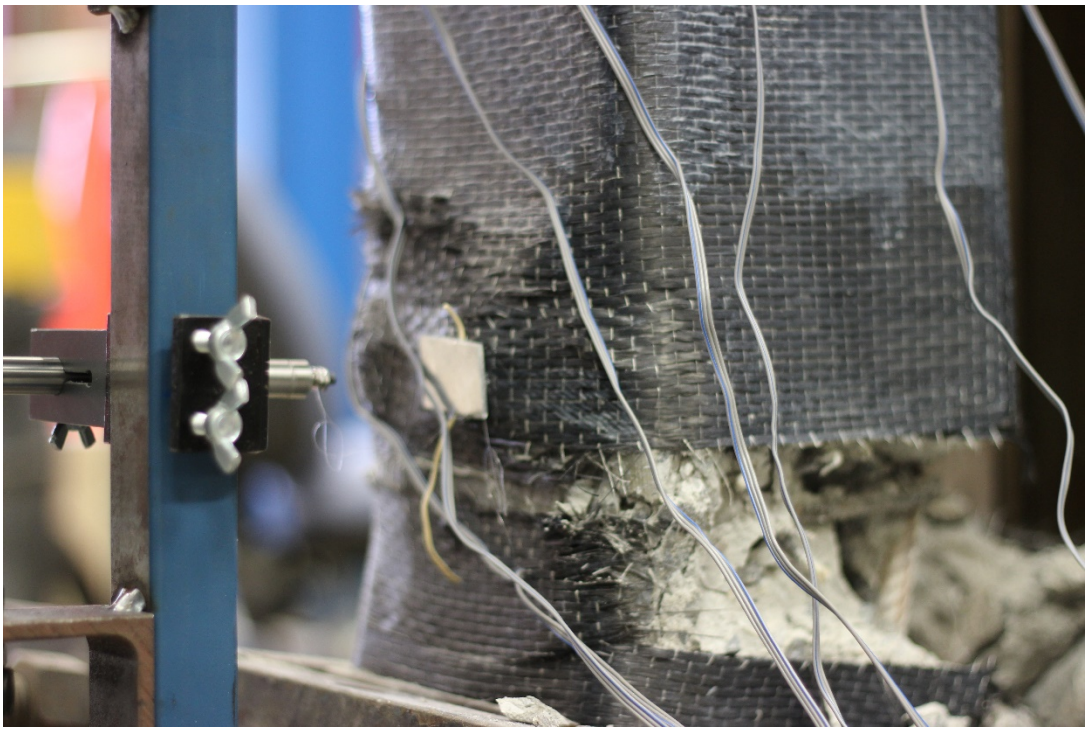

Figure 4.5.1-6 Concrete spalling at the bottom of specimen CF13

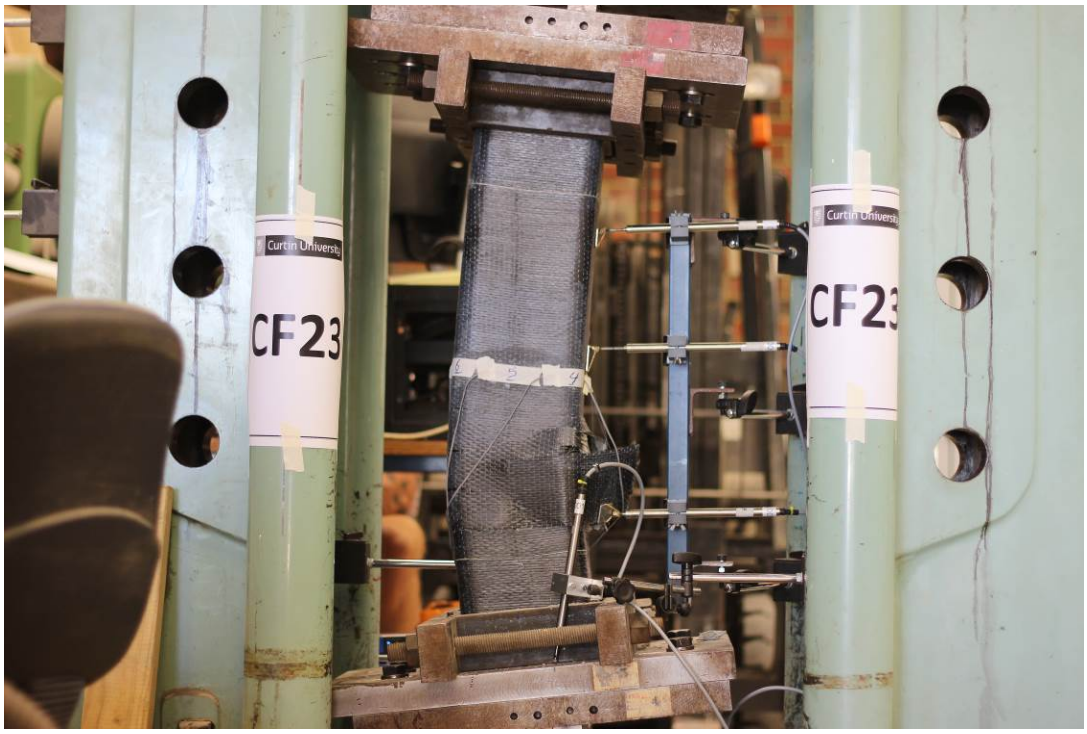

Figure 4.5.1-7 Overal view of CF23 failure

Figure 4.5.1-8 CFRP tearing in the tensile zone of CF23

Figure 4.5.1-9 Concrete crushing and CFRP rupture in the compressive zone of CF23

Figure 4.5.1-10 Overal view of CF33 failure

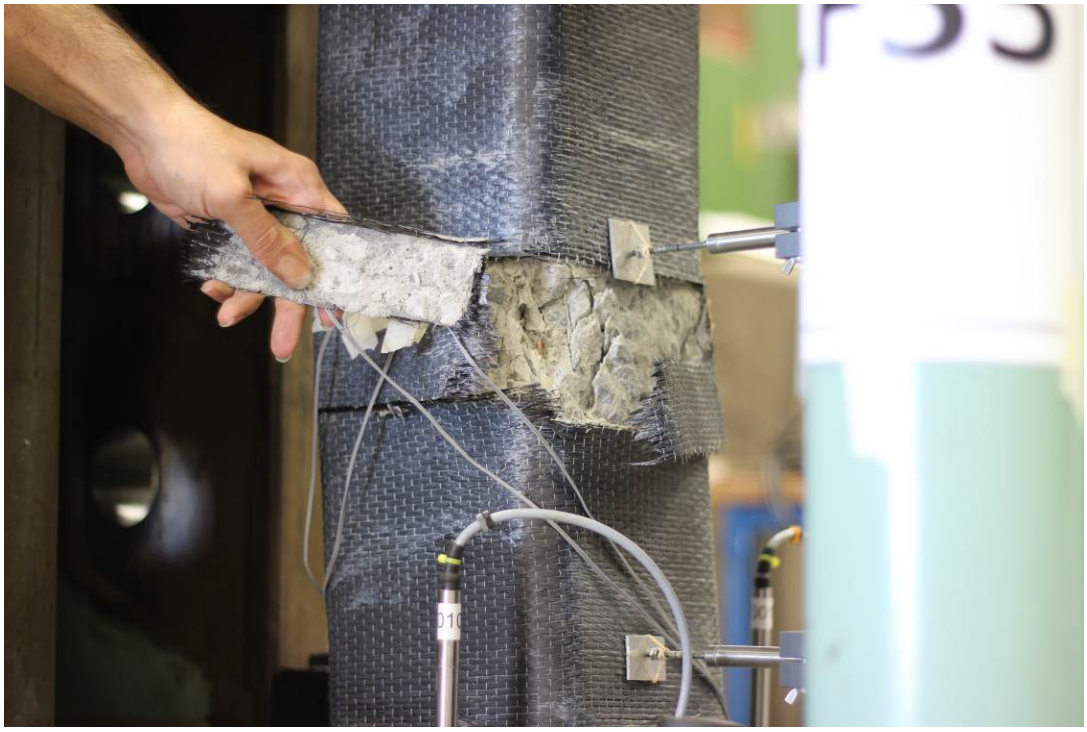

Figure 4.5.1-11 Concrete crushing and rupture of the CFRP in compressive zone of CF33

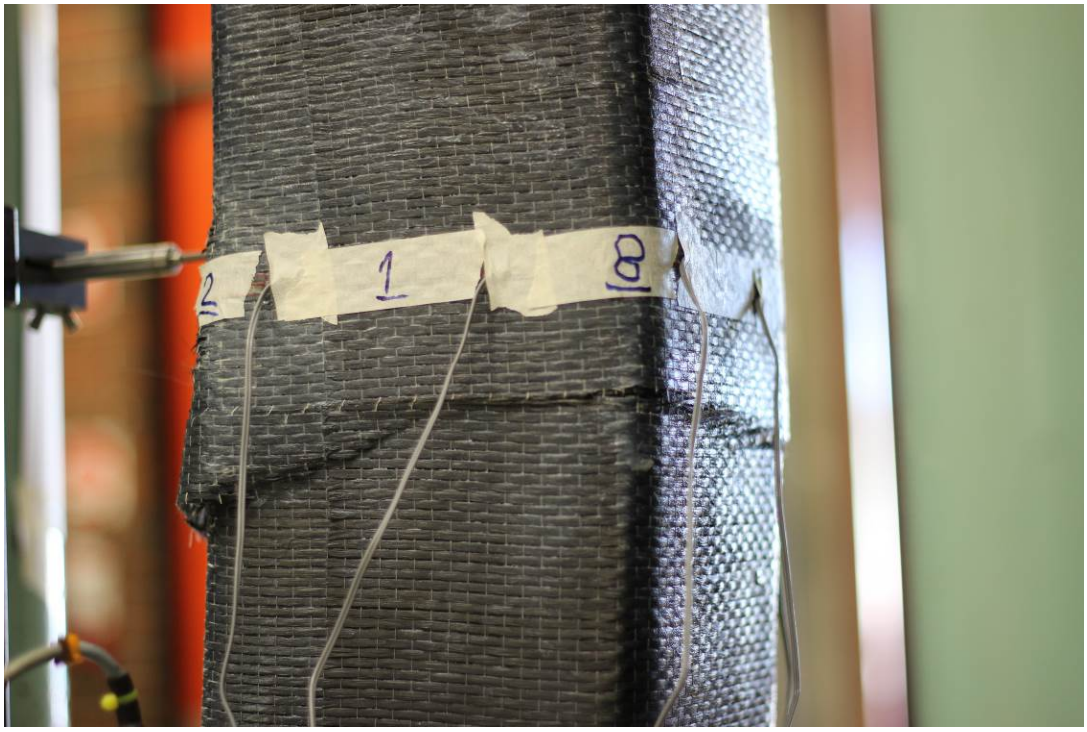

Figure 4.5.1-12 CFRP rupture and tearing in the tension zone of CF33

4.5.2 Axial load versus axial and lateral deflection behaviour

As demonstrated in Figure 4.5.2-1 the wrapped columns can sustain higher levels of peak and post-peak loads while undergoing larger axial deflections compared to CR3. Compared to the reference specimen CR3, as shown in Figure 4.5.2-1, there has been an improvement of 22%, 29%, and 28.5% in ultimate peak load of specimens CF13, CF23, and CF33 (from 654 kN to 799 kN, 845 kN, 841 kN) accordingly. The value of $P_{85\%\,u}$ has also increased by 22%, 29%, 28% for specimens CF13, CF23, and CF33 (from 556 kN to 679 kN, 718 kN, and 715 kN) correspondingly.

No clear pattern is observed for the value of lateral deflection at ultimate load (δ_u) with -98%, -89%, and +16% change for columns CF13, CF23, and CF33 correspondingly relative to column CR3. Except for column CF13 which experienced a drop of 60% in the value of $\delta_{85\%\,u}$ compared to CR3, $\delta_{85\%\,u}$ for specimens CF23 and CF33 is increased by 38% and 167% accordingly. This drop in $\delta_{85\%\,u}$ for column CF13, as already shown in Figure 4.5.2-2, can be attributed to the failure mode of the column which happened at the very bottom instead of happening at midheight.

A steady improvement pattern is observed for the ductility of the specimens when increasing the number of wraps.Compared to the reference specimen CR3, increase of 115%, 167%, 171% in ductility is achieved for specimens CF13, CF23, and CF33 as calculated in Table 4.5.2-1.

With regards to the ultimate mean hoop strain an increasing patterned is observed when the number of CFRP wraps are increased. The ultimate mean hoop strain is improved by 11%, 97%, and 111% for columns CF13, CF23, and CF33 relative to the reference column (CR3). One of the reasons for the relatively big gap in ultimate hoop strain of CF13 compared to that of CF23 and CF33 is the failure zone is located at the

bottom of the column and far from strain gauges that are located at the mid-height, so the values recorded are not the maximum hoop strains produced in the CFRP jacket.

Also an increasing trend is observed for both the ultimate load moment (M_u) as well as post-peak load moment ($M_{85\%\,u}$). Ultimate load moment (M_u) has increased by 13%, 21%, and 29% (from 35.26 kN.m to 40, 42.56, and 45.35 kN.m) for columns CF13, CF23, and CF33 compared to CR3. Furthermore the post-peak ultimate load moment ($M_{85\%\,u}$) has improved by 16%, 33%, and 44% (from 29.98 kN.m to 34.8, 39.74, and 43.14 kN.m). The increasing trend in ductility, axial and flexural capacity and lateral deformability of columns in this series of tests (50mm eccentricity) demonstrates the capability of CFRP wraps in improving the overall performance of columns under big eccentricities (tension controlled failure).

Widiarsa and Hadi (2013) reported in their study that for columns under eccentric loading with 50 mm eccentricity, the ultimate axial load has improved by 7% and 15%, the lateral deflection at ultimate load (δ_u) has changed by -13% and +21%, and the ductility is increased by 49% and 145% for columns with one and three layers of CFRP wraps accordingly. As seen, the overall increasing trend in axial load as well as ductility with respect to the number of CFRP layers confirms the trend that is reported in present experimental study.

As shown in Figure 4.5.2-3 there is an increasing trend for the axial sustained loads vs mid-height deflection as the number of wraps increase. This shows the effectiveness of CFRP wrapping in increasing the lateral deformability and energy absorption of the columns. However the lateral deflections at mid-height of specimen CF13 are even smaller than the reference columns. This can be attributed to the fact that this column failed at the bottom section for which the lateral deflections were not measured.

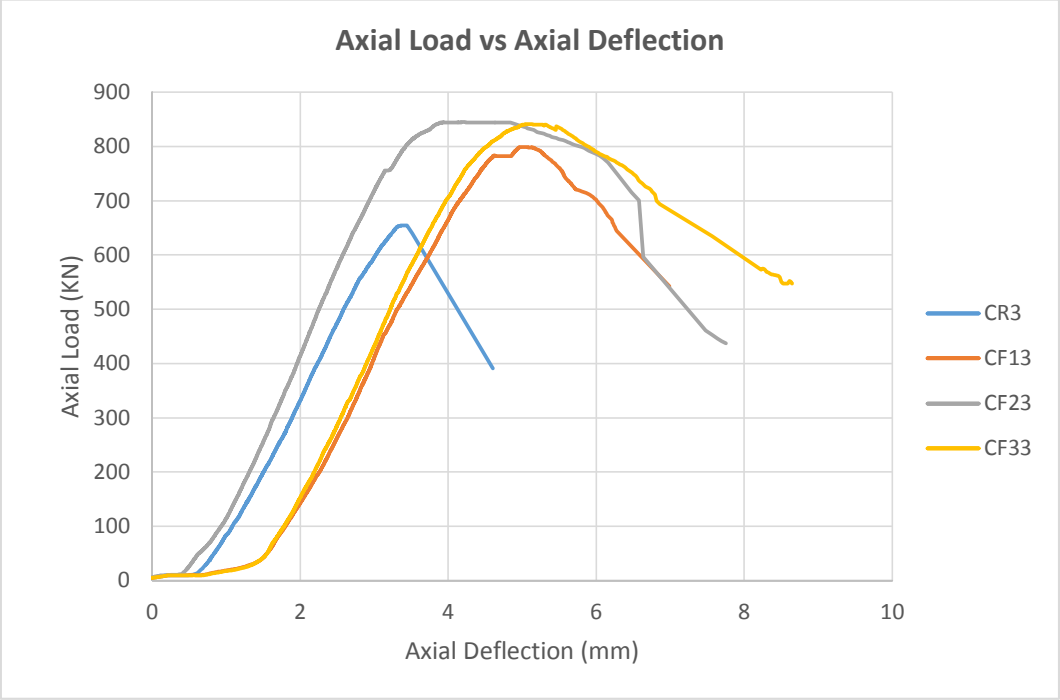

Figure 4.5.2-1 Axial load versus axial displacement behaviour of control column and column containing one, two and three layers of CFRP wrap under ecentric loading of 50mm ecentricity

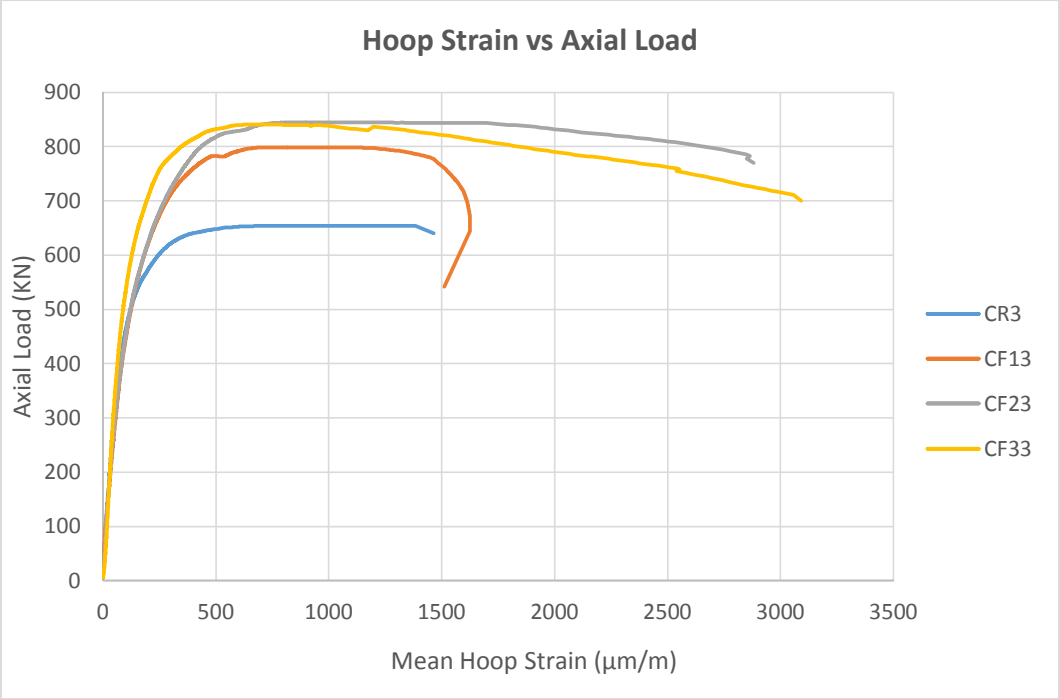

Figure 4.5.2-2 Axial load versus hoop strain of control column and column containing one, two and three layers of CFRP wrap under ecentric loading of 50mm ecentricity

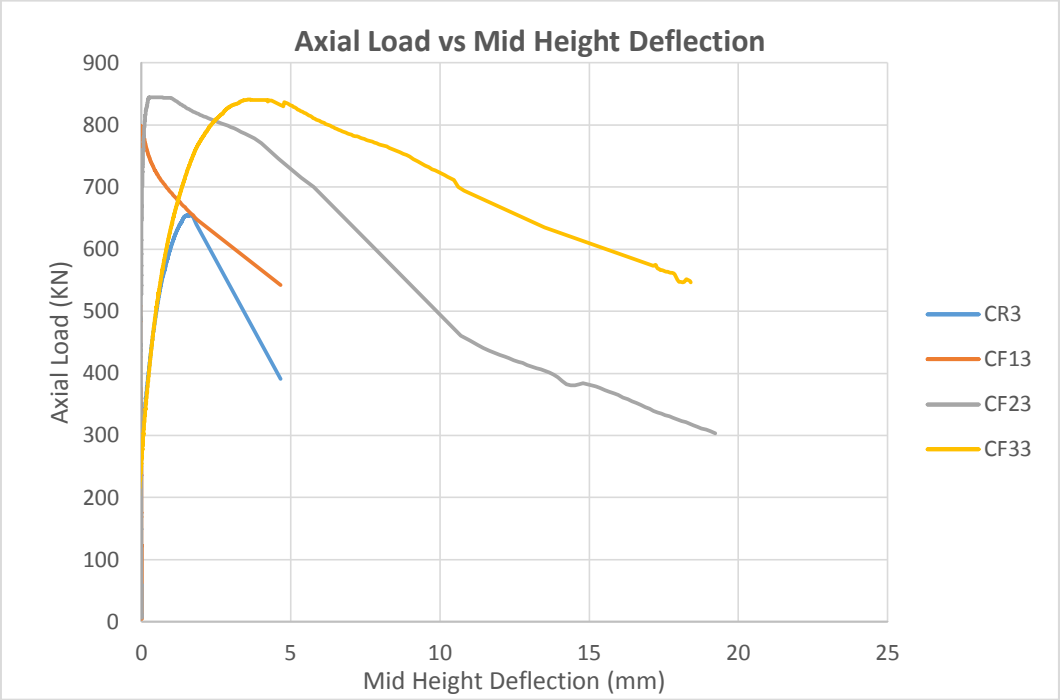

Figure 4.5.2-3 Axial load versus mid-height deflection behaviour of control column and column containing one, two and three layers of CFRP wrap under ecentric loading of 50mm ecentricity

Column code	CR3	CF13	CF23	CF33
P_y (kN)	600.00	648.86	749.94	678.01
P_u (kN)	654.48	798.92	844.57	840.92
$P_{85\%\,u}$ (kN)	556.31	679.08	717.89	714.78
δ_u (mm)	3.39	0.06	0.39	3.93
$\delta_{85\%\,u}$ (mm)	3.88	1.24	5.35	10.36
M_u (kN.m)	35.26	40.00	42.56	45.35
$M_{85\%\,u}$ (kN.m)	29.98	34.80	39.74	43.14
Ductility	1.38	2.97	3.69	3.74

Table 4.5.2-1 Summary of strength and ductility properties of columns under 50mm eccentric loading

4.6 Mechanical behaviour of Beams

4.6.1 Failure characteristics and moment-deflection behaviour

In the case of specimen CRB shear cracks (shown in Figure 4.6.1-1) started to form approximately at yield moment of 18 kN.m. These 45˚ cracks propagated from bottom to the top side of beams and then they formed localized cracks at the ultimate moment of 27 kN.m and afterwards the beam failed in a brittle manner as shown in Figure 4.6.1-2.

In the case of wrapped columns, specimens CF1B, CF2B, and CF3B there was a slight improvement in the ultimate moment to approximately 29 kN.m. However the failure behaviour of wrapped columns became ductile in dramatic way in a sense that specimens CF1B, CF2B, and CF3B undergo 18mm, 27mm, and 35mm of mid-span plastic deflection compared to that of CRB which is only 5mm (as shown in Figures 4.6.1-3, 4.6.1-6, 4.6.1-8, and 4.6.1-10). Another observation is that the CFRP wrapping changed the failure mode of the beams from brittle shear failure in CRB to a ductile flexural mode accompanied by longitudinal rebar yielding and rupture for the wrapped specimens (as shown in Figures 4.6.1-5, 4.6.1-7, and 4.6.1-9)

In the case of CF1B the moment-deflection diagram (Figure 4.6.1-10) starts at a negative strain and this is due to the fact that LVDTs were not adjusted to zero in this case, thus the first 2mm of deflection on the negative side of deflection axis is removed from the graph.

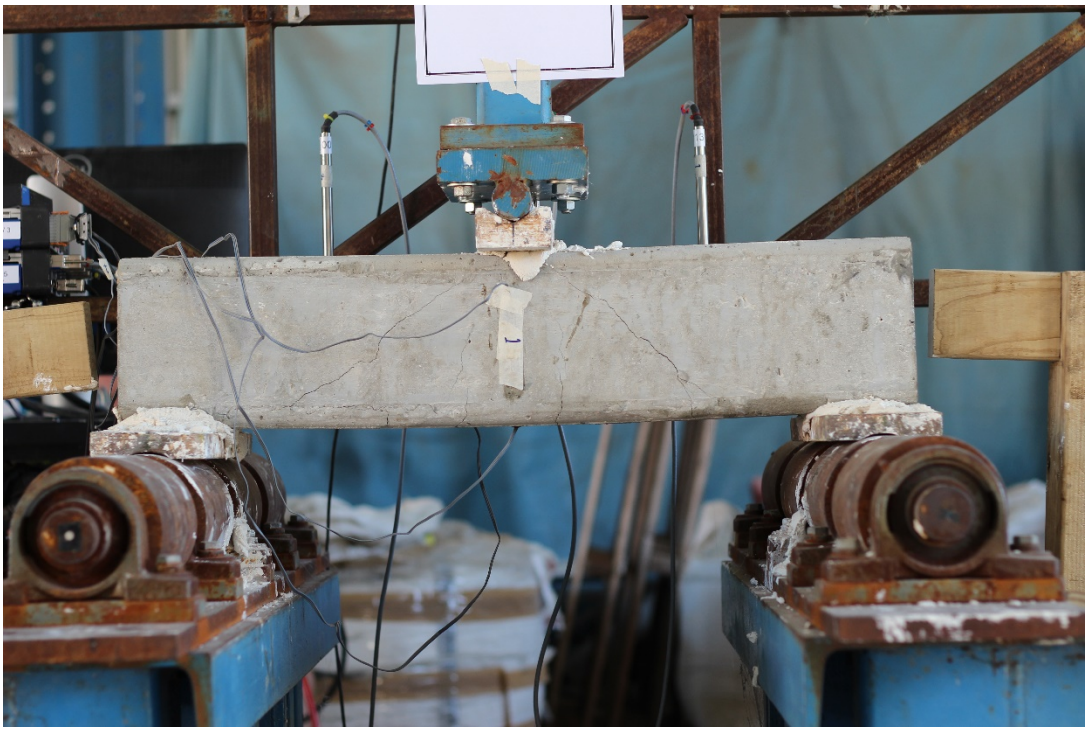

Figure 4.6.1-1 Overal view of CRB

Figure 4.6.1-2 Propagation and localization of diagonal shear cracks in CRB

Figure 4.6.1-3 Overal view of CF1B

Figure 4.6.1-4 Propogation and localization of flexural cracks in CF1B

Figure 4.6.1-5 Longitudinal rebar rupture and flexural failure in CF1B

Figure 4.6.1-6 Overal view of CF2B

Figure 4.6.1-7 Flexural failure and longitudinal rebar rupture in CF2B

Figure 4.6.1-8 Overal view of CF3B

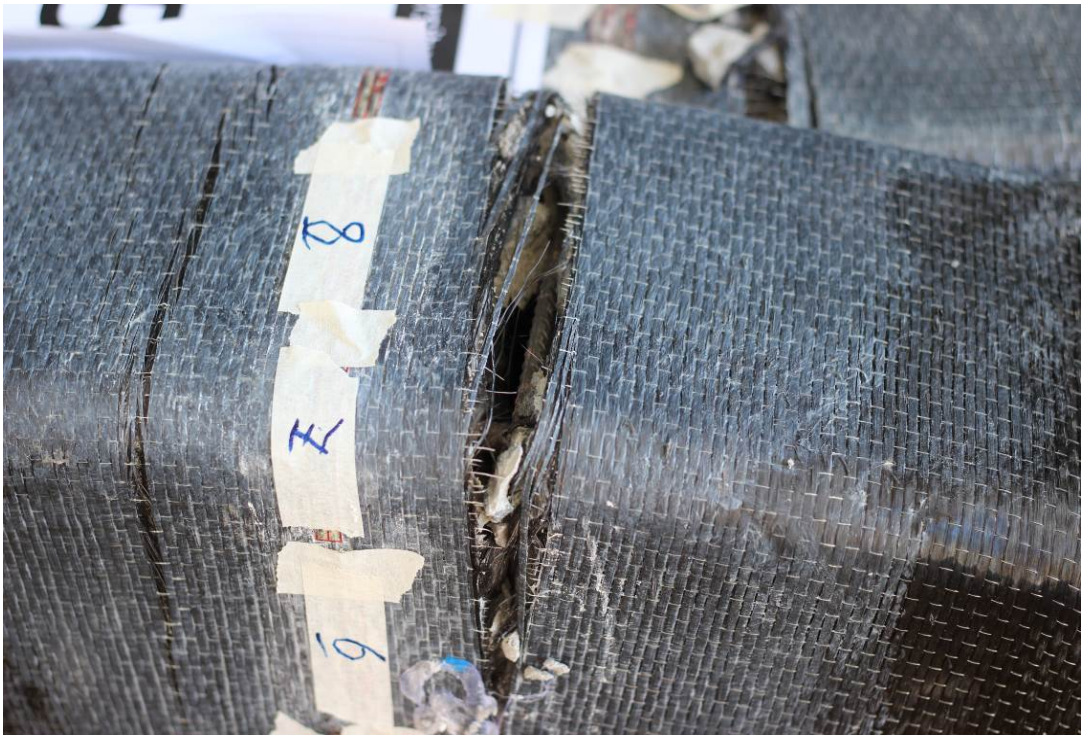

Figure 4.6.1-9 Flexural failure and longitudinal rebar rupture in CF3B

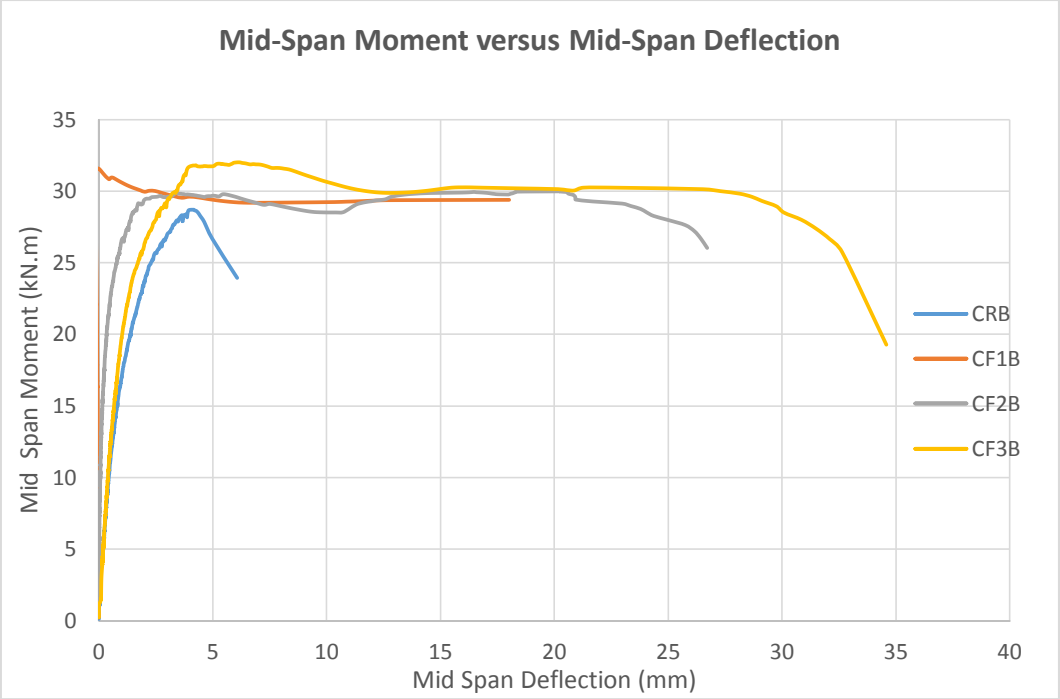

Figure 4.6.1-10 Moment versus mid-span deflection behaviour of control beam and that containing CFRP wraps (one, two and three layers) under three point bending.

4.7 Experimental P-M Interaction diagrams

Experimental load-moment (P-M) interaction diagrams of CFRP confined and unconfined columns is shown in Figure 4.7-1. It can be seen that the axial capacity of column with one CFRP wrap under pure compression (points on the vertical axis) has improved by 15%. However, in the case of pure flexure no improvement in moment capacity is observed even with 1, 2 and 3 layers of CFRP. This is due to the direction of CFRP fabric. It can be seen in Figure 4.7-2 that the CFRP fabric direction is perpendicular to the direction of beam axis meaning the developed tensile stresses in the soffit of the beam is not carried by the CFRP fibres. However, these CFRP fibres provide quite significant improvement in load and moments under applied eccentricities where combined compression and bending effects are present. Nevertheless, it can be seen that the area in the P-M diagram increases with increase in CFRP layers and an improvement in maximum flexural capacity of 13%, 21%, and 29% is observed for specimens with one, two, and three CFRP wraps compared to the unwrapped specimens. Although it seems that some points (specimen with two CFRP wraps and 35mm eccentric loading, CF22) in the interaction diagram of columns with two and three wraps exhibit lower axial capacity compared to specimens with one wrap, generally they show more significant improvements in their flexural capacities. This slight reduction of axial ultimate load of CF22 and CF32 compared to CF12 can be attributed to the variability of material properties such as concrete strength or defects in longitudinal reinforcements which can cause earlier buckling of reinforcement and delamination of wraps, but both specimens CF32 and CF22 sustained higher lateral and axial deflections while maintaining their peak axial loads whereas in the case of CF12 the failure was quite brittle and the column did not undergo large deflections. Since specimens with two and three CFRP wraps could not be

tested under concentric loading conditions due to limitations of the laboratory equipment, points of pure axial compression could not be generated in P-M interaction diagrams of such columns.

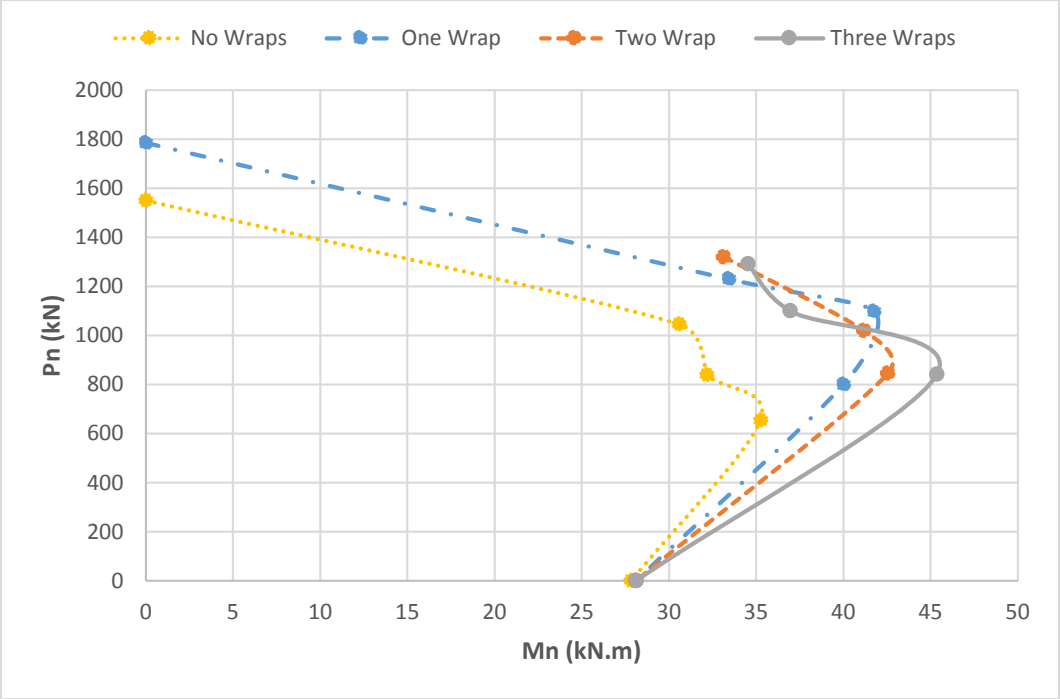

Figure 4.7-1 Experimental P-M Interaction Diagram of columns with 0, 1, 2, and 3 CFRP Wraps

Figure 4.7-2 Direction of CFRP fabrics relative to the direction of beam axis

4.8 Summary

This chapter presents the behaviour of unwrapped and wrapped columns having one, two and three CFRP layers under concentric and eccentric loadings as well as in three-point bending. It is observed that the CFRP wrapping improves the ultimate load, the ductility and deformation capacities significantly of the specimens in all eccentricities. However, with increasing eccentricities of the loading the CFRP wrapped square columns exhibited reduction in ultimate axial load. In the case of pure flexure, wraps with CFRP fibers oriented perpendicular to the longitudinal axis of the beam have minimal effect in improvement of ultimate flexural capacity although they improve the deformability of the beams.

5 Analytical Modelling

5.1 Introduction.

There are plenty of analytical stress-strain constitutive models proposed for CFRP confined columns in the literature. On the contrary there are few studies that have investigated the potential of such models to predict the load-moment (P-M) interaction diagram of these columns. It is very important to verify the capability of these Equations to predict the behaviour of CFRP confined columns under combined state of flexure and compression for design purposes. In this chapter four of the most relevant models are chosen and their performance in prediction of P-M interaction diagram of such columns is examined.

5.2 P-M interaction diagram

In this analytical study it is assumed that the behaviour of CFRP encased concrete is similar to that of the unconfined concrete except the constitutive stress-strain Equation of CFRP-confined concrete is adopted to develop the interaction diagram. In this analysis the following assumptions are considered:

1. The column under flexure follows the Euler-Bernoulli beam theory, i.e the plane sections remain plane after bending.
2. The tensile strength of the concrete is negligible.
3. The column is acting as a composite unit together with the steel reinforcement and CFRP wraps.

The loading rate of experiments in this study are kept at the minimum amount to ensure a static state of loading and thus these Equations are applicable for modelling of our experimental data. With regards to the material strength and specimen sizes, the parameters in the four chosen models are fitted using vast databases of tests which use a wide range of these variables. Therefore they theoretically should be able to predict the P-M diagram of any CFRP confined column with a reasonable margin.

All of the interaction diagrams herein are developed by connecting five critical points with straight lines as shown in Figure 5.2-1, The state of each critical point is as follows:

- **Point A:** This point corresponds to column under pure compression and a uniform distribution of ultimate strain (ε_{ccu} for FRP-confined concrete and ε_{cu} for unconfined concrete) exists all over the column cross section.
- **Point B:** This point corresponds to ultimate compressive strain (ε_{ccu} for confined concrete) at outmost compressive part of the cross section and zero strain at the level of longitudinal rebars closest to the tensile part of the cross section.
- **Point C:** This point corresponds to balanced failure of the column with maximum compressive strain of ε_{ccu} at the extreme compressive fibre of the cross section and yield tensile strain ε_{fy} at steel reinforcement layer closest to extreme tensile fibre of the cross section.
- **Point D:** This point is located at the limit of tensile-controlled failure with a compressive strain of ε_{ccu} at the extreme compressive fibre and the tensile strain of 0.005 at the longitudinal reinforcement layer closest to the extreme tensile fibre of the cross section.
- **Point E:** This point represents the pure bending state of the column and the value of the moment corresponds to the ultimate flexural capacity of the column.

In calculation of moment as well as compressive force of the columns, contribution of the CFRP confinement is only considered in compression controlled regions (Points A, B, and C). Since in this study no CFRP fibres are arranged in the longitudinal direction of the column the contribution of transverse CFRP wraps in flexural resistance is negligible. For points B and C the location of neutral axis (c) is found by applying similar triangle method for the strain distribution and the corresponding axial and flexural capacity is found by integration of stresses (or first moment of inertia of stresses) over the cross section of the column. In the case of point E the moment is found by applying the conventional beam theory to calculate the ultimate flexural capacity.

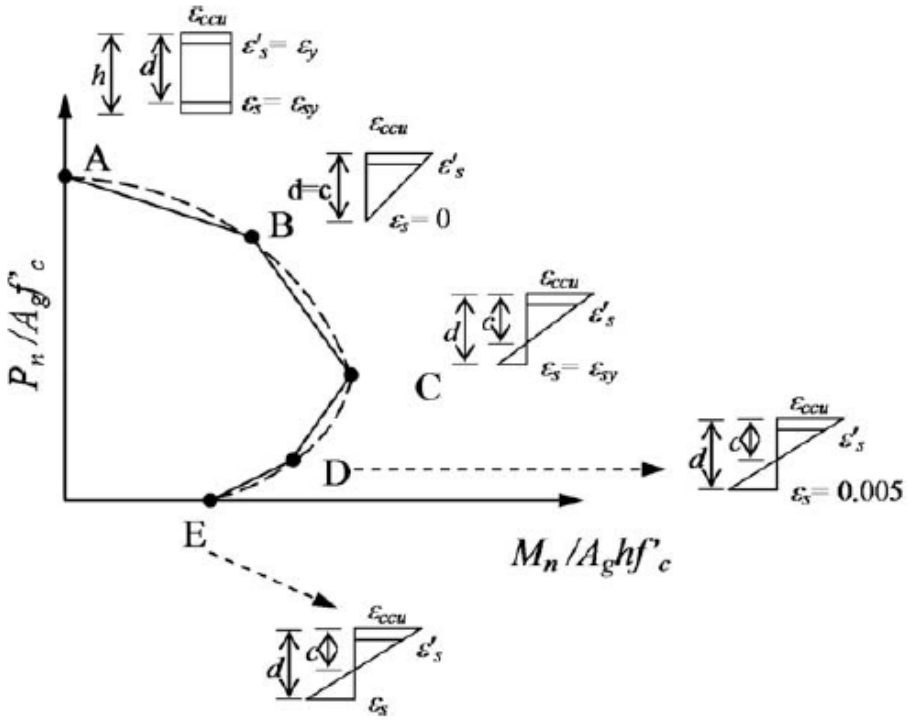

Figure 5.2-1 Strain distribution of critical points in P-M interaction diagram (Rocca et al. (2009))

5.3 Interaction diagram development based on Lam and Teng (2003a) model

Rocca et al (2009) used the model developed by Lam and Teng (2003a) with some modifications to develop the P-M interaction diagram. The model as well as parameters used by Rocca et al (2009) with their specific notations are presented herein. The notation used are summarized in Table 5.3-1

Notation	Description
A_c	Cross-sectional area of concrete in column
A_e	Effectively confined area of the column cross section
A_g	Total cross-sectional area
A_{si}	Total area of longitudinal rebars in "ith" layer from top (extreme compressive fiber) of cross section
A_s	Total area of all longitudinal rebars
b	Width of the cross section
c	Distance from neutral axis position to the extreme compression fiber in the cross-section
C_E	Environmental reduction factor (taken 0.95)
d	Depth of the cross section (distance from extreme compressive fiber to the extreme tensile reinforcement)
d_{si}	Distance from position of the "ith" layer of longitudinal steel reinforcement to geometric centroid of the cross-section
E_c	Initial modulus of elasticity of concrete
E_f	Modulus of elasticity of FRP
E_s	Modulus of elasticity of steel reinforcement
f'_c	Standard cylindrical compressive strength of concrete
f'_{cc}	Compressive strength of FRP confined concrete
f^*_{fu}	Ultimate tensile strength of FRP
f_l	Confinement pressure due to FRP jacket
f_{si}	Normal stress of longitudinal rebars in "ith" layer from top (extreme compressive fiber) of cross section
f_y	Yield strength of longitudinal steel reinforcement
h	Depth of the cross section
n	Number of FRP wraps
r	Corner radius of the cross section
t_f	FRP nominal ply thickness
y_t	Vertical coordinate within compression region measured from neutral axis position corresponding to the transition strain (ε'_t)
α	Depth of the equivalent stress block
β	The coefficient for equivalent compressive stress block ($0.65 \leq \beta = 0.85 - 0.05\frac{f'_c - 4000}{1000} \leq 0.85$)
ε'_c	Axial compressive strain corresponding to f'_c = 0.002 mm/mm
ε_{cu}	Ultimate axial compressive strain of unconfined concrete = 0.003 mm/mm
ε_{ccu}	Ultimate axial compressive strain of confined concrete
ε_{fe}	FRP effective strain reached at failure ($\varepsilon_{fe} = \kappa_\varepsilon \varepsilon_{fu}$)
ε_{fu}	Design ultimate tensile strain of FRP ($\varepsilon_{fu} = C_E \varepsilon^*_{fu}$)
ε^*_{fu}	Ultimate tensile strain of FRP
ε_{sD}	Strain of longitudinal reinforcement closest to the extreme tensile fiber at point D (0.005)
ε_{si}	Strain of longitudinal rebars in "ith" layer from top (extreme compressive fiber) of cross section
ε_{sy}	Yield strain of steel rebars
ε'_t	Transition strain in stress-strain curve of FRP-confined concrete.
ψ_f	Additional FRP strength reduction factor
ϕ_c	Strength reduction factor for compression controlled failure
ϕ_t	Strength reduction factor for tension controlled failure
κ_a	Efficiency factor for FRP reinforcement in determination of f'_{cc}
κ_b	Efficiency factor for FRP reinforcement in determination of ε_{ccu}
κ_ε	Efficiency factor for FRP strain relating the actual rupture strain to rupture strain measured from coupon tests (taken as 0.55)
ρ_g	Ratio of total longitudinal reinforcement area to total cross section area of the column A_s/A_g

Table 5.3-1 Notation for Lam and Teng model

The nominal axial load P_n for point A can be calculated using Equation 5.3.1 (Rocca et al (2009)). In this Equation f'_{cc} is calculated using Equation 5.3.2 (Rocca et al (2009)) in which the efficiency factor (κ_a) is calculated using Equation 5.3.3 (Rocca et al (2009)). In Equation 5.3.3 the ratio of A_e / A_c can be calculated by Equation 5.3.4 (Rocca et al (2009)). Finally the value of FRP confinement pressure (f_l) is calculated by Equation 5.3.5 (Rocca et al (2009)).

$$P_{n(A)} = \left[0.85 f'_{cc}\left(A_g - A_{st}\right) + f_y A_{st}\right] \tag{5.3.1}$$

$$f'_{cc} = f'_c + 3.3\kappa_a f_l \tag{5.3.2}$$

$$\kappa_a = \frac{A_e}{A_c}\left(\frac{b}{h}\right)^2 \tag{5.3.3}$$

$$\frac{A_e}{A_c} = \frac{1 - \frac{\left(\left(\frac{b}{h}\right)(h-2r)^2 + \left(\frac{h}{b}\right)(b-2r)^2\right)}{\left(3A_g\right)} - \rho_g}{1-\rho_g} \tag{5.3.4}$$

$$f_l = \frac{\psi_f 2 n t_f E_f \varepsilon_{fe}}{\sqrt{b^2 + h^2}} \tag{5.3.5}$$

Rocca et al substituted f_0 in Equations 2.6.1 through 2.6.4 by f'_c thus the Equations 5.3.6 through 5.3.11 yield for stress strain relationship of FRP confined concrete (Rocca et al (2009)):

$$f_c = E_c \varepsilon_c - \frac{(E_c - E_2)^2}{4 f'_c}(\varepsilon_c)^2 \; for \;\; 0 \le \varepsilon_c \le \varepsilon'_t \tag{5.3.6}$$

$$f_c = f'_c + E_2 \varepsilon_c \quad for \quad \varepsilon'_t \le \varepsilon_c \le \varepsilon_{ccu} \tag{5.3.7}$$

$$\varepsilon'_t = \frac{2 f'_c}{E_c - E_2} \tag{5.3.8}$$

$$\varepsilon_{ccu} = \varepsilon'_c\left(1.5 + 12\kappa_b \frac{f_l}{f'_c}\left(\frac{\varepsilon_{fe}}{\varepsilon'_c}\right)^{0.45}\right) \le 0.01 \tag{5.3.9}$$

$$\kappa_b = \frac{A_e}{A_c}\left(\frac{h}{b}\right)^{0.5} \tag{5.3.10}$$

$$E_2 = \frac{f'_{cc} - f'_c}{\varepsilon_{ccu}} \tag{5.3.11}$$

In order to be able to calculate the nominal axial force (P_n) and the nominal moment (M_n) of the column for points B, C, and D; integration of stress and first moment of stress (with respect to centroid of the section) should be calculated according to Equations 5.3.12 and 5.3.13 (Rocca et al (2009)).

$$P_{n(B,C)} = \int_0^c (b) f_c(y) dy + \sum A_{si} f_{si} \tag{5.3.12}$$

$$M_{n(B,C)} = \int_0^c (b) \left(\frac{h}{2} - c + y\right) f_c(y) dy + \sum A_{si} f_{si} d_{si} \tag{5.3.13}$$

In the case of points B and C which are located in the compression controlled region of the P-M diagram, the effect of FRP confinement is considered thus f_c is substituted by the constitutive stress-strain relationship of the FRP confined concrete. In this case f_c in Equations 5.3.12 and 5.3.13 is substituted by Equations 5.3.6 and 5.3.7. As a result Equations 5.3.14 and 5.3.15 will be formed for rectangular cross sections (Rocca et al (2009)):

$$\begin{aligned} P_{n(B,C)} = \int_0^{y_t} \left[E_c \left(\frac{\varepsilon_{ccu}}{c} y\right) - \frac{(E_c - E_2)^2}{4 f'_c} \left(\frac{\varepsilon_{ccu}}{c} y\right)^2 \right] b dy \\ + \int_{y_t}^c \left[f'_c + E_2 \left(\frac{\varepsilon_{ccu}}{c} y\right) \right] b dy + \sum A_{si} f_{si} \end{aligned} \tag{5.3.16}$$

$$\begin{aligned} M_{n(B,C)} = \int_0^{y_t} \left[E_c \left(\frac{\varepsilon_{ccu}}{c} y\right) - \frac{(E_c - E_2)^2}{4 f'_c} \left(\frac{\varepsilon_{ccu}}{c} y\right)^2 \right] b \left(\frac{h}{2} - c + y\right) dy \\ + \int_{y_t}^c \left[f'_c + E_2 \left(\frac{\varepsilon_{ccu}}{c} y\right) \right] b \left(\frac{h}{2} - c + y\right) dy + \sum A_{si} f_{si} \end{aligned} \tag{5.3.17}$$

The height of the section in compression "c" and parameter "y_t" can be calculated by Equations 5.3.18 and 5.3.19 (Rocca et al (2009)):

$$c = \begin{cases} d, & For\ point\ B \\ d \dfrac{\varepsilon_{ccu}}{\varepsilon_{sy} + \varepsilon_{ccu}}, & For\ point\ C \end{cases} \tag{5.3.20}$$

$$y_t = c \frac{\varepsilon'_t}{\varepsilon_{ccu}} \tag{5.3.21}$$

After applying integration in Equations 5.3.14 and 5.3.15 and reorganizing the terms we arrive at the more compact form in Equations 5.3.18 and 5.3.19 (Rocca et al (2009)) in which the coefficients A, B, C, D, E, F, G, H and I, are given by Equations 5.3.22 through 5.3.23 (Rocca et al (2009)).

$$P_{n(B,C)} = \left(A(y_t)^3 + B(y_t)^2 + C(y_t) + D + \sum A_{si} f_{si}\right) \tag{5.3.24}$$

$$M_{n(B,C)} = (E(y_t)^4 + F(y_t)^3 + G(y_t)^2 + H(y_t) + I) + \sum A_{si} f_{si} d_{si} \tag{5.3.25}$$

$$A = \frac{-b(E_c - E_2)^2}{12 f_c'} \left(\frac{\varepsilon_{ccu}}{c}\right)^2 \tag{5.3.26}$$

$$B = \frac{b(E_c - E_2)}{2} \left(\frac{\varepsilon_{ccu}}{c}\right) \tag{5.3.27}$$

$$C = -b f_c' \tag{5.3.28}$$

$$D = bc f_c' + \frac{bcE_2}{2} (\varepsilon_{ccu}) \tag{5.3.29}$$

$$E = \frac{-b(E_c - E_2)^2}{16 f_c'} \left(\frac{\varepsilon_{ccu}}{c}\right)^2 \tag{5.3.30}$$

$$F = b\left(c - \frac{h}{2}\right) \frac{(E_c - E_2)^2}{12 f_c'} \left(\frac{\varepsilon_{ccu}}{c}\right)^2 + \frac{b(E_c - E_2)}{3} \left(\frac{\varepsilon_{ccu}}{c}\right) \tag{5.3.31}$$

$$G = -\left(\frac{b}{2} f_c' + b\left(c - \frac{h}{2}\right) \frac{(E_c - E_2)}{2} \left(\frac{\varepsilon_{ccu}}{c}\right)\right) \tag{5.3.32}$$

$$H = b f_c' \left(c - \frac{h}{2}\right) \tag{5.3.33}$$

$$I = \frac{bc^2}{2} f_c' - bc f_c' \left(c - \frac{h}{2}\right) + \frac{bc^2 E_2}{3} (\varepsilon_{ccu}) - \frac{bcE_2}{2} \left(c - \frac{h}{2}\right) (\varepsilon_{ccu}) \tag{5.3.34}$$

For point D of the P-M interaction diagram, integrations 5.3.35 and 5.3.36 are going to be used but this time instead of constitutive stress strain relationship of confined concrete the properties of unconfined concrete is used and the stress at the extreme compressive fibre of the cross section is equal to unconfined strength of the concrete (f'_c).

In the case of point E of the P-M diagram, the nominal flexural capacity of the column is computed just as an ordinary beam. The calculation steps for all the points in the P-M diagram using Lam and Teng model are illustrated in Figure 5.3-1.

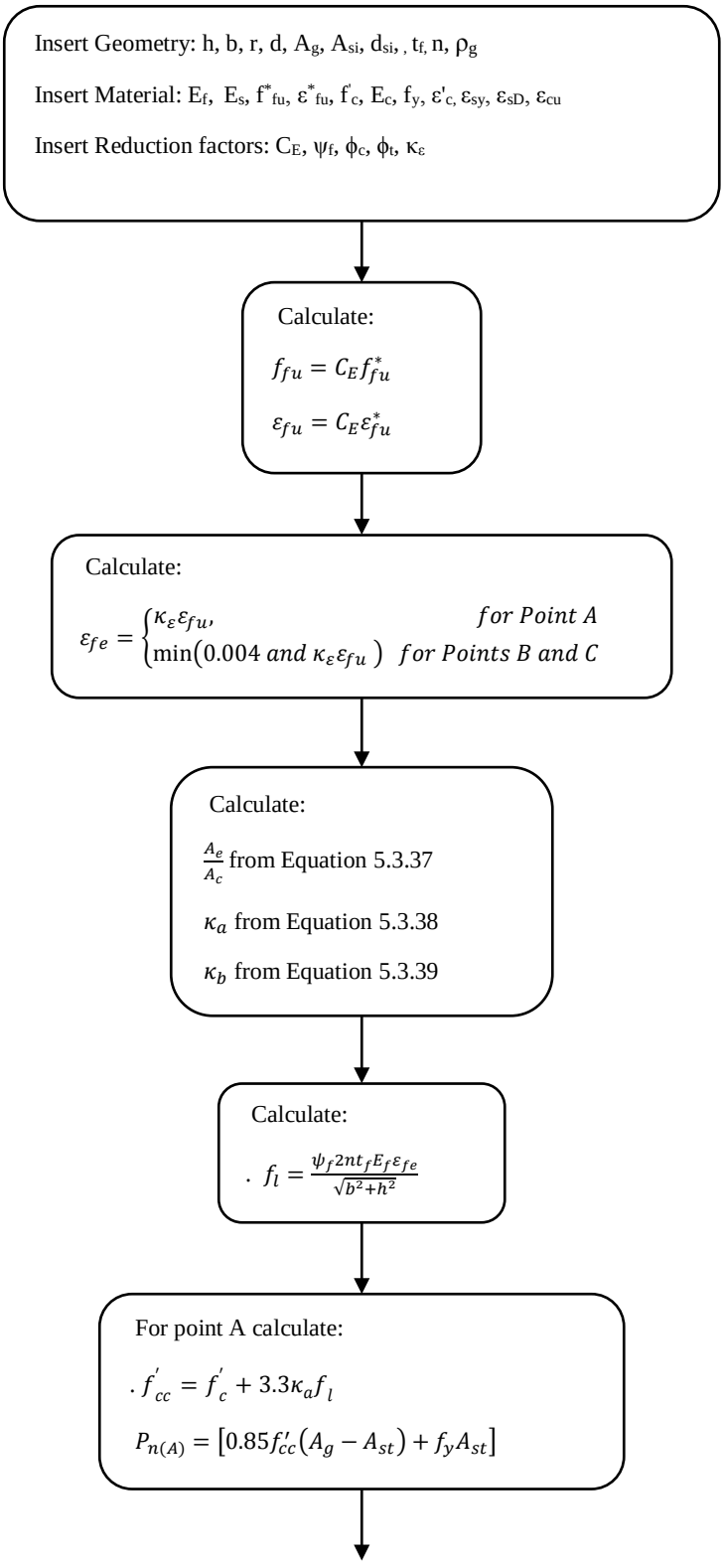
Insert Geometry: h, b, r, d, A_g, A_{si}, d_{si}, , t_f, n, ρ_g
Insert Material: E_f, E_s, f^*_{fu}, ε^*_{fu}, f'_c, E_c, f_y, ε'_c, ε_{sy}, ε_{sD}, ε_{cu}
Insert Reduction factors: C_E, ψ_f, ϕ_c, ϕ_t, κ_ε
Calculate:
$f_{fu} = C_E f^*_{fu}$
$\varepsilon_{fu} = C_E \varepsilon^*_{fu}$
Calculate:
$\varepsilon_{fe} = \begin{cases} \kappa_\varepsilon \varepsilon_{fu}, & for\ Point\ A \\ \min(0.004\ and\ \kappa_\varepsilon \varepsilon_{fu}) & for\ Points\ B\ and\ C \end{cases}$
Calculate:
$\frac{A_e}{A_c}$ from Equation 5.3.37
κ_a from Equation 5.3.38
κ_b from Equation 5.3.39
Calculate:
. $f_l = \frac{\psi_f 2nt_f E_f \varepsilon_{fe}}{\sqrt{b^2+h^2}}$
For point A calculate:
. $f'_{cc} = f'_c + 3.3\kappa_a f_l$
$P_{n(A)} = [0.85 f'_{cc}(A_g - A_{st}) + f_y A_{st}]$

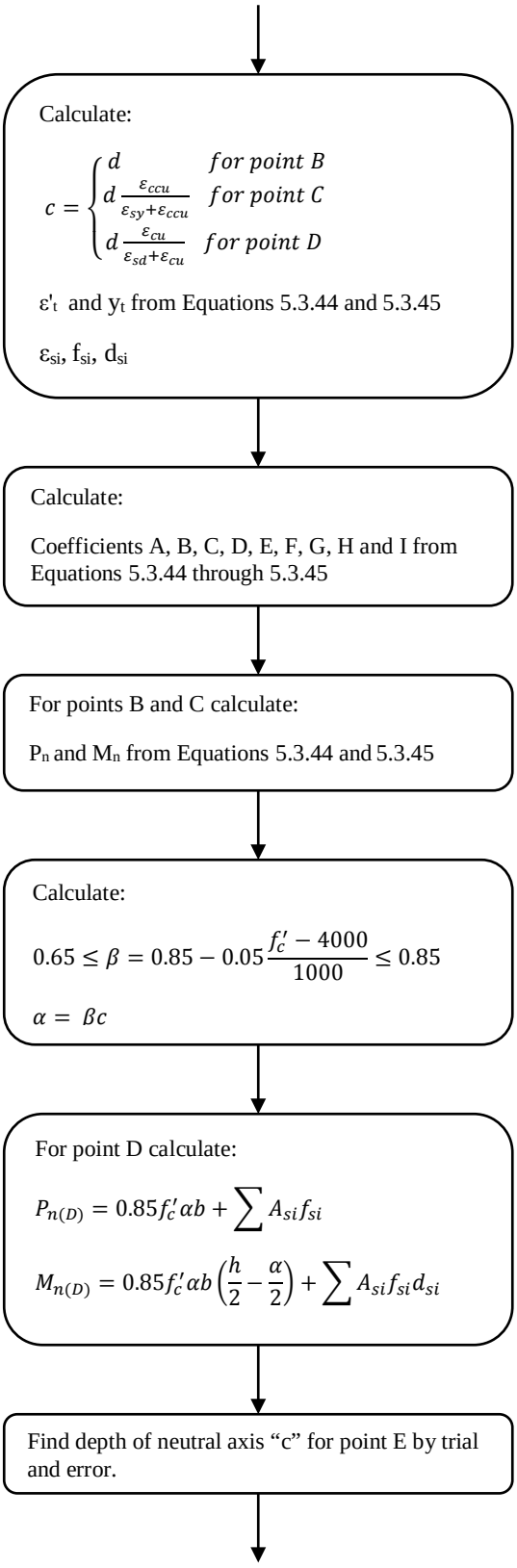
Calculate:
$c = \begin{cases} d & for\ point\ B \\ d\frac{\varepsilon_{ccu}}{\varepsilon_{sy}+\varepsilon_{ccu}} & for\ point\ C \\ d\frac{\varepsilon_{cu}}{\varepsilon_{sd}+\varepsilon_{cu}} & for\ point\ D \end{cases}$
ε't and yt from Equations 5.3.44 and 5.3.45
εsi, fsi, dsi
Calculate:
Coefficients A, B, C, D, E, F, G, H and I from Equations 5.3.44 through 5.3.45
For points B and C calculate:
Pn and Mn from Equations 5.3.44 and 5.3.45
Calculate:
$0.65 \leq \beta = 0.85 - 0.05\frac{f_c' - 4000}{1000} \leq 0.85$
$\alpha = \beta c$
For point D calculate:
$P_{n(D)} = 0.85 f_c' \alpha b + \sum A_{si} f_{si}$
$M_{n(D)} = 0.85 f_c' \alpha b \left(\frac{h}{2} - \frac{\alpha}{2}\right) + \sum A_{si} f_{si} d_{si}$
Find depth of neutral axis "c" for point E by trial and error.

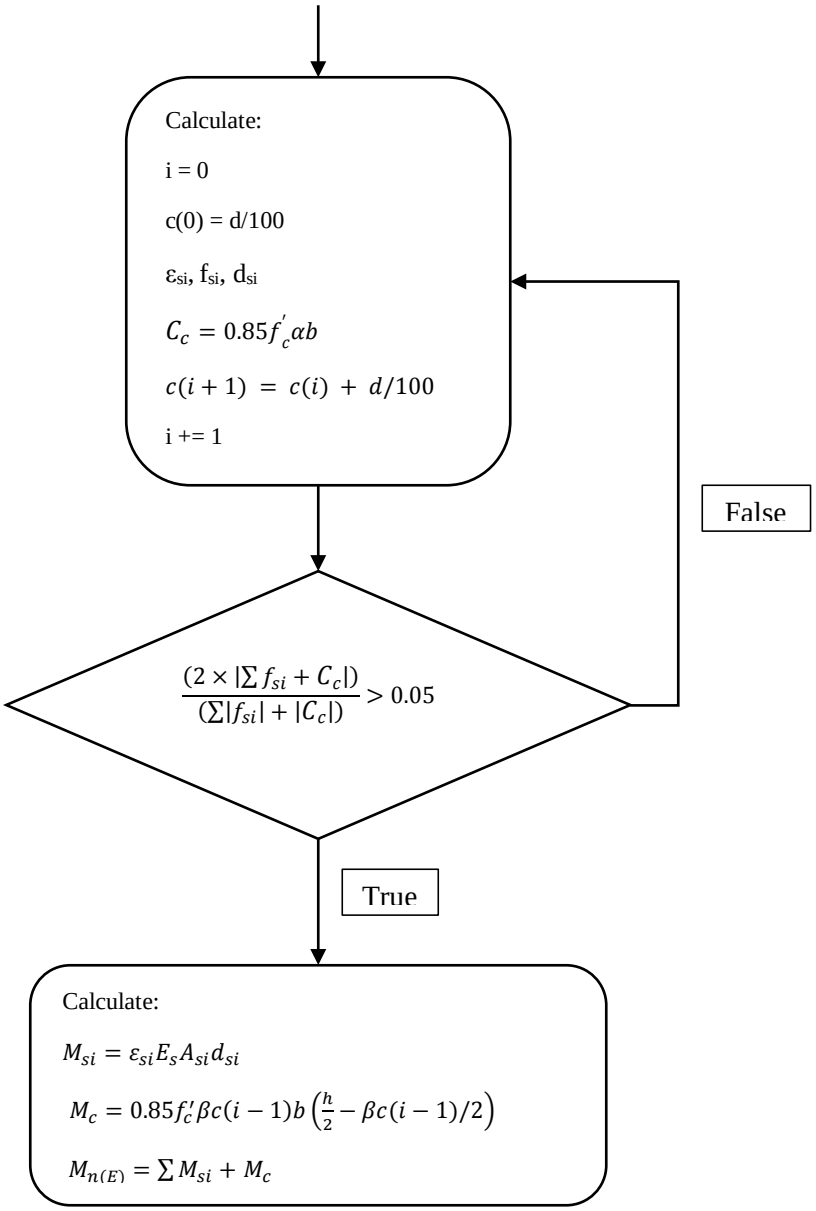

Figure 5.3-1 P-M diagram calculation algorithm based on Lam and Teng model

5.4 Interaction diagram development based on Youssef et al. (2007) Model

For developing the P-M diagram based on the constitutive model by Youssef et al (2007), points D and E can be calculated identically to that of model by Lam and Teng. However development of points A, B, and C of the P-M diagram are based on Equations proposed by Youssef et al. The procedure for calculation of these points is illustrated in Figure 5.4-1. For calculation of points B and C instead of analytical integration of Equations 5.3.46 and 5.3.47, numerical integration technique (Simpson's rule) is implemented in excel macro. All the notations used in the Equations are summarized in Table 5.4-1.

Notation	Description
A_g	Total cross-sectional area
A_{si}	Total area of longitudinal rebars in "ith" layer from top (extreme compressive fiber) of cross section
A_s	Total area of all longitudinal rebars
b	Width of the cross section
c	Distance from neutral axis position to the extreme compression fiber in the cross-section
C_E	Environmental reduction factor (taken 0.95)
d	Depth of the cross section (distance from extreme compressive fiber to the extreme tensile reinforcement)
d_{si}	Distance from position of the "ith" layer of longitudinal steel reinforcement to geometric centroid of the cross-section
D	Equivalent diameter of the rectangular section
E_c	Initial modulus of elasticity of concrete
E_j	Modulus of elasticity of FRP
E_s	Modulus of elasticity of steel reinforcement
E_2	Slope of the second (linear) branch of the stress strain curve
f'_c	Standard cylindrical compressive strength of concrete
f'_{cu}	Compressive strength of FRP confined concrete
f_{ju}	Ultimate tensile strength of FRP
f_{lu}	Lateral confining stress at ultimate condition of the FRP jacket
f'_{lu}	Effective lateral confining stress at ultimate condition of the FRP jacket
f_{si}	Normal stress of longitudinal rebars in "ith" layer from top (extreme compressive fiber) of cross section
f_t	Axial stress at the boundary point of the first and second region where the jacket is beginning to get fully activated
f_y	Yield strength of longitudinal steel reinforcement
h	Depth of the cross section
k_e	Confinement effectiveness coefficient
n_j	Number of FRP wraps
r_c	Corner radius of the cross section
t	FRP nominal ply thickness
y_t	Vertical coordinate within compression region measured from neutral axis position corresponding to the transition strain (ε'_t)
α	Depth of the equivalent stress block
β	The coefficient for equivalent compressive stress block $(0.65 \leq \beta = 0.85 - 0.05\frac{f'_c - 4000}{1000} \leq 0.85)$
ε'_c	Axial compressive strain corresponding to f'_c = 0.002 mm/mm
ε_{c0}	Ultimate axial compressive strain of unconfined concrete = 0.003 mm/mm
ε_{cu}	Ultimate axial compressive strain of confined concrete
ε_{jt}	FRP jacket strain at transition from first to second region = 0.002
ε_{ju}	Ultimate tensile strain of FRP jacket
ε_{sD}	Strain of longitudinal reinforcement closest to the extreme tensile fiber at point D (0.005)
ε_{si}	Strain of longitudinal rebars in "ith" layer from top (extreme compressive fiber) of cross section
ε_t	Axial strain at the boundary point of the first and second region where the jacket is beginning to get fully activated
ε_y	Yield strain of steel rebars
ψ_f	Additional FRP strength reduction factor
ϕ_c	Strength reduction factor for compression controlled failure
ϕ_t	Strength reduction factor for tension controlled failure
ρ_j	Volumetric ration of FRP jacket
ρ_l	Ratio of total longitudinal reinforcement area to total cross section area of the column A_s/A_g

Table 5.4-1 Notation for Youssef et al. Model

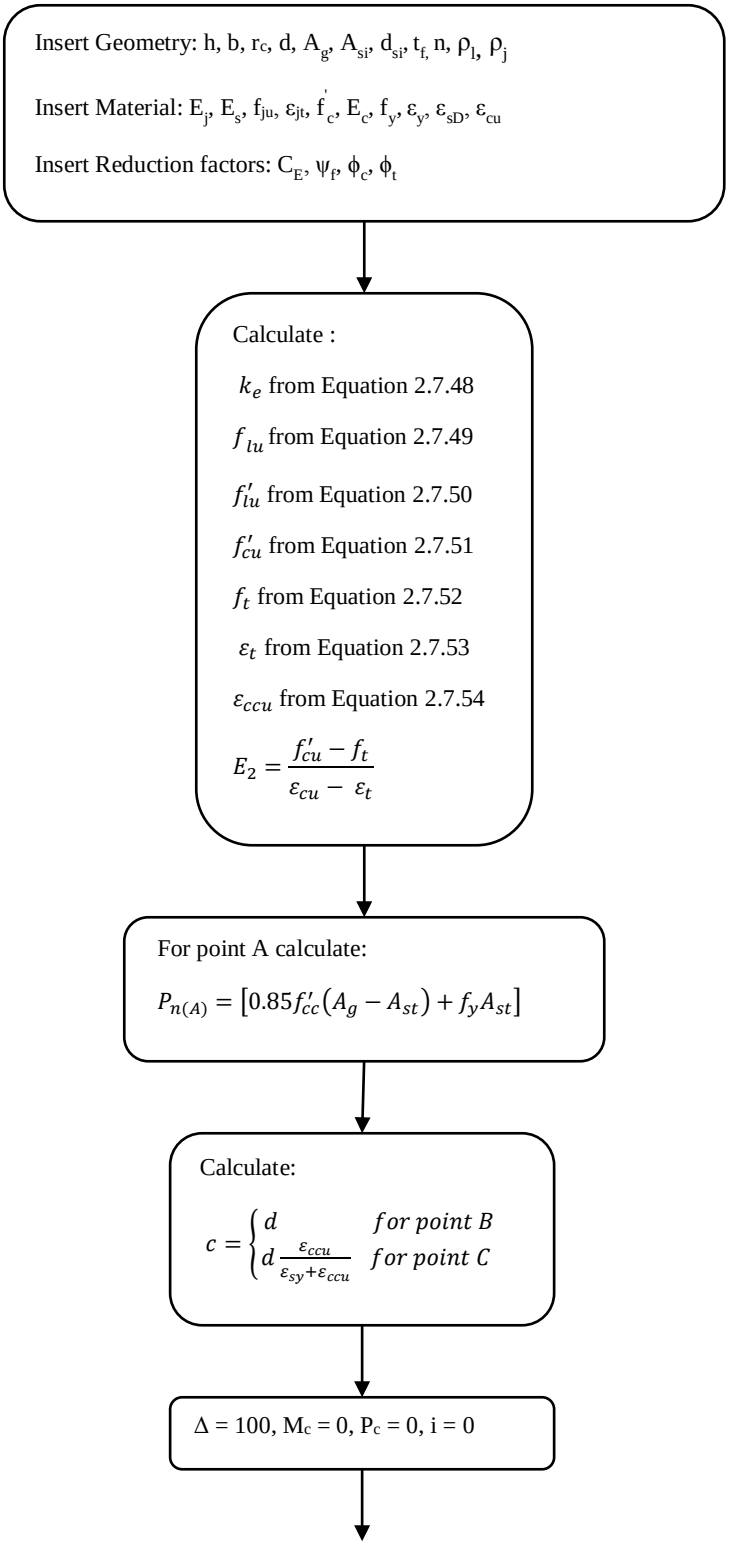
Insert Geometry: h, b, r_c, d, A_g, A_{si}, d_{si}, t_f, n, ρ_l, ρ_j
Insert Material: E_j, E_s, f_{ju}, ε_{jt}, f'_c, E_c, f_y, ε_y, ε_{sD}, ε_{cu}
Insert Reduction factors: C_E, ψ_f, ϕ_c, ϕ_t
Calculate :
k_e from Equation 2.7.48
f_{lu} from Equation 2.7.49
f'_{lu} from Equation 2.7.50
f'_{cu} from Equation 2.7.51
f_t from Equation 2.7.52
ε_t from Equation 2.7.53
ε_{ccu} from Equation 2.7.54
$E_2 = \frac{f'_{cu} - f_t}{\varepsilon_{cu} - \varepsilon_t}$
For point A calculate:
$P_{n(A)} = [0.85 f'_{cc}(A_g - A_{st}) + f_y A_{st}]$
Calculate:
$c = \begin{cases} d & for\ point\ B \\ d\frac{\varepsilon_{ccu}}{\varepsilon_{sy}+\varepsilon_{ccu}} & for\ point\ C \end{cases}$
$\Delta = 100$, $M_c = 0$, $P_c = 0$, i = 0

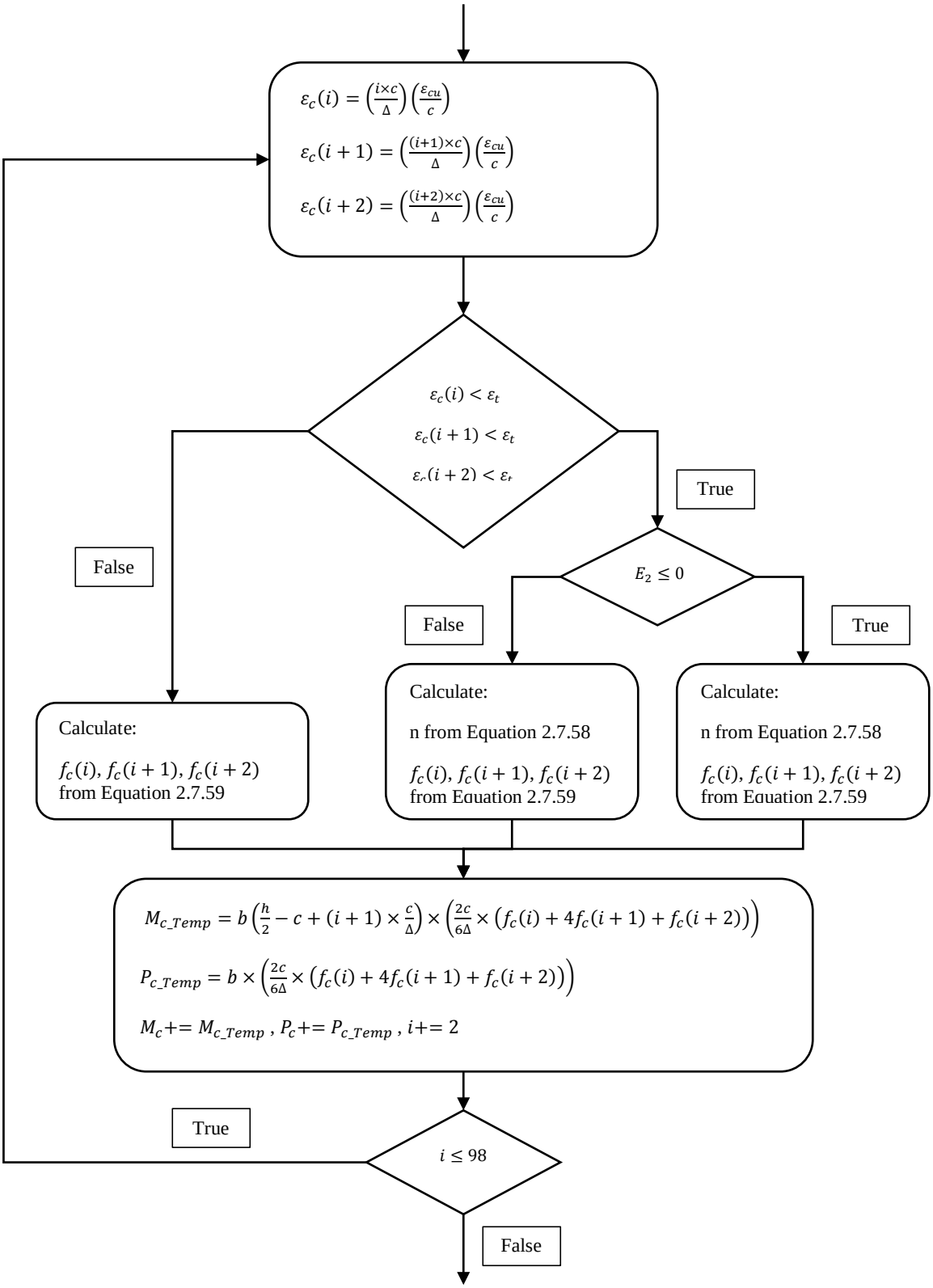
$\varepsilon_c(i) = \left(\frac{i \times c}{\Delta}\right)\left(\frac{\varepsilon_{cu}}{c}\right)$
$\varepsilon_c(i+1) = \left(\frac{(i+1) \times c}{\Delta}\right)\left(\frac{\varepsilon_{cu}}{c}\right)$
$\varepsilon_c(i+2) = \left(\frac{(i+2) \times c}{\Delta}\right)\left(\frac{\varepsilon_{cu}}{c}\right)$
$\varepsilon_c(i) < \varepsilon_t$
$\varepsilon_c(i+1) < \varepsilon_t$
$\varepsilon_c(i+2) < \varepsilon_t$
True
False
$E_2 \leq 0$
False
True
Calculate:
$f_c(i), f_c(i+1), f_c(i+2)$ from Equation 2.7.59
Calculate:
n from Equation 2.7.58
$f_c(i), f_c(i+1), f_c(i+2)$ from Equation 2.7.59
Calculate:
n from Equation 2.7.58
$f_c(i), f_c(i+1), f_c(i+2)$ from Equation 2.7.59
$M_{c\_Temp} = b\left(\frac{h}{2} - c + (i+1) \times \frac{c}{\Delta}\right) \times \left(\frac{2c}{6\Delta} \times \left(f_c(i) + 4f_c(i+1) + f_c(i+2)\right)\right)$
$P_{c\_Temp} = b \times \left(\frac{2c}{6\Delta} \times \left(f_c(i) + 4f_c(i+1) + f_c(i+2)\right)\right)$
M_c+= M_{c_Temp} , P_c+= P_{c_Temp} , i+= 2
True
$i \leq 98$
False

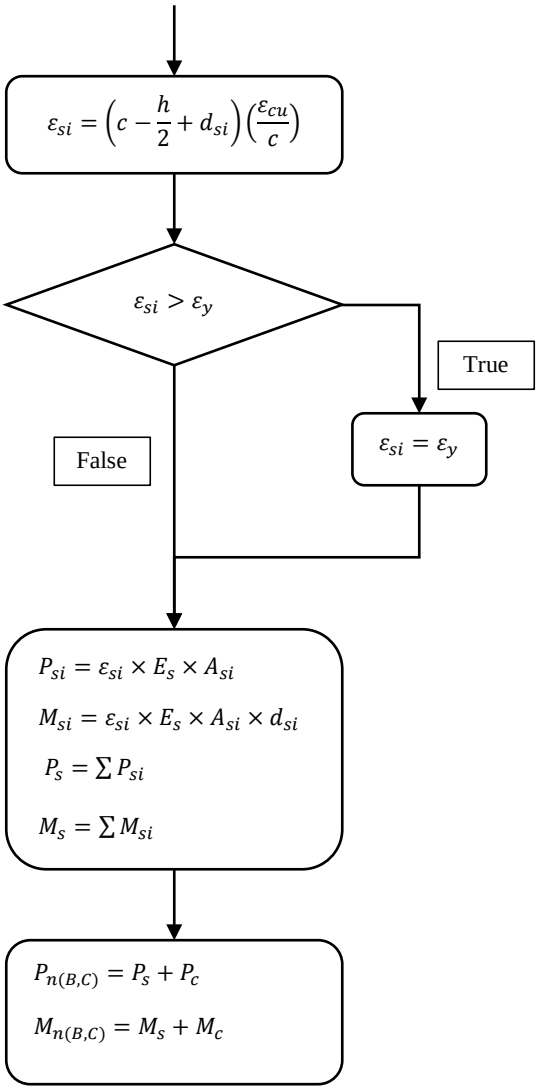

Figure 5.4-1 P-M diagram calculation algorithm based on Youssef et al. model

5.5 Interaction diagram development based on Faustino et al. (2014) model

For developing the P-M diagram based on the constitutive model by Faustino et al, points D and E can be calculated identically to that of previous models. However development of points A, B, and C of the P-M diagram are going to be based on Equations proposed by Faustino et al. The procedure for calculation of these points is illustrated in Figure 5.5-1. For calculation of points B and C instead of analytical integration of Equations 5.3.60 and 5.3.61, numerical integration technique (Simpson's rule) is implemented in excel macro. All the notations used in the Equations are summarized in Table 5.5-1.

Notation	Description
A_g	Total cross-sectional area
A_{si}	Total area of longitudinal rebars in “ith” layer from top (extreme compressive fiber) of cross section
A_s	Total area of all longitudinal rebars
A_{sw}	Total area of transverse reinforcement
b	Width of the cross section
B	Equivalent diameter of the rectangular section
b_w	Width of the transverse reinforcement
c	Distance from neutral axis position to the extreme compression fiber in the cross-section
C_E	Environmental reduction factor (taken 0.95)
d	Depth of the cross section (distance from extreme compressive fiber to the extreme tensile reinforcement)
d_{si}	Distance from position of the “ith” layer of longitudinal steel reinforcement to geometric centroid of the cross-section
d_w	Equivalent diameter of the transverse reinforcement
h	Depth of the cross section
h_w	Depth of the transverse reinforcement
R	Corner radius of the cross section
E_c	Initial modulus of elasticity of concrete
E_f	Modulus of elasticity of FRP
E_s	Modulus of elasticity of steel reinforcement
E_1	Initial slope of the first branch of stress strain curve
E_2	Slope of the second (linear) branch of the stress strain curve
f_{c0}	Standard cylindrical compressive strength of concrete
f_{cc}	Peak compressive strength of FRP confined concrete
f_{fu}	Ultimate tensile strength of FRP
f_{ju}	Lateral confining stress at ultimate condition due to FRP
f_{lu}	Lateral confining stress at ultimate condition due to FRP and transverse reinforcement
f_{shu}	Lateral confining stress at ultimate condition due to transverse reinforcement
f_{si}	Normal stress of longitudinal rebars in “ith” layer from top (extreme compressive fiber) of cross section
f_{sw}	Tensile strength of transverse reinforcement
f_t	Axial stress at the boundary point of the first and second region where the jacket is beginning to get fully activated
f_y	Yield strength of longitudinal steel reinforcement
k_1	Equation coefficient = 3.7
k_2	Equation coefficient = 18.89
n	Stress strain Equation parameter (taken as 3)
n_f	Number of FRP wraps
S	Spacing of transverse reinforcement
t	FRP nominal ply thickness
α	Depth of the equivalent stress block
β	The coefficient for equivalent compressive stress block ($0.65 \leq \beta = 0.85 - 0.05\frac{f_c' - 4000}{1000} \leq 0.85$)
ε_{c0}	Axial compressive strain corresponding to f'_c
ε_{cu}	Ultimate axial compressive strain of unconfined concrete = 0.003 mm/mm
ε_{cc}	Ultimate axial compressive strain of confined concrete
ε_{fu}	Ultimate tensile strain of FRP jacket
ε_{lu}	Lateral ultimate effective tensile strain of FRP jacket
ε_{sD}	Strain of longitudinal reinforcement closest to the extreme tensile fiber at point D (0.005)
ε_{si}	Strain of longitudinal rebars in “ith” layer from top (extreme compressive fiber) of cross section
ε_y	Yield strain of steel rebars
ψ_f	Additional FRP strength reduction factor
ϕ_c	Strength reduction factor for compression controlled failure
ϕ_t	Strength reduction factor for tension controlled failure

ρ_j	Volumetric ration of FRP jacket
ρ_g	Ratio of total longitudinal reinforcement area to total cross section area of the column A_s/A_g

Table 5.5-1 Notation for Faustino et al. model

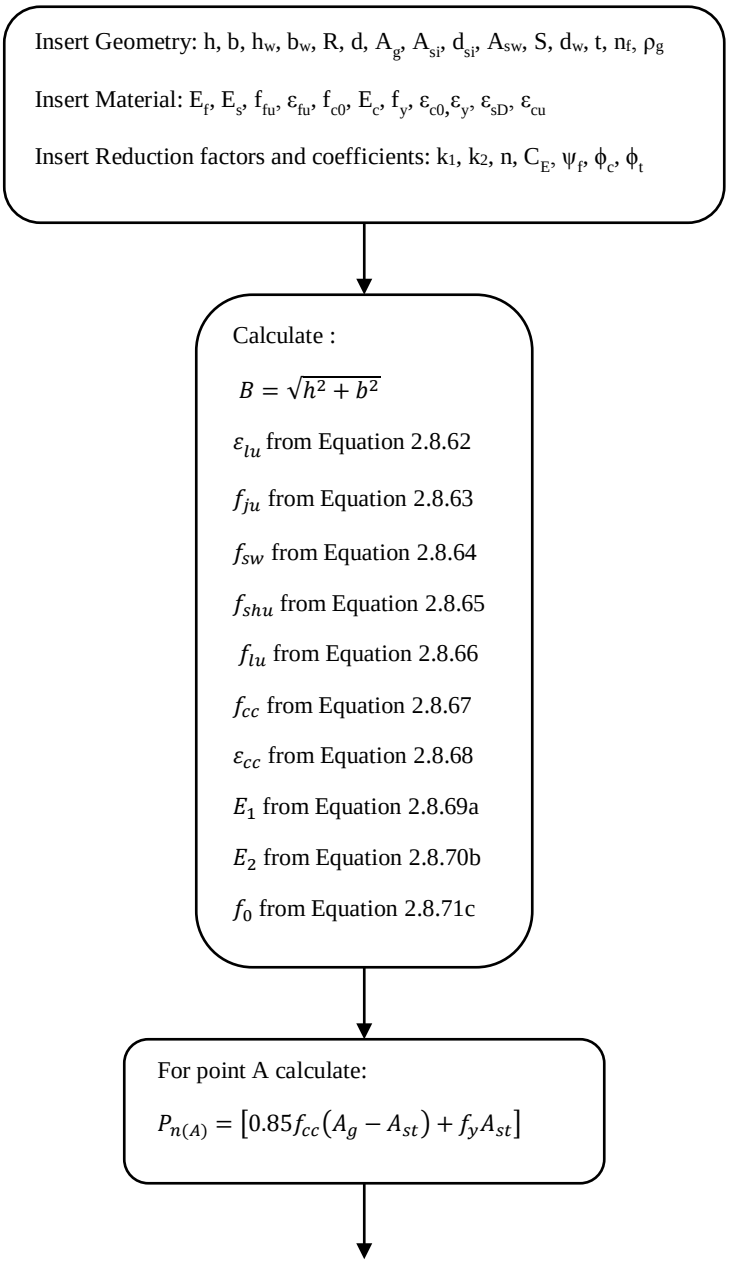

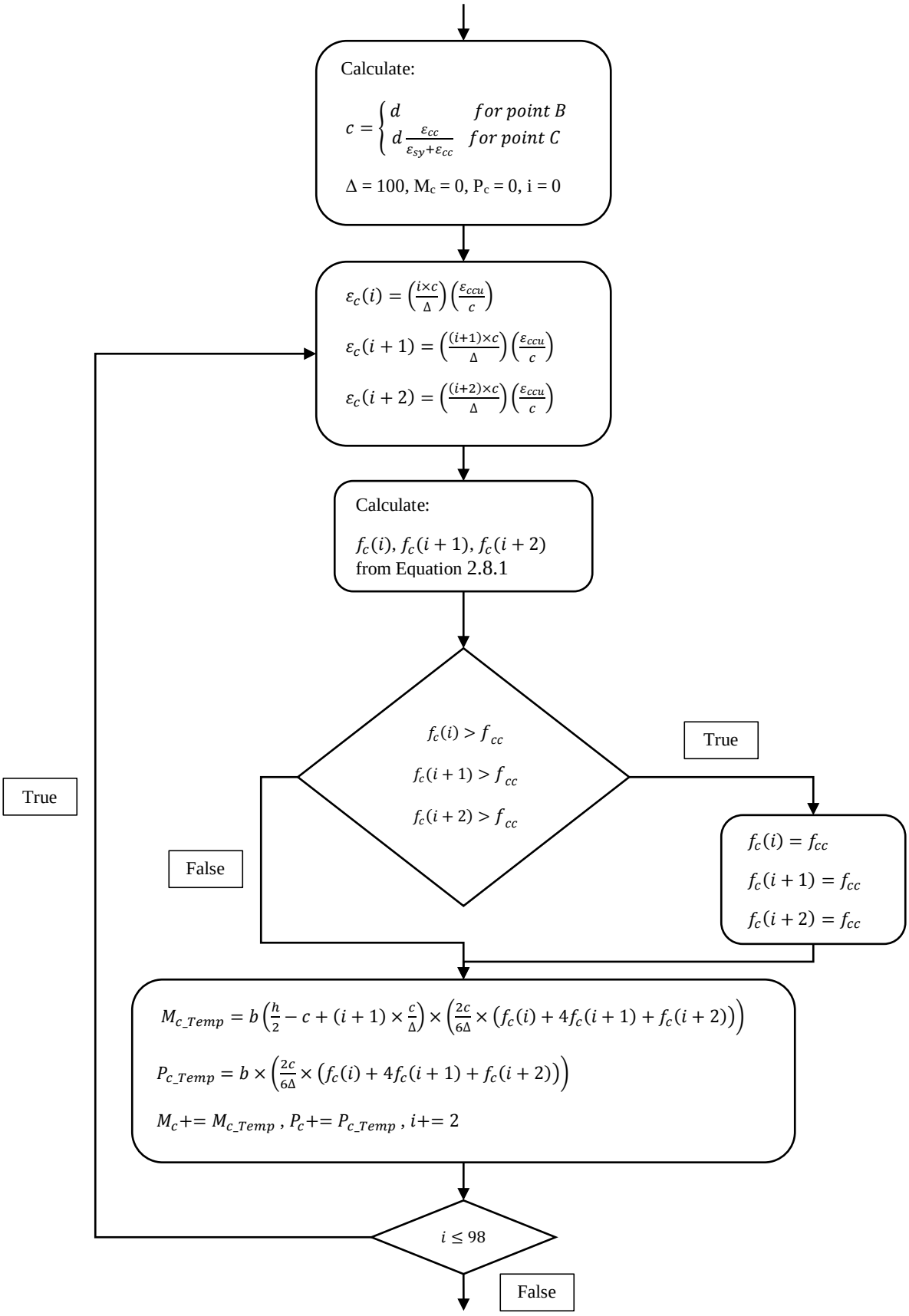
Calculate:
$c = \begin{cases} d & for\ point\ B \\ d\frac{\varepsilon_{cc}}{\varepsilon_{sy}+\varepsilon_{cc}} & for\ point\ C \end{cases}$
$\Delta = 100$, $M_c = 0$, $P_c = 0$, $i = 0$
$\varepsilon_c(i) = \left(\frac{i \times c}{\Delta}\right)\left(\frac{\varepsilon_{ccu}}{c}\right)$
$\varepsilon_c(i+1) = \left(\frac{(i+1) \times c}{\Delta}\right)\left(\frac{\varepsilon_{ccu}}{c}\right)$
$\varepsilon_c(i+2) = \left(\frac{(i+2) \times c}{\Delta}\right)\left(\frac{\varepsilon_{ccu}}{c}\right)$
Calculate:
$f_c(i), f_c(i+1), f_c(i+2)$
from Equation 2.8.1
$f_c(i) > f_{cc}$
$f_c(i+1) > f_{cc}$
$f_c(i+2) > f_{cc}$
True
False
$f_c(i) = f_{cc}$
$f_c(i+1) = f_{cc}$
$f_c(i+2) = f_{cc}$
$M_{c\_Temp} = b\left(\frac{h}{2} - c + (i+1) \times \frac{c}{\Delta}\right) \times \left(\frac{2c}{6\Delta} \times \left(f_c(i) + 4f_c(i+1) + f_c(i+2)\right)\right)$
$P_{c\_Temp} = b \times \left(\frac{2c}{6\Delta} \times \left(f_c(i) + 4f_c(i+1) + f_c(i+2)\right)\right)$
M_c+= M_{c_Temp} , P_c+= P_{c_Temp} , i+= 2
$i \leq 98$
True
False

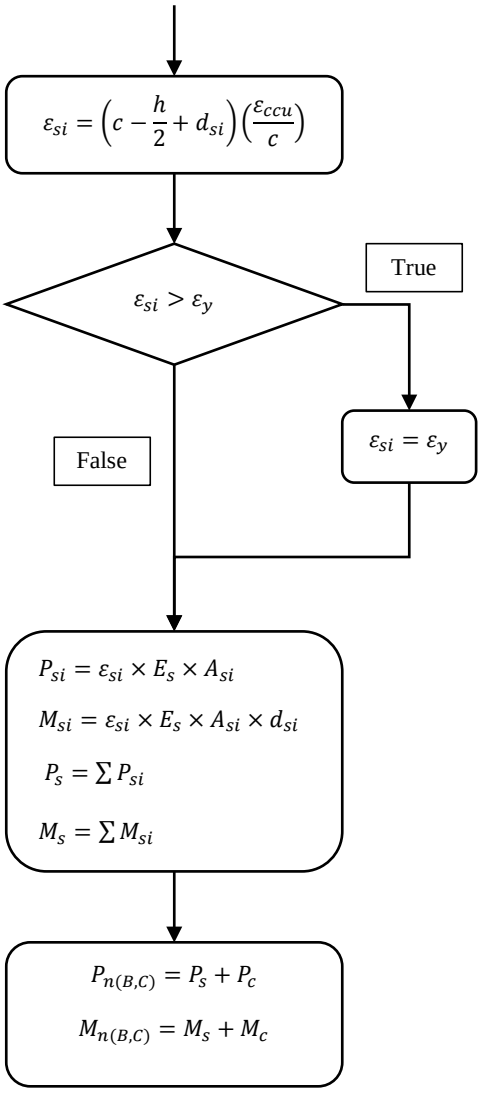

Figure 5.5-1 P-M diagram calculation algorithm based on Faustino et al. model

5.6 Interaction diagram development based on Eid and Paultre (2017) model

For developing the P-M diagram based on the constitutive model by Eid and Paultre, points D and E can be calculated identically to that of previous models. However development of points A, B, and C of the P-M diagram are going to be based on Equations proposed by Eid and Paultre. The procedure for calculation of these points is illustrated in Figure 5.6-1. For calculation of points B and C instead of analytical integration of Equations 5.3.2 and 5.3.3, numerical integration technique (Simpson's rule) is implemented in excel macro. All the notations used in the Equations are summarized in Table 5.6-1. Since after the rupture of FRP wraps specimens' strength degraded severely as mentioned in previous chapter, in Equation 2.9.4 the post FRP rupture region ($\epsilon_c > \epsilon_{cu}$) is not considered for developing P-M diagrams.

Notation	Description
A_g	Total cross-sectional area
A_{si}	Total area of longitudinal rebars in “ith” layer from top (extreme compressive fiber) of cross section
A_{st}	Total area of all longitudinal rebars
A_{shx}	Total cross-sectional area of transverse reinforcement within spacing “s” and perpendicular to direction x (rebars along width of the column cross section)
A_{shy}	Total cross-sectional area of transverse reinforcement within spacing “s” and perpendicular to direction y (rebars along depth of the column cross section)
b	Width of the cross section
c	Distance from neutral axis position to the extreme compression fiber in the cross-section
C_E	Environmental reduction factor (taken 0.95)
c_x	Width of the column’s core parallel to the x direction (along width of the column cross section)
c_y	Width of the column’s core parallel to the y direction (along depth of the column cross section)
D	Equivalent diameter of the rectangular section
d	Depth of the cross section (distance from extreme compressive fiber to the extreme tensile reinforcement)
d_{si}	Distance from position of the “ith” layer of longitudinal steel reinforcement to geometric centroid of the cross-section
E_{ct}	Tangent modulus of elasticity of concrete
E_f	Modulus of elasticity of FRP
E_{fl}	FRP lateral modulus
E_s	Modulus of elasticity of steel reinforcement
E_1	Initial slope of the first branch of stress strain curve
E_2	Slope of the second (linear) branch of the stress strain curve
f'_c	Standard cylindrical compressive strength of concrete
f_{cu}	Ultimate concrete strength
f_{hy}	Yield strength of transverse reinforcement
f_{ly}	Yield strength of longitudinal reinforcement
f_{shu}	Lateral confining stress at ultimate condition due to transverse reinforcement
f_{si}	Normal stress of longitudinal rebars in “ith” layer from top (extreme compressive fiber) of cross section
h	Depth of the cross section
I'_e	Effective confinement index evaluated at concrete peak stress
I_{e50}	Effective confinement index evaluated at ϵ_{cc50}
K_f	Geometrical effectiveness coefficient of FRP confinement
K_h	Horizontal arching geometrical effectiveness coefficient of steel reinforcement confinement
K_v	Vertical arching geometrical effectiveness coefficient of steel reinforcement confinement
k_1,k_2	Parameters controlling the shape of the stress-strain post-peak branch of stress-strain curve
n_f	Number of FRP wraps
N_{ix}	Number of spaces between longitudinal bars in x direction
N_{iy}	Number of spaces between longitudinal bars in y direction
r_c	Corner radius of the cross section
s	Center-to-center transverse reinforcement spacing
s'	Clear TSR spacing
w_{ix}	Clear horizontal spacing between two adjacent laterally supported longitudinal bars in x direction
w_{iy}	Clear horizontal spacing between two adjacent laterally supported longitudinal bars in y direction
t	FRP nominal ply thickness
α	Depth of the equivalent stress block
β	The coefficient for equivalent compressive stress block $(0.65 \leq \beta = 0.85 - 0.05\frac{f'_c - 4000}{1000} \leq 0.85)$
ϵ'_c	Axial compressive strain corresponding to f'_c
ϵ'_{cc}	Axial strain at peak strength of confined concrete
ϵ_{cu}	Ultimate axial compressive strain of unconfined concrete = 0.003 mm/mm
$\epsilon_{fu,a}$	Actual ultimate tensile strain of FRP jacket
ϵ_{fu}	Ultimate tensile strain of FRP jacket

ϵ_{hy}	Yield strain of transverse reinforcement
ϵ_{sD}	Strain of longitudinal reinforcement closest to the extreme tensile fiber at point D (0.005)
ϵ_{si}	Strain of longitudinal rebars in "ith" layer from top (extreme compressive fiber) of cross section
ϵ_{c50}	Postpeak axial strain in unconfined concrete when capacity drops to 50% of unconfined concrete
ϵ_{cc50}	Postpeak axial strain in confined concrete when capacity drops to 50% of confined strength
κ_1, κ_2	Parameters used to determine whether yielding of the lateral reinforcement occurs at peak strength of confined concrete
η	Parameter used to determine the lateral strain at concrete peak stress
γ_{sf}	Ratio of $\epsilon_{hy}/\epsilon_{fu}$
ψ_f	Additional FRP strength reduction factor
ϕ_c	Strength reduction factor for compression controlled failure
ϕ_t	Strength reduction factor for tension controlled failure
ρ_{cc}	Ratio between the longitudinal reinforcement area and the core section area
ρ_g	Ratio of total longitudinal reinforcement area to total cross section area of the column A_s/A_g
ρ_{se}	Effective sectional ratio of confinement reinforcement
ν'_{cc}	Secant Poisson's ratio of concrete at peak stress
ξ	Efficiency factor = $\epsilon_{fu,a}/\epsilon_{fu}$

Table 5.6-1 Notation for Eid and Paultre model

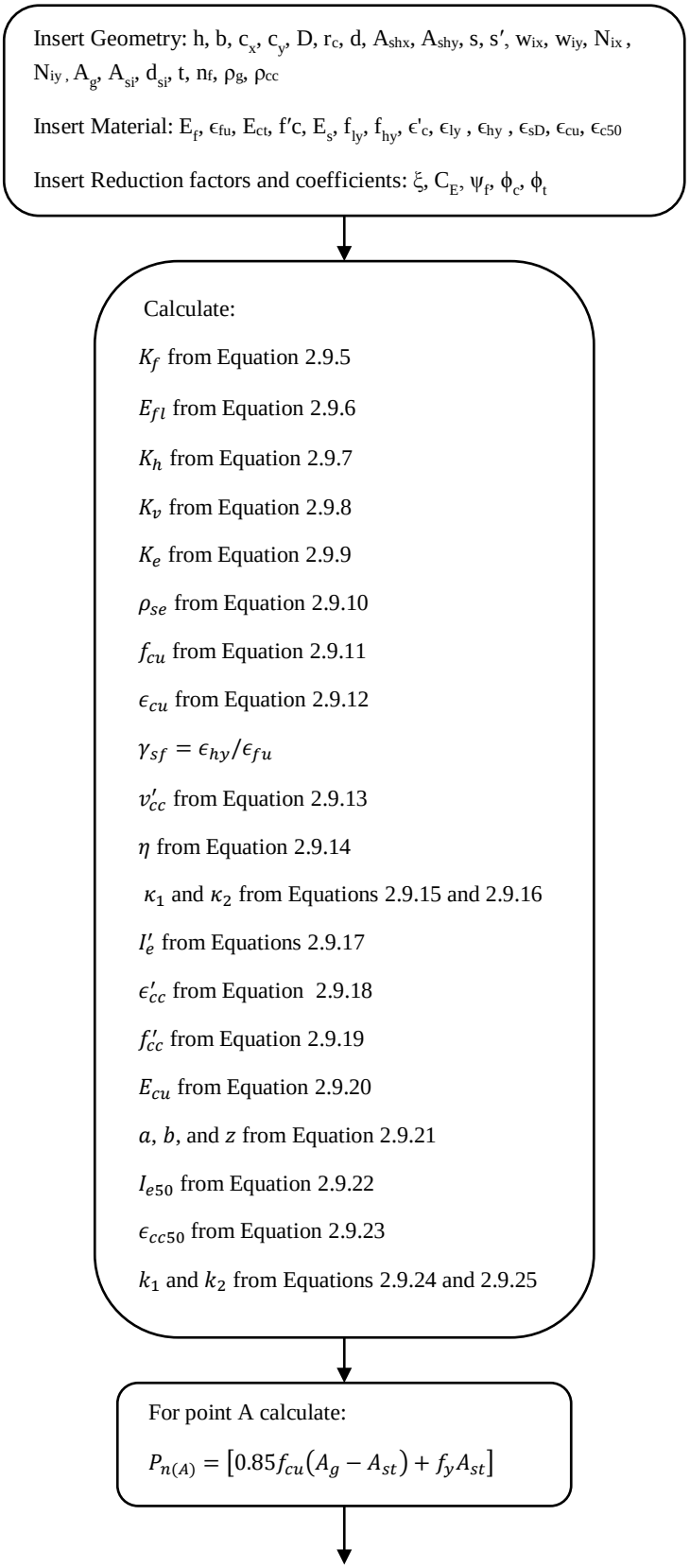
Insert Geometry: h, b, c_x, c_y, D, r_c, d, A_{shx}, A_{shy}, s, s′, w_{ix}, w_{iy}, N_{ix} , N_{iy} , A_g, A_{si}, d_{si}, t, n_f, ρ_g, ρ_{cc}
Insert Material: E_f, ϵ_{fu}, E_{ct}, f′c, E_s, f_{ly}, f_{hy}, ϵ'_c, ϵ_{ly} , ϵ_{hy} , ϵ_{sD}, ϵ_{cu}, ϵ_{c50}
Insert Reduction factors and coefficients: ξ, C_E, ψ_f, ϕ_c, ϕ_t
Calculate:
K_f from Equation 2.9.5
E_{fl} from Equation 2.9.6
K_h from Equation 2.9.7
K_v from Equation 2.9.8
K_e from Equation 2.9.9
ρ_{se} from Equation 2.9.10
f_{cu} from Equation 2.9.11
ϵ_{cu} from Equation 2.9.12
$\gamma_{sf} = \epsilon_{hy}/\epsilon_{fu}$
v'_{cc} from Equation 2.9.13
η from Equation 2.9.14
κ_1 and κ_2 from Equations 2.9.15 and 2.9.16
I'_e from Equations 2.9.17
ϵ'_{cc} from Equation 2.9.18
f'_{cc} from Equation 2.9.19
E_{cu} from Equation 2.9.20
a, b, and z from Equation 2.9.21
I_{e50} from Equation 2.9.22
ϵ_{cc50} from Equation 2.9.23
k_1 and k_2 from Equations 2.9.24 and 2.9.25
For point A calculate:
$P_{n(A)} = [0.85 f_{cu}(A_g - A_{st}) + f_y A_{st}]$

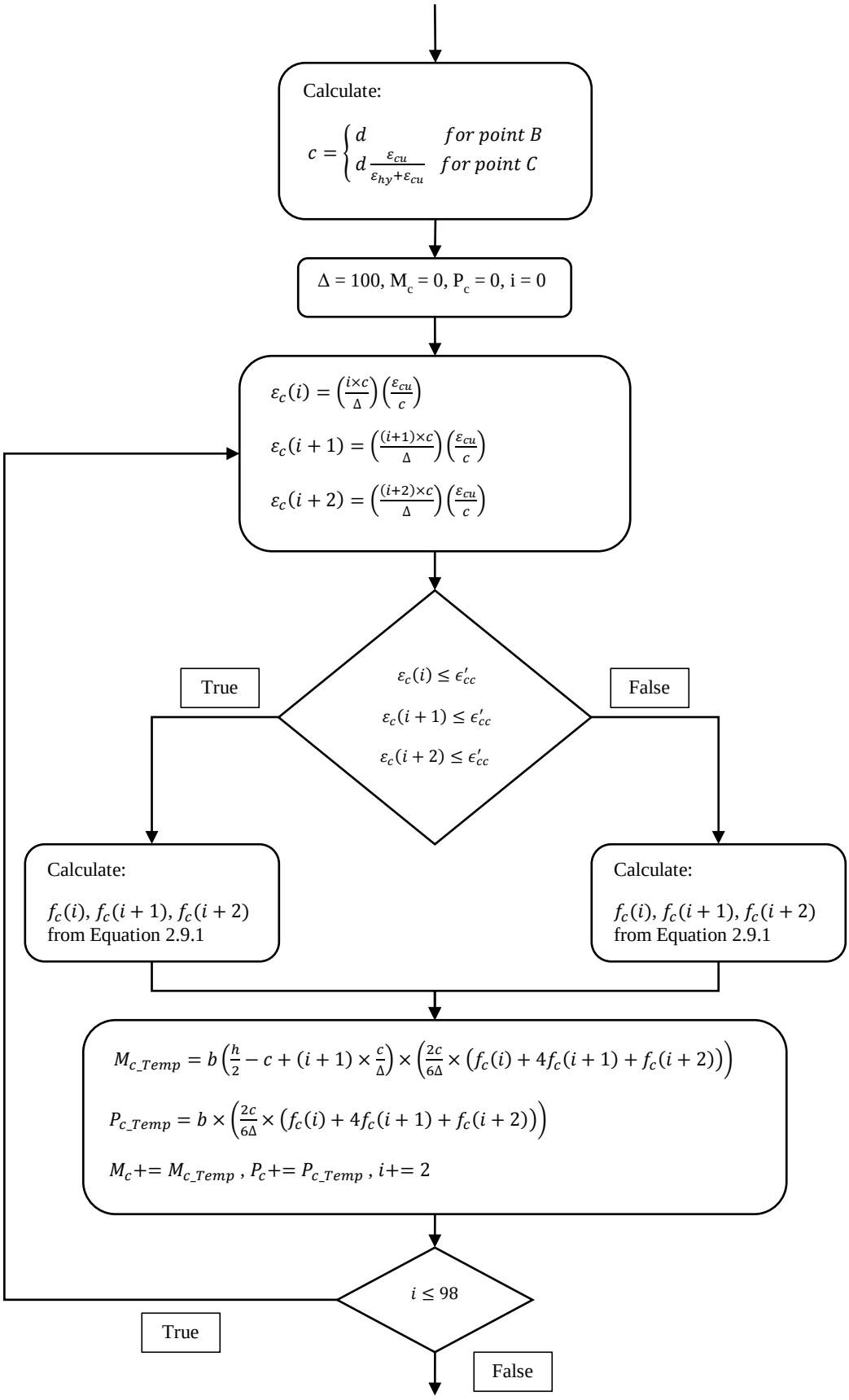
Calculate:
$c = \begin{cases} d & for\ point\ B \\ d\frac{\varepsilon_{cu}}{\varepsilon_{hy}+\varepsilon_{cu}} & for\ point\ C \end{cases}$
$\Delta = 100$, $M_c = 0$, $P_c = 0$, i = 0
$\varepsilon_c(i) = \left(\frac{i\times c}{\Delta}\right)\left(\frac{\varepsilon_{cu}}{c}\right)$
$\varepsilon_c(i+1) = \left(\frac{(i+1)\times c}{\Delta}\right)\left(\frac{\varepsilon_{cu}}{c}\right)$
$\varepsilon_c(i+2) = \left(\frac{(i+2)\times c}{\Delta}\right)\left(\frac{\varepsilon_{cu}}{c}\right)$
$\varepsilon_c(i) \le \epsilon'_{cc}$
$\varepsilon_c(i+1) \le \epsilon'_{cc}$
$\varepsilon_c(i+2) \le \epsilon'_{cc}$
True
False
Calculate:
$f_c(i), f_c(i+1), f_c(i+2)$
from Equation 2.9.1
Calculate:
$f_c(i), f_c(i+1), f_c(i+2)$
from Equation 2.9.1
$M_{c\_Temp} = b\left(\frac{h}{2} - c + (i+1)\times\frac{c}{\Delta}\right)\times\left(\frac{2c}{6\Delta}\times\left(f_c(i) + 4f_c(i+1) + f_c(i+2)\right)\right)$
$P_{c\_Temp} = b\times\left(\frac{2c}{6\Delta}\times\left(f_c(i) + 4f_c(i+1) + f_c(i+2)\right)\right)$
M_c+= M_{c_Temp} , P_c+= P_{c_Temp} , i+= 2
$i \le 98$
True
False

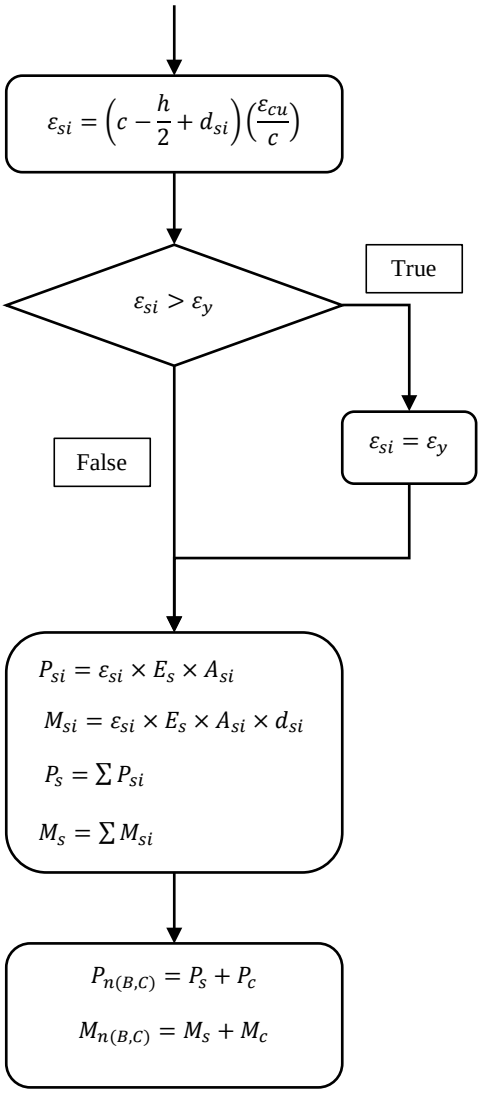

Figure 5.6-1 P-M diagram calculation algorithm based on Eid and Paultre model

5.7 Comparison of models with experimental results

The experimental P-M interaction diagrams are compared to those of the models in Figures 5.7-1**,** 5.7-2**,** and 5.7-3 for one, two, and three wrap layers of CFRP, respectively. In the case of columns with 1 CFRP wrap, as shown in Figure 5.7-1, models by Lam and Teng. (2003a), Youssef et al. (2007), and Faustino et al. (2014) predict the ultimate flexural capacity of the column in the compression controlled zone with good accuracy however in these models the axial capacity is underestimated. On the contrary, model proposed by Eid and Paultre (2017) (Figures 5.7-1 (d)) yields a closer estimation of axial capacity while flexural capacity is underestimated. Underestimation of ultimate axial load by models proposed by Lam and Teng (2003a) and Youssef et al. (2007) can be associated with the fact that they neglect the effect of transverse reinforcement in calculation of the confined concrete strength (either f'_{cc} or f'_{cu}). With regards to the model by Faustino et al (2014), the parameter k_1 in Equation 2.8.4 is based on a database of experimental studies in which the unconfined concrete was from low to mid strength (below 35 MPa) and this can create some errors when predicting the confined concrete strength and as a result axial capacity of columns in the current study with 48 MPa unconfined concrete strength.

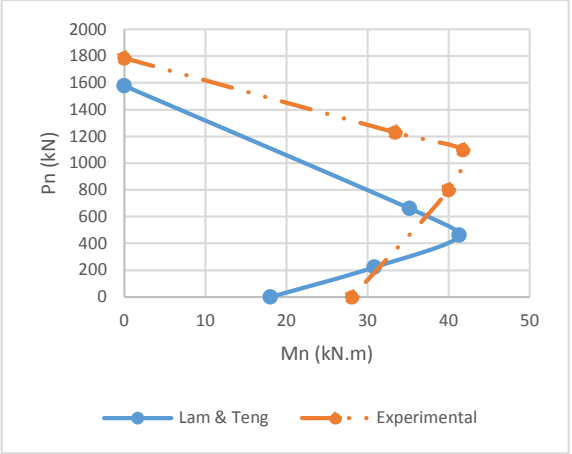

(a)

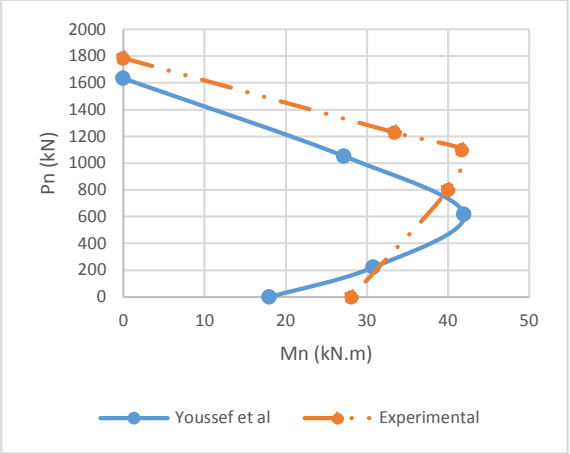

(b)

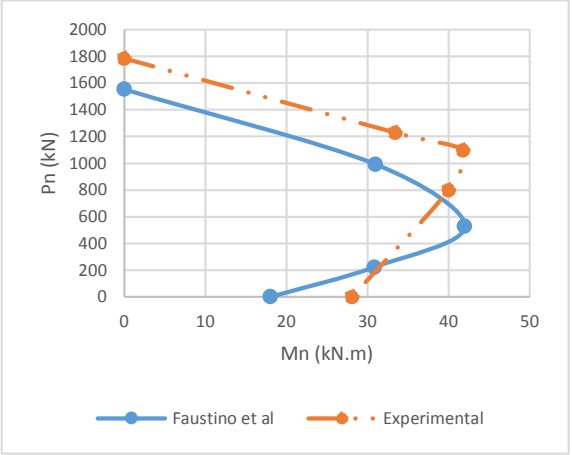

(c)

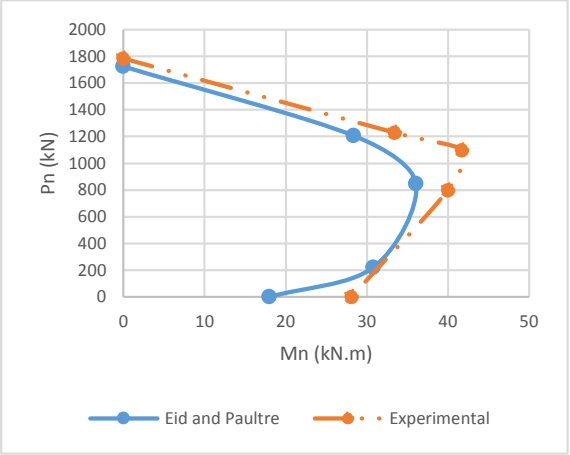

(d)

Figure 5.7-1 Experimental vs Model P-M interaction diagram (one CFRP wrap layer)

In the case of columns with two CFRP wraps, as shown in Figure 5.7-2, models by Lam and Teng (2003a), Faustino et al. (2014), and Eid & Paultre (2017) estimate the flexural capacity in compression controlled zone with a good accuracy while model by Youssef et . (2007) overestimates the flexural capacity especially at balanced failure point which is not conservative. Model by Lam and Teng (2003a) underestimates the axial capacity by a considerable margin (-32% difference with experimental results) while model by Faustino et al. (2014) has a better prediction of axial capacity, it still is conservative and is underestimating the axial force. Models by Youssef et al. (2007) and Eid & Paultre (2017) have the closest estimation of axial capacity of the columns.

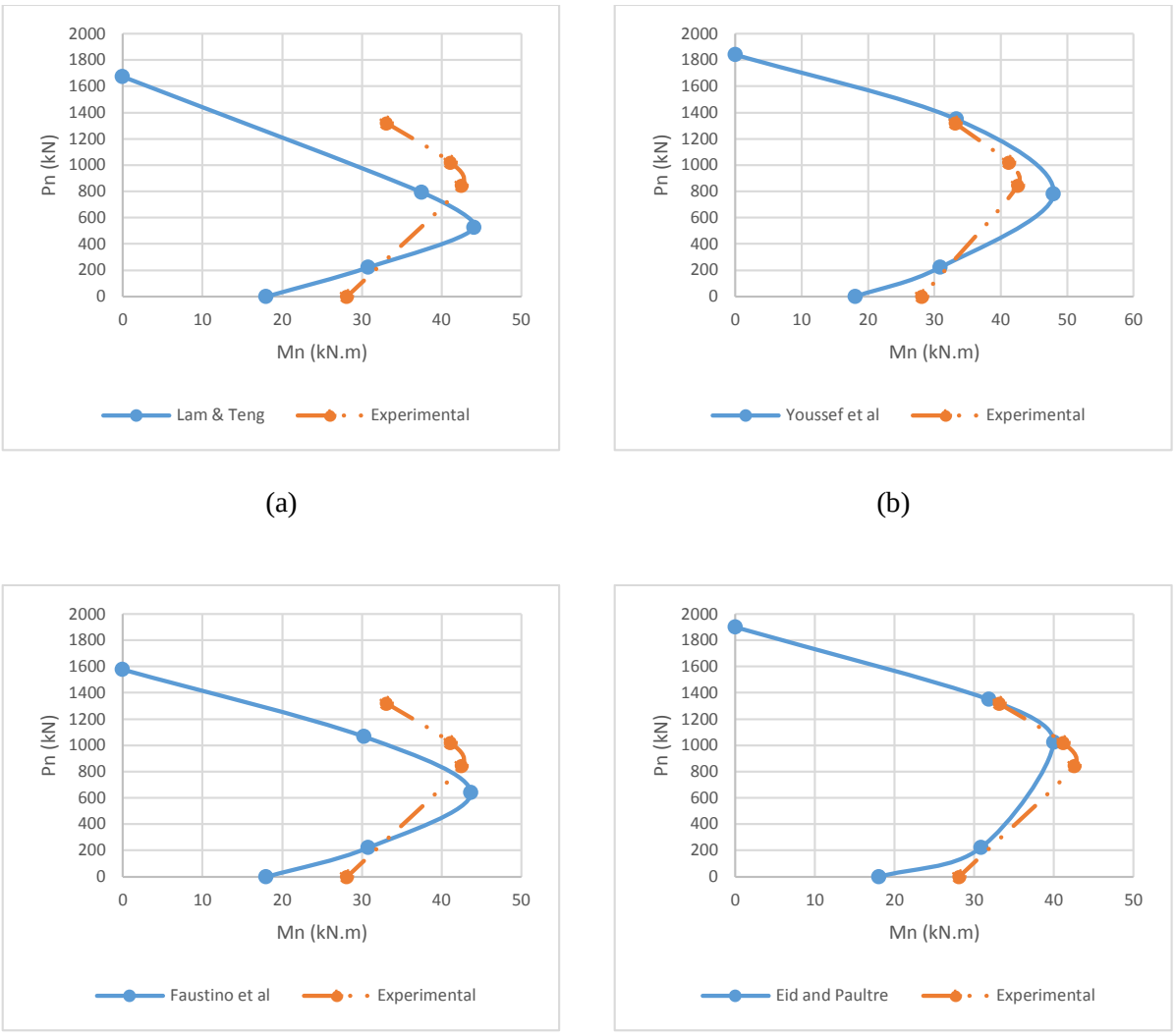

Figure 5.7-2 Experimental vs Model P-M interaction diagram (two CFRP wrap layers)

In the case of columns with three FRP wraps, as shown in Figure 5.7-3, Models by Lamand Teng (2003a), Youssef et al. (2007), and Eid & Paultre (2017) predict the flexural capacity in the compression controlled zone with good accuracy whereas model by Youssef is overestimating the flexural capacity. In terms of axial capacity, Models by Lam and Teng (2003a) and Faustino et al. (2014) underestimate while models by Youssef and Eid & Paultre overestimate the axial force of the column.

Another reason for considerable underestimation of axial forces in model by Lam and Teng (2003a) can be the fact that in the compression controlled zone (points that resemble a combined flexural and axial state of stress (Points B and C)) the ultimate strain of the concrete is limited to 0.004 following the recommendation by Rocca et al (2009).

By comparing models with results of specimens with 2 and 3 layers of wrap it can be seen that model by Eid & Paultre (2017) has a better fit to interaction diagram of specimens with 2 CFRP wraps while model

by Faustino et al. (2014) has a better fit to specimens with 3 layers of CFRP. The over estimation of axial loads for specimens with 3 CFRP wraps can be attributed to the fact that equations for calculation of f_{cu} and ϵ_{cu} (Equations 2.9.2 and 2.9.3) in Eid & Paultre model have higher coefficients and as a result higher contribution of steel and concrete confinement to the ultimate stress and strain as well as compressive resistance compared to equations developed by Faustino et al. (2.8.4 and 2.8.5). These higher coefficients in Eid and Paultre (2017) can be attributed to the fact that they included specimens with concrete strength as high as 80 MPa for calibration. Whereas the unconfined concrete compressive strength range for experimental data included in the study Faustino et al (2014) is below 35 MPa.

Overall by comparing the test results to the models for columns wrapped with 1, 2, and 3 CFRP wraps, it can be witnessed that the model developed by Eid & Paultre(2017) exhibit the best performance in predicting the P-M diagram of CFRP wrapped RC square columns. This close fit can be attributed to the fact that this model utilises the full 3D interaction of the internal reinforcement and CFRP wraps in modelling the behaviour of CFRP confined RC columns. The VBA source code and the excel spreadsheets developed for all four models have also been included in the Appendix for readers' reference.

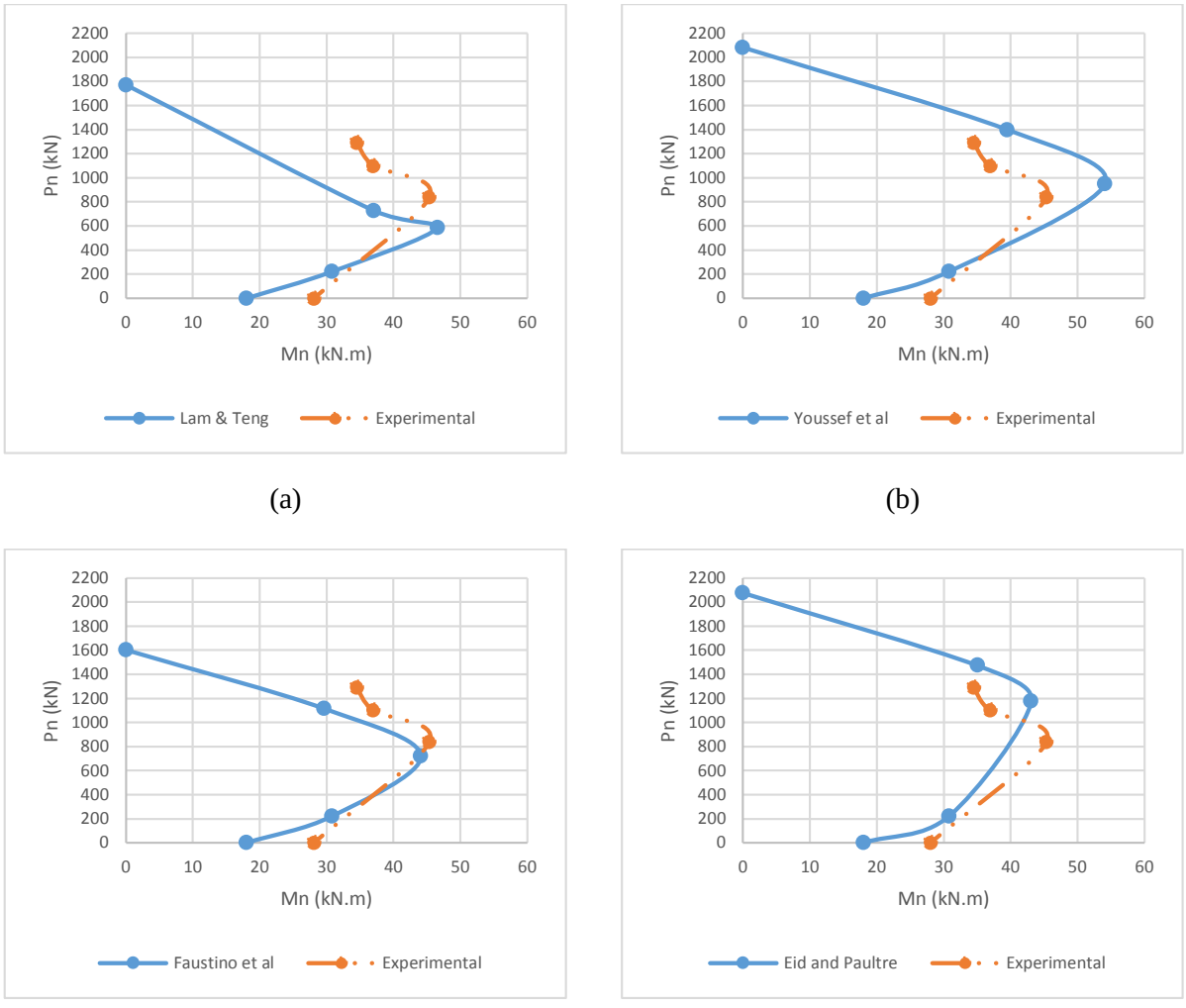

Figure 5.7-3 Experimental vs Model P-M interaction diagram (three CFRP wrap layers)

5.8 Summary

In this chapter four constitutive models for CFRP confined concrete column, namely Lam and Teng, Youssef et al, Faustino et al, and Eid & Paultre are considered for developing the P-M interaction diagram of the square shaped FRP confined RC columns. The algorithms for calculation of critical points using analytical as well as numerical stress integrations were developed. And finally the results are compared to those of the column tests. Among these models, the model proposed by Eid & Paultre demonstrated the best performance in the prediction of P-M interaction diagram. This can be attributed to consideration of interaction of CFRP and internal transverse reinforcement in developing this constitutive model.

6 Conclusions and recommendations

6.1 Introduction

In this study the behaviour of square shaped CFRP confined RC columns under combined flexure and compression is investigated. Due to scarcity of experimental data, tests were undertaken and potential of four analytical constitutive models in the calculation of P-M interaction diagram of these columns was investigated.

In the experimental phase, 18 RC columns with no wraps as well as one to three CFRP wraps were tested under concentric loading, eccentric loading (with three different eccentricities), and pure flexural loading and their corresponding axial stress, axial deflections, lateral deflections, and mid-height hoop strains were measured.

In the theoretical phase models by Lam and Teng, (2007), Youssef et al. (2007), Faustino et al. (2014), and Eid & Paultre (2017) were used to develop the P-M interaction diagrams and the accuracy of their estimations versus test results are compared. The conclusions of this study are as follows:

6.2 Conclusions

1. From column test results it is apparent that the ultimate load of the specimens for each eccentricity is increased by wrapping of the specimens. However there seems to be an ultimate load threshold by comparing the results of specimens with two and three wraps for which there is not much ultimate load improvement is observed and sometimes there are even some drops in ultimate load are observed.
2. Although in general an improvement in average hoop strain and mid-height lateral deflection of the wrapped columns is witnessed compared to that of unwrapped columns, no clear trend exists for these values when wrapped columns are compared to each other. The variability of average ultimate hoop strains can be attributed to longitudinal reinforcement buckling that causes high localized tensile strains in the CFRP jacket at the ultimate load. The longitudinal reinforcement buckling itself is a random phenomenon thus it creates discrepancies in the results.
3. Among the wrapped columns a clear increasing pattern is observed in the ductility of specimens when increasing the number of CFRP wraps. This trend in ductility improvement indicates the energy absorption capacity of columns can be increased by providing thicker jackets and resulting higher confinement pressures.
4. There is little evidence that CFRP wrapping increases the ultimate flexural capacity of the beam specimens, although their deformability is increased significantly. Also the brittle shear failure mode in unwrapped beams is changed to a ductile flexural failure mode in the CFRP wrapped specimens.
5. Among the models used in this study for calculation of P-M diagram, the model by Eid and Paultre (2008) seems to have the best fit with the experimental data. The reason for that can be attributed to the fact that this model considers a 3D refined interaction of internal transverse steel and the CFRP jacket when it is calculating the lateral confinement pressure.

6.3 Recommendation for future research

Although there are many studies on the behaviour of FRP wrapped columns under concentric load, performance of these columns (specifically with rectangular cross sections) under eccentric loading remains under investigated in terms both of experimental as well as theoretical studies.

Due to complexity of the nature of stress in FRP-encased rectangular RC columns under combined flexure and compression as well as tediousness of carrying out such tests on columns with real world dimensions, there needs to be a numerical (FEA) study conducted that adopts the advanced plasticity models to study this complex stress-strain field. Also, the interaction of internal transverse reinforcement as well as buckling of longitudinal reinforcement should be considered in such numerical studies.

Once the constitutive plasticity based models are verified with test results, they can be adopted to perform parametric study and propose more refined analytical constitutive models. Such models can also be adopted to develop P-M interaction diagrams that can be used by the codes and design specifications which assist structural engineers with their design calculations for the wrapped columns.

References

ASTM (2011). “Standard test method for compressive strength of cylindrical concrete specimens” C39/C39M-14a, West Conshohocken, PA.

ASTM (2014) “Standard test method for splitting tensile strength of cylindrical concrete specimens” C496/496M-11, West Conshohocken, PA.

Balmer, G. G. (1944). "Shearing strength of concrete under high triaxial stress computation of Mohr's envelope as a curve." *SP-23*, Structural Research Laboratory, U.S. Bureau of Reclamation.

Chaallal, O., and Shahawy, M. (2000). "Performance of fiber-reinforced polymer wrapped reinforced concrete column under combined axial-flexural loading." *ACI Struct. J.*, 97(4), 659–688.

Eid R, and Paultre P. (2008) "Analytical model for FRP-confined circular reinforced concrete columns." ASCE J Compos Construct ; 12(5):541–52.

Eid, R., and Paultre, P. (2017) "Compressive behavior of FRP-confined reinforced concrete columns" Engineering Structures, 132, 518-530.

Fam, A., Flisak, B., and Rizkalla, S. (2003). "Experimental and analytical modeling of concrete-filled fiber-reinforced polymer tubes subjected to combined bending and axial loads." *ACI Struct. J.*, 100(4), 1–11.

Fardis, M.N. and Khalili, H.(1982). "FRP-encased concrete as a structural material. " Magazine of Concrete Research, 34(122): 191-202.

Faustino, P., Chastre, C., and Paula, R. (2014) "Design model for square RC columns under compression confined with CFRP" Composites: Part B, 57, 187-198.

Hadi, M. N. S., and Li, J. (2004). "External reinforcement of high strength concrete columns." *Compos. Struct.*, 65(3–4), 279–287.

Hadi, M. N. S. (2006a). "Behaviour of FRP wrapped normal strength concrete columns under eccentric loading." *Compos. Struct.*, 72(4), 503–511.

Hadi, M. N. S. (2006b). "Comparative study of eccentrically loaded FRP wrapped columns." *Compos. Struct.*, 74(2), 127–35.

Hadi, M. N. S. (2007a). "Behaviour of FRP strengthened concrete columns under eccentric compression loading." *Compos. Struct.*, 77(1), 92–96.

Hadi, M. N. S. (2007b). "The behaviour of FRP wrapped HSC columns under different eccentric loads." *Compos. Struct.*, 78(4), 560–566.Hadi, M. N. S. and Widiarsa, I. B R., (2012) "Axial and flexural performance of square RC columns wrapped with CFRP under eccentric Loading".

Hognestad E. (1951) "A study of combined bending and axial load in reinforced concrete members." Bulletin no. 399, Univ. of Illinois, Eng. Experimental Station, Champaign.

Hoshikuma J, Kawashima K, Nagaya K, and Taylor AW. (1997) "Stress–strain model for confined reinforced concrete in bridge piers." J Struct Eng, 123(5): 624-633.

Karbhari, V.M. and Gao, Y. (1997). "Composite jacketed concrete under uniaxial compression – verification of simple design equations, " Journal of Materials in Civil Engineering, ASCE, 9(4): 185-193.

Lam, L. and Teng, JG. (2002) "Strength models for FRP-confined concrete." J Struct Eng, ASCE;128(5): 612 –23.

Lam, L. and Teng, J.G. (2003a) "Design-oriented stress-strain model for FRP-confined concrete" Construction and Building Materials, 17, 471-489

Lam, L. and Teng, J.G. (2003b) "Design-oriented stress-strain model for FRP-confined concrete in rectangular columns" Journal of Reinforced Plastics and Composites, 22(13), 1149-1186.

Legeron, F. and Paultre, P. (2003) "Uniaxial confinement model for normal- and high-strength concrete columns." J Struct Eng, 129(2):241-252.

Lei, X., Pham, T.M. and Hadi, M.N.S. (2012) "Behaviour of CFRP wrapped square RC columns under eccentric loading." Australasian structural engineering conference, Perth, Australia.

Li, J. and Hadi, M. N. S. (2003). "Behaviour of externally confined high strength concrete columns under eccentric loading." *Compos. Struct.*, 62(2), 145–153.

Lignola, G. P., Prota, A., Manfredi, G., Cosenza, E. (2007). "Experimental performance of RC hollow columns confined with CFRP. " *J. Compos. Constr.*, 11(1), 42–49.

Mander, J. B., Priestley, M. J. N., and Park, R. (1984). "Seismic design of bridge piers." *Research Report No. 84-2,* Univ. of Canterbury, New Zealand.

Mander, J.B., Priestley, M.J.N., and Park, R. (1988) "Theoretical Stress-Strain Model For Confined Concrete" J. Struct. Eng., 114(8), 1804-1826.

Mirrniran, A. (1996). "Analytical and experimental investigation of reinforced concrete columns encased in fiberglass tubular jackets and use of fiber jacket for pile splicing." *Final Rep.. Contract No. B-9135,* Florida Dept. of Transp., Tallahassee, Fla.

Mirmiran, A., and Shahawy, M. (1996). "A new concrete-filled hollow FRP composite column." *Composites Part B: Engrg.*, 27B(3-4), 263-268, Elsevier Science Ltd., London, U.K.

Mirmiran, A., Shahawy, M. (1997). "Behavior of concrete columns confined by fiber composites" J. Struct. Eng. 123(5), 583-590.

Mirmiran, A., Shahawy, M., Samaan, M., Echary, H. E., Mastrapa, J. C., and Pico, O. (1998). "Effect of Column Parameters on FRP-Confined Concrete." Journal of Composites for Construction, 2(4), 175.

Miyauchi, K., Inoue, S., Kuroda, T. and Kobayashi, A. (1999). "Strengthening effects of concrete columns with carbon fiber sheet." Transactions of The Japan Concrete Institute, 21:143-150.

Ozbakkaloglu, T., Lim, J. C., Vincent, T. (2013). "FRP-confined concrete in circular sections: Review and assessment of stress-strain models" Engineering Structures, 49, 1068-1088.

Parvin A., and Wang, W. (2001). "Behaviour of FRP jacketed concrete columns under eccentric loading." *J. Compos. Constr.*, 5(3), 146–152.

Parvin, A., and Wang, W. (2002). "Concrete columns confined by fiber composite wraps under combined axial and cyclic lateral loads." Composite Structures, 58(4), 539-549.

Richard RM, Abbott BJ. (1975) "Versatile elastic-plastic stress–strain formula." ASCE J Eng Mech Div; 101(4):511–5.

Richart, F. E., Brandtzaeg, A., and Brown, R. L. (1928). "A study of the failure of concrete under combined compressive stresses." *Bulletin 185,* Univ. of Illinois Engineering Experimental Station, Champaign, 111.

Rocca, S., Galati, N., Nanni, A. (2009) "Interaction diagram methodology for design of FRP-confined reinforced concrete columns." Construction and Building Materials. 23, 1508-1520.

Rochette, P., and Labossiere, P. (2000) "Axial testing of rectangular column models confined with composites." Journal of Composites for Construction, 4(3), 129-136.

Saadatmanesh, H., Ehsani, M. R., and Li, M. W. (1994). "Strength and ductility of concrete columns externally reinforced with fiber composite straps." *ACI Struct. J.*, 91(4), 434-447.

Saafi, M., Touranji, H.A. and Li, Z. (1999). "Behavior of concrete columns confined with fiber reinforced polymer tubes." ACI Materials Journal, 96(4): 500-509.

Sadeghian, P., Rahai, A. and Ehsani, M.R. (2010) "Experimental study of rectangular RC columns strengthened with CFRP composites under eccentric loading." Journal of composites for construction.Samaan, M., Mirmiran, A., Shahawy, M. (1998) "Model of concrete confined by fiber composites" J. Struct. Eng., 124(9), 1025-1031.

Sargin M. (1971) "Stress–strain relationship for concrete and the analysis of structural concrete section." Univ. of Waterloo: Ontario, Canada.

Schickert, G., and Winkler, H. (1979). "Results of tests concerning strength and strain of concrete subjected to multiaxial compressive stresses." *Deutscher Ausschuss fur Stahlbeton*, Heft 277, Berlin, West Germany.

Spoelstra, M.R. and Monti, G. (1999). "FRP-confined concrete model." Journal of Composites for Construction, ASCE, 3(3): 143-150.

Toutanji, H.A. (1999) "Stress–strain characteristics of concrete columns externally confined with advanced fiber composite sheets." ACI Mater J;96(3): 397–404.

Widiarsa, I.B.R. and Hadi, M.N.S. (2013) "Performance of CFRP wrapped square reinforced concrete columns subjected to eccentric loading." Procedia Engineering, 54:365-376.

William, K. J., and Warnke, E. P. (1975). "Constitutive model for the triaxial behavior of concrete." Proc, International Association for Bridge and Structural Engineering, vol. 19, 1-30.

Youssef, M.N., Feng, Q.F., and Mosallam, A. S. (2007) "Stress-strain model for concrete confined by FRP composites" Composites: Part B, 38, 614-628.

Yu, T., Teng, J.G., Wong, Y.L., Dong S.L., (2010a) "Finite element modeling of confined concrete-I: Drucker-Prager type plasticity model" Engineering Structures 32, 665-679.

Yu, T., Teng, J.G., Wong, Y.L., Dong S.L., (2010b) "Finite element modeling of confined concrete-II: Plastic-damage model" Engineering Structures 32, 665-679.

Xiao, Y. and Wu, H. (2000). "Compressive behavior of concrete confined by carbon fiber composite jackets." Journal of Materials in Civil Engineering, ASCE, 12(2): 139-146.

Xiao, Y. and Wu, H. (2003). "Compressive behavior of concrete confined by various types of FRP composite jackets." *J. Reinf. Plast. Compos.*, 22(13), 1187–1201.

Xiao Q, Teng JG, Yu T. (2010) "Behavior and modeling of confined high-strength concrete." ASCE J Compos Constr;14(3): 249–59.

SikaWrap Hex 230C. Carbon fiber fabric for structural strengthening system, product datasheet, Sika Edition 03, 2003.

Appendix - Spreadsheets and VBA codes for calculation of interaction diagrams

Model by Teng et al.

h	175.00	mm	t_f	0.13	mm	C_E	0.95
b	175.00	mm	n	1.00		ψ_f	0.95
r	20.00	mm	ρ_g	1.477	%	φ_c	0.65
d	148.00	mm	E_f	216000.00	MPa	φ_t	0.90
A_g	30625.00	mm^2	E_s	200000.00	MPa	κ_ε	0.55
A_{s1}	226.19	mm^2	f^*_{fu}	3176.00	MPa		
A_{s2}	0.00	mm^2	ε^*_{fu}	0.017	mm/mm		
A_{s3}	0.00	mm^2	f'_c	47.77	MPa		
A_{s4}	226.19	mm^2	E_c	32484.45	MPa		
d_{s1}	60.50	mm	f_y	560.00	MPa		
d_{s2}	0.00	mm	ε'_c	0.0020	mm/mm		
d_{s3}	0.00	mm	ε_{sy}	0.0028	mm/mm		
d_{s4}	-60.50	mm	ε_{sD}	0.0050	mm/mm		
			ε_{cu}	0.0030	mm/mm		

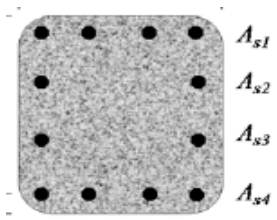

1. Calculation of Point A and A'

$f_{fu} = C_E f^*_{fu}$ 3017.20 MPa

$\varepsilon_{fu} = C_E \varepsilon^*_{fu}$ 0.0162 %

$f_l = \dfrac{\psi_f 2 n t_f E_f \varepsilon_{fe}}{\sqrt{b^2 + h^2}}$ 1.93 MPa

$$\frac{A_e}{A_c} = \frac{1 - \dfrac{\left(\left(\frac{b}{h}\right)(h-2r)^2 + \left(\frac{h}{b}\right)(b-2r)^2\right)}{(3A_g)} - \rho_g}{1-\rho_g}$$ 0.60

$\kappa_a = \dfrac{A_e}{A_c}\left(\dfrac{b}{h}\right)^2$ 0.60

$f'_{cc} = f'_c + 3.3\kappa_a f_l$ 51.57

$P_{n(A)} = \left[0.85 f'_{cc}(A_g - A_{st}) + f_y A_{st}\right]$ 1576.02 kN

$\varphi P_{n(A)}$ 1024.42

2. Calculation of point B & B'

$\varepsilon_{fe} = min[0.004, \kappa_\varepsilon \varepsilon_{fu}]$ 0.004

$f_l = \frac{\psi_f 2nt_f E_f \varepsilon_{fe}}{\sqrt{b^2 + h^2}}$ 0.87 MPa

$f_l / f_c' \geq 0.08$ 0.02 Failure

$\kappa_a = \frac{A_e}{A_c}\left(\frac{b}{h}\right)^2$ 0.60

$\kappa_b = \frac{A_e}{A_c}\left(\frac{h}{b}\right)^{0.5}$ 0.60

$\varepsilon_{ccu} = \varepsilon_c'\left(1.5 + 12\kappa_b \frac{f_l}{f_c'}\left(\frac{\varepsilon_{fe}}{\varepsilon_c'}\right)^{0.45}\right) \leq 0.01$ 0.0034

$f_{cc}' = f_c' + 3.3\kappa_a f_l$ 49.48 MPa

$E_2 = \frac{f_{cc}' - f_c'}{\varepsilon_{ccu}}$ 510.33 MPa

$\varepsilon_t' = \frac{2f_c'}{E_c - E_2}$ 0.0030

c 148.00 mm

$y_t = c\frac{\varepsilon_t'}{\varepsilon_{ccu}}$ 131.76

$A = \frac{-b(E_c - E_2)^2}{12f_c'}\left(\frac{\varepsilon_{ccu}}{c}\right)^2$ -1.60E-04 kN/mm^3

$B = \frac{b(E_c - E_2)}{2}\left(\frac{\varepsilon_{ccu}}{c}\right)$ 63.44 MPa

$C = -bf_c'$ -8.36 kN/mm

$$D = bcf_c' + \frac{bcE_2}{2}(\varepsilon_{ccu})$$ 1259.42 kN

$$E = \frac{-b(E_c - E_2)^2}{16f_c'}\left(\frac{\varepsilon_{ccu}}{c}\right)^2$$ -1.20E-04 kN/mm^3

$$F = b\left(c - \frac{h}{2}\right)\frac{(E_c - E_2)^2}{12f_c'}\left(\frac{\varepsilon_{ccu}}{c}\right)^2 + \frac{b(E_c - E_2)}{3}\left(\frac{\varepsilon_{ccu}}{c}\right)$$ 52.01 MPa

$$G = -\left(\frac{b}{2}f_c' + b\left(c - \frac{h}{2}\right)\frac{(E_c - E_2)}{2}\left(\frac{\varepsilon_{ccu}}{c}\right)\right)$$ -8.02 kN/mm

$$H = bf_c'\left(c - \frac{h}{2}\right)$$ 505.76 kN

$$I = \frac{bc^2}{2}f_c' - bcf_c'\left(c - \frac{h}{2}\right) + \frac{bc^2E_2}{3}(\varepsilon_{ccu}) - \frac{bcE_2}{2}\left(c - \frac{h}{2}\right)(\varepsilon_{ccu})$$ 17549.34 kN mm

d_{s1} 60.50 mm

$d_{s2}=d_{s3}$ 0.00 mm

ε_{s1}	0.0027	f_{s1}	548.79
ε_{s2}	0.0014	f_{s2}	274.39
ε_{s3}	0.0014	f_{s3}	274.39
ε_{s4}	0.0000	f_{s4}	0.00

$$P_{n(B)} = \left[\left(A(y_t)^3 + B(y_t)^2 + C(y_t) + D + \sum A_{si}f_{si}\right)\right]$$ 660.65 kN

$\varphi P_{n(B)}$ 429.42

$$M_{n(B)} = \left[(E(y_t)^4 + F(y_t)^3 + G(y_t)^2 + H(y_t) + I) + \sum A_{si}f_{si}d_{si}\right]$$ 35.18 kN m

$\varphi M_{n(B)}$ 22.87

2. Calculation of point C & C'

$$\varepsilon_{fe} = min\left[0.004, \kappa_\varepsilon\varepsilon_{fu}\right]$$ 0.0040

$$f_l = \frac{\psi_f 2nt_f E_f \varepsilon_{fe}}{\sqrt{b^2 + h^2}}$$ 0.87 MPa

$f_l/f_c' \geq 0.08$ 0.02 Failure

$$\kappa_a = \frac{A_e}{A_c}\left(\frac{b}{h}\right)^2$$ 0.60

$$\kappa_b = \frac{A_e}{A_c}\left(\frac{h}{b}\right)^{0.5}$$ 0.60

$$\varepsilon_{ccu} = \varepsilon_c'\left(1.5 + 12\kappa_b \frac{f_l}{f_c'}\left(\frac{\varepsilon_{fe}}{\varepsilon_c'}\right)^{0.45}\right) \leq 0.01$$ 0.0034

$$f_{cc}' = f_c' + 3.3\kappa_a f_l$$ 49.48 MPa

$$E_2 = \frac{f_{cc}' - f_c'}{\varepsilon_{ccu}}$$ 510.33 MPa

$$\varepsilon_t' = \frac{2f_c'}{E_c - E_2}$$ 0.0030

$$c = \left(\frac{\varepsilon_{ccu}}{\varepsilon_{ccu} + \varepsilon_y}\right)d$$ 80.69 mm

$$y_t = c\frac{\varepsilon_t'}{\varepsilon_{ccu}}$$ 71.83

$$A = \frac{-b(E_c - E_2)^2}{12f_c'}\left(\frac{\varepsilon_{ccu}}{c}\right)^2$$ -5.40E-04 kN/mm^3

$$B = \frac{b(E_c - E_2)}{2}\left(\frac{\varepsilon_{ccu}}{c}\right)$$ 116.37 MPa

$$C = -bf_c'$$ -8.36 kN/mm

$$D = bcf_c' + \frac{bcE_2}{2}(\varepsilon_{ccu})$$ 686.61 kN

$$E = \frac{-b(E_c - E_2)^2}{16f_c'}\left(\frac{\varepsilon_{ccu}}{c}\right)^2$$ -4.05E-04 kN/mm^3

$$F = b\left(c - \frac{h}{2}\right)\frac{(E_c - E_2)^2}{12f_c'}\left(\frac{\varepsilon_{ccu}}{c}\right)^2 + \frac{b(E_c - E_2)}{3}\left(\frac{\varepsilon_{ccu}}{c}\right)$$ 73.90 MPa

$$G = -\left(\frac{b}{2}f_c' + b\left(c - \frac{h}{2}\right)\frac{(E_c - E_2)}{2}\left(\frac{\varepsilon_{ccu}}{c}\right)\right)$$ -3.39 kN/mm

$$H = bf_c'\left(c - \frac{h}{2}\right)$$ -56.96 kN

$$I = \frac{bc^2}{2}f_c' - bcf_c'\left(c - \frac{h}{2}\right) + \frac{bc^2E_2}{3}(\varepsilon_{ccu}) - \frac{bcE_2}{2}\left(c - \frac{h}{2}\right)(\varepsilon_{ccu})$$ 32540.94 kN mm

d_{s1}	60.50 mm
d_{s2}	0.00 mm
d_{s3}	0.00 mm
d_{s4}	-60.50 mm

ε_{s1}	0.0022	f_{s1}	446.62
ε_{s2}	-0.0003	f_{s2}	-56.69
ε_{s3}	-0.0003	f_{s3}	-56.69
ε_{s4}	-0.0028	f_{s4}	-560.00

$$P_{n(C)} = \left[\left(A(y_t)^3 + B(y_t)^2 + C(y_t) + D + \sum A_{si}f_{si}\right)\right]$$ 460.79 kN

$\varphi P_{n(C)}$ 299.51 kN

$$M_{n(C)} = \left[(E(y_t)^4 + F(y_t)^3 + G(y_t)^2 + H(y_t) + I) + \sum A_{si}f_{si}d_{si}\right]$$ 41.36 kN.m

$\varphi M_{n(C)}$ 26.88 kN.m

2. Calculation of point D & D'

c 55.50 mm

$$0.65 \le \beta = 0.85 - 0.05\frac{f_c' - 4000}{1000} \le 0.85$$ 0.71

$\varepsilon_{cu} = \varepsilon_{c0}$ 0.0030

$P_{n(D)} = 0.85 f_c' \alpha b + \sum A_{si} f_{si}$ 222.55 kN

$\varphi P_{n(D)}$ 200.29 kN

$M_{n(D)} = 0.85 f_c' \alpha b \left(\frac{h}{2} - \frac{\alpha}{2}\right) + \sum A_{si} f_{si} d_{si}$ 30.84 kN.m

$\varphi M_{n(D)}$ 27.76 kN.m

5. Calculation of Point E & E'

$0.65 \leq \beta = 0.85 - 0.05 \frac{f_c' - 4000}{1000} \leq 0.85$ 0.71

$M_{n(E)} = 0.85 f_c' \alpha b \left(\frac{h}{2} - \frac{\alpha}{2}\right) + \sum A_{si} f_{si} d_{si}$ 18.03 kN.m

$\varphi M_{n(E)}$ 16.22 kN.m

Model by Youssef et al

h	175.00	mm	t	0.13	mm	φ_c	0.65
b	175.00	mm	n_j	1.00		φ_t	0.90
D	247.49	mm	ρ_j	0.21	%	C_E	0.95
r_c	20.00	mm	E_j	216000.00	MPa	ψ_f	0.95
d	148.00	mm	f_{ju}	3176.00	MPa		
A_g	30625.00	mm^2	ε_{jt}	0.018	mm/mm		
A_{s1}	226.19	mm^2	ρ_l	1.477	%		
A_{s2}	0.00	mm^2	E_s	200000.00	MPa		
A_{s3}	0.00	mm^2	f_y	560.00	MPa		
A_{s4}	226.19	mm^2	E_c	32484.45	MPa		
d_{s1}	60.50	mm	f'_c	47.77	MPa		
d_{s2}	0.00	mm	ε_y	0.0028	mm/mm		
d_{s3}	0.00	mm	ε_{sD}	0.0050	mm/mm		
d_{s4}	-60.50	mm	ε_{cu}	0.0030	mm/mm		

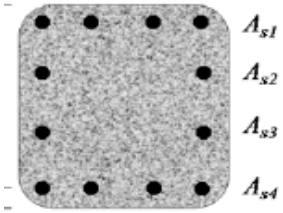

1. Calculation of Point A & A'

$$k_e = \frac{1 - \left[\frac{(b-2r_c)^2 + (h-2r_c)^2}{3hb}\right] - \rho_l}{1 - \rho_l} \qquad 0.60$$

$$f_{lu} = \frac{1}{2}\rho_j f_{ju} \qquad 3.34 \text{ MPa}$$

$$f'_{lu} = k_e f_{lu} \qquad 1.99 \text{ MPa}$$

$$f'_{cu} = f'_c\left[0.5 + 1.225\left(\frac{f'_{lu}}{f'_c}\right)^{0.6}\right] \qquad 32.58 \text{ MPa}$$

$$f_t = f'_c\left[1 + 1.135\left(\frac{\rho_j E_j \varepsilon_{jt}}{f'_c}\right)^{\frac{5}{4}}\right] \qquad 53.73 \text{ MPa}$$

$P_{n(A)} = [0.85f_c'(A_g - A_{st}) + f_y A_{st}]$ 1631.40 kN

$\varphi P_{n(A)}$ 1060.41 kN

2. Calculation of Point B & B'

$$k_e = \frac{1 - \left[\frac{(b-2r_c)^2 + (h-2r_c)^2}{3hb}\right] - \rho_l}{1 - \rho_l}$$ 0.60

$f_{lu} = \frac{1}{2}\rho_j f_{ju}$ 3.34 MPa

$f'_{lu} = k_e f_{lu}$ 1.99 MPa

$$f'_{cu} = f'_c\left[0.5 + 1.225\left(\frac{f'_{lu}}{f'_c}\right)^{0.6}\right]$$ 32.58 MPa

$$\varepsilon_{cu} = \left[0.00433 + 0.260\left(\frac{f'_{lu}}{f'_c}\right)\left(\frac{f_{ju}}{E_j}\right)^{\frac{1}{2}}\right]$$ 0.0056

c 148.00 mm

$$f_t = f'_c\left[1 + 1.135\left(\frac{\rho_j E_j \varepsilon_{jt}}{f'_c}\right)^{\frac{5}{4}}\right]$$ 53.73 MPa

$$\varepsilon_t = \left[0.0020 + 0.078\left(\frac{\rho_j E_j \varepsilon_{jt}}{f'_c}\right)^{\frac{6}{7}}\left(\frac{f_{ju}}{E_j}\right)^{\frac{1}{2}}\right]$$ 0.0041

$$E_2 = \frac{f'_{cu} - f_t}{\varepsilon_{cu} - \varepsilon_t}$$ -13523.93 MPa

$$f(c) = \begin{cases} f_c = E_c\varepsilon_c\left[1 - \frac{1}{n}\left(1 - \frac{E_2}{E_c}\right)\left(\frac{\varepsilon_c}{\varepsilon_t}\right)^{n-1}\right], & E_2 > 0 \\ f_c = E_c\varepsilon_c\left[1 - \frac{1}{n}\left(\frac{\varepsilon_c}{\varepsilon_t}\right)^{n-1}\right], & E_2 \le 0 \\ f_c = f_t + E_2(\varepsilon_c - \varepsilon_t), & \end{cases}, \quad 0 \le \varepsilon_c < \varepsilon_t \quad \varepsilon_t \le \varepsilon_c \le \varepsilon_{cu}$$

$$P_{n(B)} = \int_0^c (b) f_c(y) dy + \sum A_{si} f_{si}$$ 1051.33 kN

$\varphi P_{n(B)}$ 683.36 kN

$$M_{n(B)} = \int_0^c (b)\left(\frac{h}{2} - c + y\right) f_c(y) dy + \sum A_{si} f_{si} d_{si}$$ 27.18 kN.m

$\varphi M_{n(B)}$ 17.67 kN

3. Calculation of Point C & C'

$$k_e = \frac{1 - \left[\frac{(b - 2r_c)^2 + (h - 2r_c)^2}{3hb}\right] - \rho_l}{1 - \rho_l}$$ 0.60

$$f_{lu} = \frac{1}{2}\rho_j f_{ju}$$ 3.34 MPa

$$f'_{lu} = k_e f_{lu}$$ 1.99 MPa

$$f'_{cu} = f'_c\left[0.5 + 1.225\left(\frac{f'_{lu}}{f'_c}\right)^{0.6}\right]$$ 32.58 MPa

$$\varepsilon_{ccu} = \left[0.00433 + 0.260\left(\frac{f'_{lu}}{f'_c}\right)\left(\frac{f_{ju}}{E_j}\right)^{\frac{1}{2}}\right]$$ 0.0056

c 98.93 mm

$$f_t = f'_c\left[1 + 1.135\left(\frac{\rho_j E_j \varepsilon_{jt}}{f'_c}\right)^{\frac{5}{4}}\right]$$ 53.73 MPa

$$\varepsilon_t = \left[0.0020 + 0.078\left(\frac{\rho_j E_j \varepsilon_{jt}}{f'_c}\right)^{\frac{6}{7}}\left(\frac{f_{ju}}{E_j}\right)^{\frac{1}{2}}\right]$$ 0.0041

$$E_2 = \frac{f'_{cu} - f_t}{\varepsilon_{cu} - \varepsilon_t}$$ -13523.93 MPa

$$f(c) = \begin{cases} f_c = E_c\varepsilon_c\left[1 - \frac{1}{n}\left(1 - \frac{E_2}{E_c}\right)\left(\frac{\varepsilon_c}{\varepsilon_t}\right)^{n-1}\right], & E_2 > 0 \\ f_c = E_c\varepsilon_c\left[1 - \frac{1}{n}\left(\frac{\varepsilon_c}{\varepsilon_t}\right)^{n-1}\right], & E_2 \le 0 \end{cases}, \quad 0 \le \varepsilon_c < \varepsilon_t$$
$$f_c = f_t + E_2(\varepsilon_c - \varepsilon_t), \quad \varepsilon_t \le \varepsilon_c \le \varepsilon_{cu}$$

$$P_{n(C)} = \int_0^c (b) f_c(y)dy + \sum A_{si} f_{si}$$ 618.10 kN

$\varphi P_{n(C)}$ 401.76 kN

$$M_{n(C)} = \int_0^c (b)\left(\frac{h}{2} - c + y\right) f_c(y)dy + \sum A_{si} f_{si} d_{si}$$ 41.98 kN.m

$\varphi M_{n(C)}$ 27.29 kN

4. Calculation of Point D & D'

c 55.50 mm

$$0.65 \leq \beta = 0.85 - 0.05\frac{f_c' - 4000}{1000} \leq 0.85$$ 0.71

$\varepsilon_{cu} = \varepsilon_{c0}$ 0.0030

$P_{n(D)} = 0.85 f_c' \alpha b + \sum A_{si} f_{si}$ 222.55 kN

$\varphi P_{n(D)}$ 200.29 kN

$M_{n(D)} = 0.85 f_c' \alpha b \left(\frac{h}{2} - \frac{\alpha}{2}\right) + \sum A_{si} f_{si} d_{si}$ 30.84 kN.m

$\varphi M_{n(D)}$ 27.76 kN.m

5. Calculation of Point E & E'

$$0.65 \leq \beta = 0.85 - 0.05\frac{f_c' - 4000}{1000} \leq 0.85$$ 0.71

$M_{n(E)} = 0.85 f_c' \alpha b \left(\frac{h}{2} - \frac{\alpha}{2}\right) + \sum A_{si} f_{si} d_{si}$ 18.03 kN.m

$\varphi M_{n(E)}$ 16.22 kN.m

Model by Faustino et al.

h	175.00	mm	t	0.13	mm	k_1	3.70
b	175.00	mm	n_f	1.00		k_2	18.89
h_w	145.00	mm	ρ_g	1.48	%	φ_c	0.65
b_w	145.00	mm	E_f	216000.00	MPa	φ_t	0.90
R	20.00	mm	f_{fu}	3176.00	MPa	C_E	0.95
d	148.00	mm	ε_{fu}	0.018	mm/mm	ψ_f	0.95
A_g	30625.00	mm^2	f_{c0}	47.77	MPa	n	3.00
A_{s1}	226.19	mm^2	E_c	32484.45	MPa	E_s	200000.00 mm
A_{s2}	0.00	mm^2	f_y	560.00	MPa		
A_{s3}	0.00	mm^2	ε_{c0}	0.0023	mm/mm		
A_{s4}	226.19	mm^2	ε_y	0.0028	mm/mm		
d_{s1}	60.50	mm	ε_{sD}	0.0050	mm/mm		
d_{s2}	0.00	mm	ε_{cu}	0.0030	mm/mm		
d_{s3}	0.00	mm					
d_{s4}	-60.50	mm					
A_{sw}	56.55	mm^3					
S	100.00	mm					
d_w	205.06	mm					

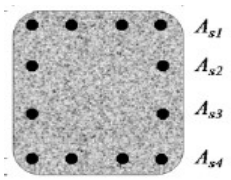

1. Calculation of Point A & A'

B 247.49 mm

$$\varepsilon_{lu} = C_E * 0.7\left(\frac{2R}{B}\right)^{0.23} \varepsilon_{fu}$$ 0.01 mm/mm

$$f_{ju} = \frac{\psi_f 2 n_f t}{B} E_f \varepsilon_{lu}$$ 1.70 MPa

$$f_{sw} = \begin{cases} E_s \times \frac{d_w}{B}\varepsilon_{lu}, & for \quad \varepsilon_{lu} < \frac{B}{d_w}\varepsilon_y \\ f_y \quad , & for \quad \varepsilon_{lu} \geq \frac{B}{d_w}\varepsilon_y \end{cases}$$ 560.00 MPa

$$f_{shu} = \frac{2A_{sw}}{d_w S} f_{sw}$$ 3.09 MPa

$$f_{lu} = f_{ju} + f_{shu}$$ 4.79 MPa

$$f_{cc} = f_{c0} + k_1\left(\frac{2R}{B}\right) f_{lu}$$ 50.63 MPa

$$P_{n(A)} = \left[0.85 f_{cc}\left(A_g - A_{st}\right) + f_y A_{st}\right]$$ 1551.87 MPa

$\varphi_c P_{n(A)}$ 1008.72 MPa

2. Calculation of Point B & B'

$\varepsilon_{c0} = \frac{0.7}{1000}(f_{c0})^{0.31}$ 0.0023

$\varepsilon_{cc} = k_2\varepsilon_{c0}\left(\frac{f_{lu}}{f_{c0}}\right) \leq 0.01$ 0.0044

c 148.00 mm

$E_1 = 3950\sqrt{f_{c0}}$ 27300.76 MPa

$E_2 = 510\left(\frac{2R}{B}f_{lu}\right)^{0.04} f_{c0}^{0.95} - 440f_{c0}$ -1143.89 Mpa

$f_0 = f_{c0} + 0.5\left(\frac{2R}{B}\right)f_{lu}$ 48.16 MPa

$$f_c = \frac{(E_1 - E_2)\varepsilon_c}{\left[1 + \left(\frac{(E_1 - E_2)\varepsilon_c}{f_0}\right)^n\right]^{\frac{1}{n}}} + E_2\varepsilon_c \leq f_{cc}$$

$P_{n(B)} = \int_0^c (b)f_c(y)dy + \sum A_{si}f_{si}$ 991.50 kN

$\varphi P_{n(B)}$ 644.48 kN

$M_{n(B)} = \int_0^c (b)\left(\frac{h}{2} - c + y\right)f_c(y)dy + \sum A_{si}f_{si}d_{si}$ 30.99 kN.m

$\varphi M_{n(B)}$ 20.14 kN.m

3. Calculation of Point C & C'

$\varepsilon_{c0} = \frac{0.7}{1000}(f_{c0})^{0.31}$ 0.0023

$\varepsilon_{cc} = k_2\varepsilon_{c0}\left(\frac{f_{lu}}{f_{c0}}\right) \leq 0.01$ 0.0044

c 90.38 mm

$E_1 = 3950\sqrt{f_{c0}}$ 27300.76 MPa

$E_2 = 510\left(\frac{2R}{B}f_{lu}\right)^{0.04} f_{c0}^{0.95} - 440f_{c0}$ -1143.89 MPa

$f_0 = f_{c0} + 0.5\left(\frac{2R}{B}\right)f_{lu}$ 48.16 MPa

$$f_c = \frac{(E_1 - E_2)\varepsilon_c}{\left[1 + \left(\frac{(E_1 - E_2)\varepsilon_c}{f_0}\right)^n\right]^{\frac{1}{n}}} + E_2\varepsilon_c \leq f_{cc}$$

$P_{n(c)} = \int_0^c (b) f_c(y) dy + \sum A_{si} f_{si}$ 528.13 kN

$\varphi P_{n(c)}$ 343.28 kN

$M_{n(c)} = \int_0^c (b)\left(\frac{h}{2} - c + y\right) f_c(y) dy + \sum A_{si} f_{si} d_{si}$ 42.02 kN.m

$\varphi M_{n(c)}$ 27.31 kN.m

4. Calculation of Point D & D'

c 55.50 mm

$0.65 \leq \beta = 0.85 - 0.05\frac{f_c' - 4000}{1000} \leq 0.85$ 0.71

ε_{cu} 0.0030

$P_{n(D)} = 0.85 f_c' \alpha b + \sum A_{si} f_{si}$ 222.55 kN

$\varphi P_{n(D)}$ 200.29 kN

$M_{n(D)} = 0.85 f_c' \alpha b\left(\frac{h}{2} - \frac{\alpha}{2}\right) + \sum A_{si} f_{si} d_{si}$ 30.84 kN.m

$\varphi M_{n(D)}$ 27.76 kN.m

5. Calculation of Point E & E'

$0.65 \leq \beta = 0.85 - 0.05\frac{f_c' - 4000}{1000} \leq 0.85$ 0.71

$M_{n(E)} = 0.85 f_c' \alpha b\left(\frac{h}{2} - \frac{\alpha}{2}\right) + \sum A_{si} f_{si} d_{si}$ 18.03 kN.m

$\varphi M_{n(E)}$ 16.22 kN.m

Model by Eid & Paultre

h	175.00	mm	t	0.13	mm	φ_c	0.65
b	175.00	mm	n_f	1.00		φ_t	0.90
c_x	145.00	mm	E_f	216000.00	MPa	C_E	0.95
c_y	145.00	mm	ϵ_{fu}	0.0180		ψ_f	0.95
D	247.49	mm	E_{ct}	32484.45	MPa	ξ	0.50
r_c	20.00	mm	f'_c	47.77	MPa		
d	148.00	mm	E_s	200000.00	MPa		
A_{shx}	56.55	mm^2	f_{ly}	560.00	MPa		
A_{shy}	56.55	mm^2	f_{hy}	560.00	MPa		
s	100.00	mm	ρ_g	1.48	%		
s'	94.00	mm	ρ_{cc}	2.15	%		
w_{ix}	109.00	mm	ϵ'_c	0.0023	mm/mm		
w_{iy}	109.00	mm	ϵ_{ly}	0.0028	mm/mm		
N_{ix}	1.00		ϵ_{hy}	0.0028	mm/mm		
N_{iy}	1.00		ϵ_{sD}	0.0050	mm/mm		
A_g	30625.00	mm^2	ϵ_{cu}	0.0030	mm/mm		
A_{s1}	226.19	mm^2	ϵ_{c50}	0.0040	mm/mm		
A_{s2}	0.00	mm^2					
A_{s3}	0.00	mm^2					
A_{s4}	226.19	mm^2					
d_{s1}	60.50	mm					
d_{s2}	0.00	mm					
d_{s3}	0.00	mm					
d_{s4}	-60.50	mm					

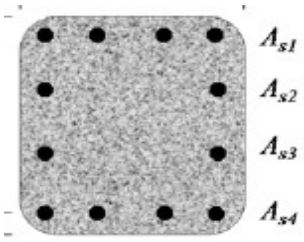

1. Calculation of Point A & A'

$$K_f = \frac{1 - \frac{\left[\left(\frac{b}{h}\right)(h-2r_c)^2 + \left(\frac{h}{b}\right)(b-2r_c)^2\right]}{3A_g} - \rho_g}{(1-\rho_g)} \geq 0$$ 0.60

$E_{fl} = 2K_f E_f \left(\frac{2n_{fl}t}{c_x+c_y}\right)$ 231.35 MPa

$K_h = 1 - \frac{\sum w_i^2}{6c_x c_y}$ 0.81

$$K_v = \frac{\left(1 - \frac{s'}{2c_x}\right)\left(1 - \frac{s'}{2c_y}\right)}{(1 - \rho_{cc})} \geq 0$$ 0.47

$K_e = K_h K_v$ 0.38

$$\rho_{se} = \frac{K_e}{s}\left(\frac{A_{shx} + A_{shy}}{c_x + c_y}\right)$$ 0.0015

$$f_{cu} = f_c'\left(1 + 3.3\left(\frac{b}{h}\right)^2\left(\frac{\rho_{se} f_{hy}}{f_c'} + \frac{E_{fl}\epsilon_{fu}}{f_c'}.\xi\right)\right)$$ 57.37 MPa

$$P_{n(A)} = \left[0.85 f_{cu}(A_g - A_{st}) + f_y A_{st}\right]$$ 1724.58 kN

$\varphi_c P_{n(A)}$ 1120.98 kN

2. Calculation of Point B & B'

$$K_f = \frac{1 - \frac{\left[\left(\frac{b}{h}\right)(h - 2r_c)^2 + \left(\frac{h}{b}\right)(b - 2r_c)^2\right]}{3A_g} - \rho_g}{(1 - \rho_g)} \geq 0$$ 0.60

$E_{fl} = 2K_f E_f \left(\frac{2n_{fl}t}{c_x + c_y}\right)$ 231.35 MPa

$$K_h = 1 - \frac{\sum w_i^2}{6c_x c_y}$$ 0.81

$$K_v = \frac{\left(1 - \frac{s'}{2c_x}\right)\left(1 - \frac{s'}{2c_y}\right)}{(1 - \rho_{cc})} \geq 0$$ 0.47

$K_e = K_h K_v$ 0.38

$$\rho_{se} = \frac{K_e}{s}\left(\frac{A_{shx} + A_{shy}}{c_x + c_y}\right)$$ 0.0015

$$f_{cu} = f_c'\left(1 + 3.3\left(\frac{b}{h}\right)^2\left(\frac{\rho_{se} f_{hy}}{f_c'} + \frac{E_{fl}\epsilon_{fu}}{f_c'}.\xi\right)\right)$$ 57.37 MPa

$$\epsilon_{cu} = \epsilon_c'\left(1.56 + 12\left(\frac{\rho_{se} f_{hy}}{f_c' K_h^2} + \frac{E_{fl}\epsilon_{fu}}{f_c'}.\xi\right)\left(\frac{\epsilon_{fu,a}}{\epsilon_c'}\right)^{0.45}\right)$$ 0.0066

c 148.00 mm

$\gamma_{sf} = \epsilon_{hy}/\epsilon_{fu}$ 0.16

$$v_{c0} \le v_{cc}' = 10\left[\frac{f_c'}{E_{fl} + \rho_{se} E_s \gamma_{sf}}\right]^{0.9} \le 0.5$$ 0.50

$\eta = 29.8 v_{cc}' - 3.56$ 11.34

$$\kappa_1 = \frac{f_c'}{\rho_{se} E_s \epsilon_c' + E_{fl}\epsilon_c'}$$ 39.11

$$\kappa_2 = \frac{f_c'}{E_{fl}\epsilon_c'} = \frac{E_c'}{E_{fl}}$$ 88.97

$$I_e' = \begin{cases} I_{e1}' = \dfrac{v_{cc}'}{\kappa_1 - \eta} \le I_{e2}' & if\ \kappa_1 > \eta\ \ (\kappa_2 \gg \eta) \\ I_{e2}' = \dfrac{v_{cc}' f_c' + \kappa_2 \rho_{se} f_{hy}}{f_c'(\kappa_2 - \eta)} \le I_{e,max} & if\ \kappa_1 \le \eta\ and\ (\kappa_2 > \eta) \\ I_{e,max} = \dfrac{\rho_{se} f_{hy}}{f_c'} + \dfrac{E_{fl}\epsilon_{fu}\xi}{f_c'} & if\ \kappa_1 \le \eta\ and\ (\kappa_2 \ll \eta) \end{cases}$$ 0.02

$\epsilon'_{cc} = \epsilon'_c(1 + 35(I'_e)^{1.2})$ 0.0030

$f'_{cc} = f'_c(1 + 2.4(I'_e)^{0.7})$ 54.66

$E_{cu} = \frac{f_{cu} - f'_{cc}}{\epsilon_{cu} - \epsilon'_{cc}} \leq \frac{f_{cu} - f'_{cc}}{\epsilon_{cu}}$ 749.55

$a = E_{ct}$ 32484.45

$b = \frac{E_{ct}}{f'_{cc}} - \frac{2}{\epsilon'_{cc}} + \frac{E_{ct}E_{cu}\epsilon'_{cc}}{{f'_{cc}}^2}$ -53.56

$z = \frac{1}{{\epsilon'_{cc}}^2} - \frac{E_{ct}E_{cu}}{{f'_{cc}}^2}$ 104791.17

$I_{e50} = \frac{\rho_{sey} f_{hy}}{f'_c} + \frac{E_{fl}\epsilon_{fu}}{f'_c}$ 0.10

$\epsilon_{cc50} = \epsilon_{c50}(1 + 60I_{e50})$ 0.03

$k_1 = \frac{\ln(0.5)}{(\epsilon_{cc50} - \epsilon'_{cc})^{k_2}}$ -71.82

$k_2 = 1 + 25(I_{e50})^2$ 1.27

$$f_c = \begin{cases} f_c = \dfrac{a\epsilon_c}{1 + b\epsilon_c + z\epsilon_c^2} & for\ \epsilon_c \leq \epsilon'_{cc} \\ f'_{cc}\exp\left(k_1(\epsilon_c - \epsilon'_{cc})^{k_2}\right) + E_{cu}(\epsilon_c - \epsilon'_{cc}) & for\ \epsilon_{cu} \geq \epsilon_c > \epsilon'_{cc} \end{cases}$$

$$P_{n(B)} = \int_0^c (b) f_c(y) dy + \sum A_{si} f_{si}$$ 1205.69 kN

$\varphi P_{n(B)}$ 783.70 kN

$$M_{n(B)} = \int_0^c (b) \left(\frac{h}{2} - c + y\right) f_c(y) dy + \sum A_{si} f_{si} d_{si}$$ 28.40 kN.m

$\varphi M_{n(B)}$ 18.46 kN.m

3. Calculation of Point C & C'

$$K_f = \frac{1 - \frac{\left[\left(\frac{b}{h}\right)(h - 2r_c)^2 + \left(\frac{h}{b}\right)(b - 2r_c)^2\right]}{3A_g} - \rho_g}{(1 - \rho_g)} \geq 0$$ 0.60

$E_{fl} = 2K_f E_f \left(\frac{2n_{fl}t}{c_x + c_y}\right)$ 231.35 MPa

$$K_h = 1 - \frac{\sum w_i^2}{6c_x c_y}$$ 0.81

$$K_v = \frac{\left(1 - \frac{s'}{2c_x}\right)\left(1 - \frac{s'}{2c_y}\right)}{(1 - \rho_{cc})} \geq 0$$ 0.47

$K_e = K_h K_v$ 0.38

$$\rho_{se} = \frac{K_e}{s}\left(\frac{A_{shx} + A_{shy}}{c_x + c_y}\right)$$ 0.0015

$$f_{cu} = f_c'\left(1 + 3.3\left(\frac{b}{h}\right)^2\left(\frac{\rho_{se} f_{hy}}{f_c'} + \frac{E_{fl}\epsilon_{fu}}{f_c'}.\xi\right)\right)$$ 57.37 MPa

$$\epsilon_{cu} = \epsilon_c' \left(1.56 + 12 \left(\frac{\rho_{se} f_{hy}}{f_c' K_h^2} + \frac{E_{fl} \epsilon_{fu}}{f_c'} . \xi \right) \left(\frac{\epsilon_{fu,a}}{\epsilon_c'} \right)^{0.45} \right)$$ 0.0066

c 103.86 mm

$\gamma_{sf} = \epsilon_{hy} / \epsilon_{fu}$ 0.16

$$v_{c0} \leq v_{cc}' = 10 \left[\frac{f_c'}{E_{fl} + \rho_{se} E_s \gamma_{sf}} \right]^{0.9} \leq 0.5$$ 0.50

$\eta = 29.8 v_{cc}' - 3.56$ 11.34

$$\kappa_1 = \frac{f_c'}{\rho_{se} E_s \epsilon_c' + E_{fl} \epsilon_c'}$$ 39.11

$$\kappa_2 = \frac{f_c'}{E_{fl} \epsilon_c'} = \frac{E_c'}{E_{fl}}$$ 88.97

$$I_e' = \begin{cases} I_{e1}' = \dfrac{v_{cc}'}{\kappa_1 - \eta} \leq I_{e2}' & if\ \kappa_1 > \eta\ \ (\kappa_2 \gg \eta) \\ I_{e2}' = \dfrac{v_{cc}' f_c' + \kappa_2 \rho_{se} f_{hy}}{f_c' (\kappa_2 - \eta)} \leq I_{e,max} & if\ \kappa_1 \leq \eta\ and\ (\kappa_2 > \eta) \\ I_{e,max} = \dfrac{\rho_{se} f_{hy}}{f_c'} + \dfrac{E_{fl} \epsilon_{fu} \xi}{f_c'} & if\ \kappa_1 \leq \eta\ and\ (\kappa_2 \ll \eta) \end{cases}$$ 0.02

$\epsilon_{cc}' = \epsilon_c' (1 + 35 (I_e')^{1.2})$ 0.0030

$f_{cc}' = f_c' (1 + 2.4 (I_e')^{0.7})$ 54.66

$$E_{cu} = \frac{f_{cu} - f_{cc}'}{\epsilon_{cu} - \epsilon_{cc}'} \leq \frac{f_{cu} - f_{cc}'}{\epsilon_{cu}}$$ 749.55

$a = E_{ct}$ 32484.45

$$b = \frac{E_{ct}}{f'_{cc}} - \frac{2}{\epsilon'_{cc}} + \frac{E_{ct}E_{cu}\epsilon'_{cc}}{{f'_{cc}}^2}$$ -53.56

$$z = \frac{1}{{\epsilon'_{cc}}^2} - \frac{E_{ct}E_{cu}}{{f'_{cc}}^2}$$ 104791.17

$$I_{e50} = \frac{\rho_{sey} f_{hy}}{f'_c} + \frac{E_{fl}\epsilon_{fu}}{f'_c}$$ 0.10

$$\epsilon_{cc50} = \epsilon_{c50}(1 + 60I_{e50})$$ 0.0291

$$k_1 = \frac{\ln(0.5)}{(\epsilon_{cc50} - \epsilon'_{cc})^{k_2}}$$ -71.82

$$k_2 = 1 + 25(I_{e50})^2$$ 1.27

$$f_c = \begin{cases} f_c = \dfrac{a\epsilon_c}{1 + b\epsilon_c + z\epsilon_c^2} & for\ \epsilon_c \le \epsilon'_{cc} \\ f'_{cc}\exp\left(k_1(\epsilon_c - \epsilon'_{cc})^{k_2}\right) + E_{cu}(\epsilon_c - \epsilon'_{cc}) & for\ \epsilon_{cu} \ge \epsilon_c > \epsilon'_{cc} \end{cases}$$

$$P_{n(C)} = \int_0^c (b) f_c(y) dy + \sum A_{si} f_{si}$$ 846.09 kN

$\varphi P_{n(C)}$ 549.96 kN

$$M_{n(C)} = \int_0^c (b)\left(\frac{h}{2} - c + y\right) f_c(y) dy + \sum A_{si} f_{si} d_{si}$$ 36.07 kN.m

$\varphi M_{n(C)}$ 23.44 kN.m

4. Calculation of Point D & D'

c 55.50 mm

$$0.65 \le \beta = 0.85 - 0.05\frac{f_c' - 4000}{1000} \le 0.85$$ 0.71

$\varepsilon_{cu} = \varepsilon_{c0}$ 0.0030

$P_{n(D)} = 0.85 f_c' \alpha b + \sum A_{si} f_{si}$ 222.55 kN

$\varphi P_{n(D)}$ 200.29 kN

$M_{n(D)} = 0.85 f_c' \alpha b \left(\frac{h}{2} - \frac{\alpha}{2}\right) + \sum A_{si} f_{si} d_{si}$ 30.84 kN.m

$\varphi M_{n(D)}$ 27.76 kN.m

5. Calculation of Point E & E'

$$0.65 \le \beta = 0.85 - 0.05\frac{f_c' - 4000}{1000} \le 0.85$$ 0.71

$M_{n(E)} = 0.85 f_c' \alpha b \left(\frac{h}{2} - \frac{\alpha}{2}\right) + \sum A_{si} f_{si} d_{si}$ 18.03 kN.m

$\varphi M_{n(E)}$ 16.22 kN.m

```
Function Betha(fPrime_c)
Betha = 0.85 - 0.05 * ((fPrime_c - 28) / 7)
If Betha < 0.65 Then
    Betha = 0.65
ElseIf Betha > 0.85 Then
    Betha = 0.85
End If
End Function
================================================================================
Function Pd_(Es, ep_y, fPrime_c, ep_cu, d, c, Betha, h, b, As1, As2, As3, As4, ds1,
ds2, ds3, ds4)

'Calculating the axial capacity of the section for point "D" of the interaction
diagram.

Dim Pc As Double            'Compressive force in concrete.
Dim ep_s1 As Double         'Strain in reinforcement layer 1.
Dim ep_s2 As Double         'Strain in reinforcement layer 2.
Dim ep_s3 As Double         'Strain in reinforcement layer 3.
Dim ep_s4 As Double         'Strain in reinforcement layer 4.
Dim fs1 As Double           'Stress in reinforcement layer 1.
Dim fs2 As Double           'Stress in reinforcement layer 2.
Dim fs3 As Double           'Stress in reinforcement layer 3.
Dim fs4 As Double           'Stress in reinforcement layer 4.
Dim Ps As Double            'Sum of the forces due to steel tension/compression.

'Calculate compressive force in concrete.
Pc = 0.85 * fPrime_c * Betha * c * b


'Calculate strain in each reinforcement layer.
ep_s1 = (c - h / 2 + ds1) * ep_cu / c
If ep_s1 >= 0 Then
   If ep_s1 > ep_y Then
      ep_s1 = ep_y
   End If
Else
     If ep_s1 < -ep_y Then
        ep_s1 = -ep_y
     End If
End If

ep_s2 = (c - h / 2 + ds2) * ep_cu / c
If ep_s2 >= 0 Then
   If ep_s2 > ep_y Then
      ep_s2 = ep_y
   End If
Else
     If ep_s2 < -ep_y Then
        ep_s2 = -ep_y
     End If
End If

ep_s3 = (c - h / 2 + ds3) * ep_cu / c
If ep_s3 >= 0 Then
   If ep_s3 > ep_y Then
      ep_s3 = ep_y
   End If
```

```
Else
     If ep_s3 < -ep_y Then
        ep_s3 = -ep_y
   End If
End If

ep_s4 = (c - h / 2 + ds4) * ep_cu / c
If ep_s4 >= 0 Then
   If ep_s4 > ep_y Then
      ep_s4 = ep_y
   End If
Else
     If ep_s4 < -ep_y Then
        ep_s4 = -ep_y
   End If
End If

'Calculate the stress in each reinforcement layer.
fs1 = ep_s1 * Es * As1
fs2 = ep_s2 * Es * As2
fs3 = ep_s3 * Es * As3
fs4 = ep_s4 * Es * As4

'Calculate sum of steel forces.
'Calculate axial capacity of the section.
Ps = fs1 + fs2 + fs3 + fs4
Pd_ = (Ps + Pc) / 1000

End Function

================================================================================
Function Md_(Es, ep_y, fPrime_c, ep_cu, d, c, Betha, h, b, As1, As2, As3, As4, ds1,
ds2, ds3, ds4)

'Calculating the flexural capacity of the section for point "D" of interaction
diagram.

Dim Mc As Double            'Flexural moment due to concrete compression.
Dim Ms As Double            'Sum of flexural moments due to steel tension/compression.
Dim ep_s1 As Double         'Strain in reinforcement layer 1.
Dim ep_s2 As Double         'Strain in reinforcement layer 2.
Dim ep_s3 As Double         'Strain in reinforcement layer 3.
Dim ep_s4 As Double         'Strain in reinforcement layer 4.
Dim Ms1 As Double           'Moment created by tension/compression in steel layer 1.
Dim Ms2 As Double           'Moment created by tension/compression in steel layer 2.
Dim Ms3 As Double           'Moment created by tension/compression in steel layer 3.
Dim Ms4 As Double           'Moment created by tension/compression in steel layer 4.

''Calculating the moment caused by concrete compression with respect to-
''-the central horizontal axis of the section.
Mc = 0.85 * fPrime_c * Betha * c * b * (h / 2 - Betha * c / 2)

'Calculating strain in each layer of reinforcement.
ep_s1 = (c - h / 2 + ds1) * ep_cu / c
If ep_s1 >= 0 Then
   If ep_s1 > ep_y Then
      ep_s1 = ep_y
   End If
```

```
113   Else
114        If ep_s1 < -ep_y Then
115           ep_s1 = -ep_y
116        End If
117   End If
118
119   ep_s2 = (c - h / 2 + ds2) * ep_cu / c
120   If ep_s2 >= 0 Then
121      If ep_s2 > ep_y Then
122         ep_s2 = ep_y
123      End If
124   Else
125        If ep_s2 < -ep_y Then
126           ep_s2 = -ep_y
127        End If
128   End If
129
130   ep_s3 = (c - h / 2 + ds3) * ep_cu / c
131   If ep_s3 >= 0 Then
132      If ep_s3 > ep_y Then
133         ep_s3 = ep_y
134      End If
135   Else
136        If ep_s3 < -ep_y Then
137           ep_s3 = -ep_y
138      End If
139   End If
140
141   ep_s4 = (c - h / 2 + ds4) * ep_cu / c
142   If ep_s4 >= 0 Then
143      If ep_s4 > ep_y Then
144         ep_s4 = ep_y
145      End If
146   Else
147        If ep_s4 < -ep_y Then
148           ep_s4 = -ep_y
149      End If
150   End If
151
152   ''Calculate moment created for each layer of reinforcement-
153   ''-with respect to the central horizontal axis of the section.
154   Ms1 = ep_s1 * Es * As1 * ds1
155   Ms2 = ep_s2 * Es * As2 * ds2
156   Ms3 = ep_s3 * Es * As3 * ds3
157   Ms4 = ep_s4 * Es * As4 * ds4
158
159   ''Calculate sum of reinforcement moments.
160   ''Calculate the flexural capacity of the section.
161   Ms = Ms1 + Ms2 + Ms3 + Ms4
162   Md_ = (Ms + Mc) / 1000000
163
164   End Function
165   ================================================================================
166   Function Me_(Es, ep_y, fPrime_c, ep_cu, d, Betha, h, b, As1, As2, As3, As4, ds1,
      ds2, ds3, ds4)
167
168   'Calculating the flexural capacity of the section for point "E" of interaction
      diagram.
```

```
169
170   Dim Mc As Double            'Flexural moment due to concrete compression.
171   Dim Ms As Double            'Sum of flexural moments due to steel tension/compression.
172   Dim c(1000) As Double       'Depth to neutral axis array.
173   Dim ep_s1 As Double         'Strain in reinforcement layer 1.
174   Dim ep_s2 As Double         'Strain in reinforcement layer 2.
175   Dim ep_s3 As Double         'Strain in reinforcement layer 3.
176   Dim ep_s4 As Double         'Strain in reinforcement layer 4.
177   Dim C_c As Double           'Concrete net compression force.
178   Dim fs1 As Double           'Stress in reinforcement layer 1.
179   Dim fs2 As Double           'Stress in reinforcement layer 2.
180   Dim fs3 As Double           'Stress in reinforcement layer 3.
181   Dim fs4 As Double           'Stress in reinforcement layer 4.
182   Dim Ms1 As Double           'Moment created by tension/compression in steel layer 1.
183   Dim Ms2 As Double           'Moment created by tension/compression in steel layer 2.
184   Dim Ms3 As Double           'Moment created by tension/compression in steel layer 3.
185   Dim Ms4 As Double           'Moment created by tension/compression in steel layer 4.
186   Dim i As Integer            'Loop counter.
187
188
189   'Find the depth of neutral axis "C" through trial & error.
190   c(0) = d / 100
191   i = 0
192   Do
193       ep_s1 = (c(i) - h / 2 + ds1) * ep_cu / c(i)
194           If ep_s1 >= 0 Then
195               If ep_s1 > ep_y Then
196                   ep_s1 = ep_y
197               End If
198           Else
199               If ep_s1 < -ep_y Then
200                   ep_s1 = -ep_y
201               End If
202           End If
203
204       ep_s2 = (c(i) - h / 2 + ds2) * ep_cu / c(i)
205           If ep_s2 >= 0 Then
206               If ep_s2 > ep_y Then
207                   ep_s2 = ep_y
208               End If
209           Else
210               If ep_s2 < -ep_y Then
211                   ep_s2 = -ep_y
212               End If
213           End If
214
215       ep_s3 = (c(i) - h / 2 + ds3) * ep_cu / c(i)
216           If ep_s3 >= 0 Then
217               If ep_s3 > ep_y Then
218                   ep_s3 = ep_y
219               End If
220           Else
221               If ep_s3 < -ep_y Then
222                   ep_s3 = -ep_y
223               End If
224           End If
225
226       ep_s4 = (c(i) - h / 2 + ds4) * ep_cu / c(i)
```

```
        If ep_s4 >= 0 Then
            If ep_s4 > ep_y Then
                ep_s4 = ep_y
            End If
        Else
            If ep_s4 < -ep_y Then
                ep_s4 = -ep_y
            End If
        End If

    fs1 = ep_s1 * Es * As1
    fs2 = ep_s2 * Es * As2
    fs3 = ep_s3 * Es * As3
    fs4 = ep_s4 * Es * As4
    C_c = 0.85 * fPrime_c * Betha * c(i) * b
    c(i + 1) = c(i) + d / 100
    i = i + 1

Loop While Abs(fs1 + fs2 + fs3 + fs4 + C_c) * 2 / (Abs(fs1) + Abs(fs2) + Abs(fs3) + Abs(fs4) + Abs(C_c)) > 0.05

''Calculate moment created for each layer of reinforcement-
''-with respect to the central horizontal axis of the section.
''Calculate the moment created due to concrete compression-
''-with respect to the central horizontal axis of the section.
Ms1 = ep_s1 * Es * As1 * ds1
Ms2 = ep_s2 * Es * As2 * ds2
Ms3 = ep_s3 * Es * As3 * ds3
Ms4 = ep_s4 * Es * As4 * ds4
Mc = 0.85 * fPrime_c * Betha * c(i - 1) * b * (h / 2 - Betha * c(i - 1) / 2)

''Calculate sum of reinforcement moments.
''Calculate the flexural capacity of the section.
Ms = Ms1 + Ms2 + Ms3 + Ms4
Me_ = (Ms + Mc) / 1000000

End Function
================================================================================
Function Pbc_Youssef(E_c, Es, E2, fprime_cu, f_t, ep_y, ep_cu, ep_t, d, c, h, b, As1, As2, As3, As4, ds1, ds2, ds3, ds4)

'Calculating the axial capacity of the section for point "B" & "C" of the interaction diagram.
'Based on Model by Youssef et al.

Dim Delta As Integer        'Number of iteration steps for integration.
Dim E2_temp As Double       'Modulus of elasticity of the post-peak branch.
Dim n As Double             'Stress strain equation constant.
Dim i As Integer            'Loop Counter.
Dim ep_c(101) As Double     'Array of concrete strains.
Dim fc(101) As Double       'Array of concrete stresses.
Dim Pc_temp As Double       'Compressive force due to concrete compression at each level of depth.
Dim Pc As Double            'Sum of compressive force due to concrete compression.
Dim ep_s1 As Double         'Strain in reinforcement layer 1.
Dim ep_s2 As Double         'Strain in reinforcement layer 2.
Dim ep_s3 As Double         'Strain in reinforcement layer 3.
Dim ep_s4 As Double         'Strain in reinforcement layer 4.
```

```
281   Dim fs1 As Double           'Tension/compression in steel layer 1.
282   Dim fs2 As Double           'Tension/compression in steel layer 2.
283   Dim fs3 As Double           'Tension/compression in steel layer 3.
284   Dim fs4 As Double           'Tension/compression in steel layer 4.
285   Dim Ps As Double            'Sum of forces due to steel tension/compression.
286
287   ''Calculating the force caused by concrete compression-
288   ''-using numerical integration.
289   Delta = 100
290   Pc = 0
291   For i = 0 To 98 Step 2
292       ep_c(i) = (i * c / Delta) * (ep_cu / c)
293       ep_c(i + 1) = ((i + 1) * c / Delta) * (ep_cu / c)
294       ep_c(i + 2) = ((i + 2) * c / Delta) * (ep_cu / c)
295
296       If ep_c(i) < ep_t Then
297           If E2 <= 0 Then
298               E2_temp = 0
299           End If
300           n = ((E_c - E2_temp) * ep_t) / (E_c * ep_t - f_t)
301           fc(i) = E_c * ep_c(i) * (1 - (1 / n) * (1 - E2_temp / E_c) * (ep_c(i) /
              ep_t) ^ (n - 1))
302       Else
303           fc(i) = f_t + E2 * (ep_c(i) - ep_t)
304           If fc(i) > fprime_cu Then
305               fc(i) = fprime_cu
306           End If
307       End If
308
309       If ep_c(i + 1) < ep_t Then
310           If E2 <= 0 Then
311               E2_temp = 0
312           End If
313           n = ((E_c - E2_temp) * ep_t) / (E_c * ep_t - f_t)
314           fc(i + 1) = E_c * ep_c(i + 1) * (1 - (1 / n) * (1 - E2_temp / E_c) * (ep_c(i
              + 1) / ep_t) ^ (n - 1))
315       Else
316           fc(i + 1) = f_t + E2 * (ep_c(i + 1) - ep_t)
317           If fc(i + 1) > fprime_cu Then
318               fc(i + 1) = fprime_cu
319           End If
320       End If
321
322       If ep_c(i + 2) < ep_t Then
323           If E2 <= 0 Then
324               E2_temp = 0
325           End If
326           n = ((E_c - E2_temp) * ep_t) / (E_c * ep_t - f_t)
327           fc(i + 2) = E_c * ep_c(i + 2) * (1 - (1 / n) * (1 - E2_temp / E_c) * (ep_c(i
              + 2) / ep_t) ^ (n - 1))
328       Else
329           fc(i + 2) = f_t + E2 * (ep_c(i + 2) - ep_t)
330           If fc(i + 2) > fprime_cu Then
331               fc(i + 2) = fprime_cu
332           End If
333       End If
334
335           Pc_temp = b * (((2 * c) / Delta) * (fc(i) + 4 * fc(i + 1) + fc(i + 2)) / 6)
```

```
        Pc = Pc + Pc_temp
Next i

'Calculating strain in each layer of reinforcement.
ep_s1 = (c - h / 2 + ds1) * ep_cu / c
If ep_s1 > ep_y Then
    ep_s1 = ep_y
End If
ep_s2 = (c - h / 2 + ds2) * ep_cu / c
If ep_s2 > ep_y Then
    ep_s2 = ep_y
End If
ep_s3 = (c - h / 2 + ds3) * ep_cu / c
If ep_s3 > ep_y Then
    ep_s3 = ep_y
End If
ep_s4 = (c - h / 2 + ds4) * ep_cu / c
If ep_s4 > ep_y Then
    ep_s4 = ep_y
End If

''Calculate force created in each layer of reinforcement.
fs1 = ep_s1 * Es * As1
fs2 = ep_s2 * Es * As2
fs3 = ep_s3 * Es * As3
fs4 = ep_s4 * Es * As4

''Calculate sum of reinforcement forces.
''Calculate the compressive capacity of the section.
Ps = fs1 + fs2 + fs3 + fs4
Pbc_Youssef = (Ps + Pc) / 1000

End Function
================================================================================
Function Mbc_Youssef(E_c, Es, E2, fprime_cu, f_t, ep_y, ep_cu, ep_t, d, c, h, b,
As1, As2, As3, As4, ds1, ds2, ds3, ds4)

'Calculating the flexural capacity of the section for point "B" & "C" of the
interaction diagram.
'Based on Model by Youssef et al.

Dim Delta As Integer            'Number of iteration steps for integration.
Dim E2_temp As Double           'Modulus of elasticity of the post-peak branch.
Dim n As Double                 'Stress strain equation constant.
Dim i As Integer                'Loop Counter.
Dim ep_c(101) As Double         'Array of concrete strains.
Dim fc(101) As Double           'Array of concrete stresses.
Dim Mc_temp As Double           'Sum of flexural moment due to concrete compression.
Dim Mc As Double                'Flexural moment due to concrete compression at each
level of depth.
Dim ep_s1 As Double             'Strain in reinforcement layer 1.
Dim ep_s2 As Double             'Strain in reinforcement layer 2.
Dim ep_s3 As Double             'Strain in reinforcement layer 3.
Dim ep_s4 As Double             'Strain in reinforcement layer 4.
Dim Ms1 As Double               'Moment created by tension/compression in steel
layer 1.
Dim Ms2 As Double               'Moment created by tension/compression in steel
layer 2.
```

```
389   Dim Ms3 As Double                'Moment created by tension/compression in steel
      layer 3.
390   Dim Ms4 As Double                'Moment created by tension/compression in steel
      layer 4.
391   Dim Ms As Double                 'Sum of flexural moments due to steel
      tension/compression.
392
393   ''Calculating the moment caused by concrete compression with respect to-
394   ''-the central horizontal axis of the section using numerical integration.
395   Delta = 100
396   Mc = 0
397   For i = 0 To 98 Step 2
398       ep_c(i) = (i * c / Delta) * (ep_cu / c)
399       ep_c(i + 1) = ((i + 1) * c / Delta) * (ep_cu / c)
400       ep_c(i + 2) = ((i + 2) * c / Delta) * (ep_cu / c)
401
402       If ep_c(i) < ep_t Then
403           If E2 <= 0 Then
404               E2_temp = 0
405           End If
406           n = ((E_c - E2_temp) * ep_t) / (E_c * ep_t - f_t)
407           fc(i) = E_c * ep_c(i) * (1 - (1 / n) * (1 - E2_temp / E_c) * (ep_c(i) /
          ep_t) ^ (n - 1))
408       Else
409           fc(i) = f_t + E2 * (ep_c(i) - ep_t)
410           If fc(i) > fprime_cu Then
411               fc(i) = fprime_cu
412           End If
413       End If
414
415       If ep_c(i + 1) < ep_t Then
416           If E2 <= 0 Then
417               E2_temp = 0
418           End If
419           n = ((E_c - E2_temp) * ep_t) / (E_c * ep_t - f_t)
420           fc(i + 1) = E_c * ep_c(i + 1) * (1 - (1 / n) * (1 - E2_temp / E_c) * (ep_c(i
          + 1) / ep_t) ^ (n - 1))
421       Else
422           fc(i + 1) = f_t + E2 * (ep_c(i + 1) - ep_t)
423           If fc(i + 1) > fprime_cu Then
424               fc(i + 1) = fprime_cu
425           End If
426       End If
427
428       If ep_c(i + 2) < ep_t Then
429           If E2 <= 0 Then
430               E2_temp = 0
431           End If
432           n = ((E_c - E2_temp) * ep_t) / (E_c * ep_t - f_t)
433           fc(i + 2) = E_c * ep_c(i + 2) * (1 - (1 / n) * (1 - E2_temp / E_c) * (ep_c(i
          + 2) / ep_t) ^ (n - 1))
434       Else
435           fc(i + 2) = f_t + E2 * (ep_c(i + 2) - ep_t)
436           If fc(i + 2) > fprime_cu Then
437               fc(i + 2) = fprime_cu
438           End If
439       End If
440
```

```
        Mc_temp = b * (h / 2 - c + (i + 1) * c / Delta) * (((2 * c) / Delta) *
        (fc(i) + 4 * fc(i + 1) + fc(i + 2)) / 6)
        Mc = Mc + Mc_temp
Next i

'Calculating strain in each layer of reinforcement.
ep_s1 = (c - h / 2 + ds1) * ep_cu / c
If ep_s1 > ep_y Then
   ep_s1 = ep_y
End If
ep_s2 = (c - h / 2 + ds2) * ep_cu / c
If ep_s2 > ep_y Then
   ep_s2 = ep_y
End If
ep_s3 = (c - h / 2 + ds3) * ep_cu / c
If ep_s3 > ep_y Then
   ep_s3 = 0.00207
End If
ep_s4 = (c - h / 2 + ds4) * ep_cu / c
If ep_s4 > ep_y Then
   ep_s4 = ep_y
End If

''Calculate moment created for each layer of reinforcement-
''-with respect to the central horizontal axis of the section.
Ms1 = ep_s1 * Es * As1 * ds1
Ms2 = ep_s2 * Es * As2 * ds2
Ms3 = ep_s3 * Es * As3 * ds3
Ms4 = ep_s4 * Es * As4 * ds4

''Calculate sum of reinforcement moments.
''Calculate the flexural capacity of the section.
Ms = Ms1 + Ms2 + Ms3 + Ms4
Mbc_Youssef = (Ms + Mc) / 1000000

End Function
================================================================================
Function Pbc_Faustino(E1, E2, Es, ep_y, ep_ccu, d, c, h, b, n, f0, fcc, As1, As2,
As3, As4, ds1, ds2, ds3, ds4)

'Calculating the axial capacity of the section for point "B" & "C" of the
interaction diagram.
'Based on Model by Faustino et al.

Dim Delta As Integer        'Number of iteration steps for integration.
Dim i As Integer            'Loop Counter.
Dim ep_c(101) As Double     'Array of concrete strains.
Dim fc(101) As Double       'Array of concrete stresses.
Dim Pc_temp As Double       'Compressive force due to concrete compression at each
level of depth.
Dim Pc As Double            'Sum of compressive force due to concrete compression.
Dim ep_s1 As Double         'Strain in reinforcement layer 1.
Dim ep_s2 As Double         'Strain in reinforcement layer 2.
Dim ep_s3 As Double         'Strain in reinforcement layer 3.
Dim ep_s4 As Double         'Strain in reinforcement layer 4.
Dim fs1 As Double           'Tension/compression in steel layer 1.
Dim fs2 As Double           'Tension/compression in steel layer 2.
Dim fs3 As Double           'Tension/compression in steel layer 3.
```

```
Dim fs4 As Double           'Tension/compression in steel layer 4.
Dim Ps As Double            'Sum of forces due to steel tension/compression.

''Calculating the force caused by concrete compression-
''-using numerical integration.
Delta = 100
Pc = 0
For i = 0 To 98 Step 2
    ep_c(i) = (i * c / Delta) * (ep_ccu / c)
    ep_c(i + 1) = ((i + 1) * c / Delta) * (ep_ccu / c)
    ep_c(i + 2) = ((i + 2) * c / Delta) * (ep_ccu / c)
    fc(i) = ((E1 - E2) * ep_c(i) / (1 + ((E1 - E2) * ep_c(i) / f0) ^ n) ^ (1 / n)) +
    E2 * ep_c(i)
    If fc(i) > fcc Then
       fc(i) = fcc
    End If
    fc(i + 1) = ((E1 - E2) * ep_c(i + 1) / (1 + ((E1 - E2) * ep_c(i + 1) / f0) ^ n)
    ^ (1 / n)) + E2 * ep_c(i + 1)
    If fc(i + 1) > fcc Then
       fc(i + 1) = fcc
    End If
    fc(i + 2) = ((E1 - E2) * ep_c(i + 2) / (1 + ((E1 - E2) * ep_c(i + 2) / f0) ^ n)
    ^ (1 / n)) + E2 * ep_c(i + 2)
    If fc(i + 2) > fcc Then
       fc(i + 2) = fcc
    End If
    Pc_temp = b * (((2 * c) / Delta) * (fc(i) + 4 * fc(i + 1) + fc(i + 2)) / 6)
    Pc = Pc + Pc_temp
Next i

'Calculating strain in each layer of reinforcement.
ep_s1 = (c - h / 2 + ds1) * ep_ccu / c
If ep_s1 > ep_y Then
    ep_s1 = ep_y
End If
ep_s2 = (c - h / 2 + ds2) * ep_ccu / c
If ep_s2 > ep_y Then
    ep_s2 = ep_y
End If
ep_s3 = (c - h / 2 + ds3) * ep_ccu / c
If ep_s3 > ep_y Then
    ep_s3 = ep_y
End If
ep_s4 = (c - h / 2 + ds4) * ep_ccu / c
If ep_s4 > ep_y Then
    ep_s4 = ep_y
End If

''Calculate force created in each layer of reinforcement.
fs1 = ep_s1 * Es * As1
fs2 = ep_s2 * Es * As2
fs3 = ep_s3 * Es * As3
fs4 = ep_s4 * Es * As4

''Calculate sum of reinforcement forces.
''Calculate the compressive capacity of the section.
Ps = fs1 + fs2 + fs3 + fs4
Pbc_Faustino = (Ps + Pc) / 1000
```

```
550
551 End Function
552 ================================================================================
553 Function Mbc_Faustino(E1, E2, Es, ep_y, ep_ccu, d, c, h, b, n, f0, fcc, As1, As2,
    As3, As4, ds1, ds2, ds3, ds4)
554
555 'Calculating the flexural capacity of the section for point "B" & "C" of the
    interaction diagram.
556 'Based on Model by Faustino et al.
557
558 Dim Delta As Integer        'Number of iteration steps for integration.
559 Dim i As Integer            'Loop Counter.
560 Dim ep_c(101) As Double     'Array of concrete strains.
561 Dim fc(101) As Double       'Array of concrete stresses.
562 Dim Mc_temp As Double       'Flexural moment due to concrete compression at each
    level of depth.
563 Dim Mc As Double            'Sum of flexural moment due to concrete compression.
564 Dim ep_s1 As Double         'Strain in reinforcement layer 1.
565 Dim ep_s2 As Double         'Strain in reinforcement layer 2.
566 Dim ep_s3 As Double         'Strain in reinforcement layer 3.
567 Dim ep_s4 As Double         'Strain in reinforcement layer 4.
568 Dim Ms1 As Double           'Moment created by tension/compression in steel layer 1.
569 Dim Ms2 As Double           'Moment created by tension/compression in steel layer 2.
570 Dim Ms3 As Double           'Moment created by tension/compression in steel layer 3.
571 Dim Ms4 As Double           'Moment created by tension/compression in steel layer 4.
572 Dim Ms As Double            'Sum of flexural moments due to steel tension/compression.
573
574 ''Calculating the moment caused by concrete compression with respect to-
575 ''-the central horizontal axis of the section using numerical integration.
576 Delta = 100
577 Mc = 0
578 For i = 0 To 98 Step 2
579     ep_c(i) = (i * c / Delta) * (ep_ccu / c)
580     ep_c(i + 1) = ((i + 1) * c / Delta) * (ep_ccu / c)
581     ep_c(i + 2) = ((i + 2) * c / Delta) * (ep_ccu / c)
582     fc(i) = ((E1 - E2) * ep_c(i) / (1 + ((E1 - E2) * ep_c(i) / f0) ^ n) ^ (1 / n)) +
    E2 * ep_c(i)
583     If fc(i) > fcc Then
584        fc(i) = fcc
585     End If
586     fc(i + 1) = ((E1 - E2) * ep_c(i + 1) / (1 + ((E1 - E2) * ep_c(i + 1) / f0) ^ n)
    ^ (1 / n)) + E2 * ep_c(i + 1)
587     If fc(i + 1) > fcc Then
588        fc(i + 1) = fcc
589     End If
590     fc(i + 2) = ((E1 - E2) * ep_c(i + 2) / (1 + ((E1 - E2) * ep_c(i + 2) / f0) ^ n)
    ^ (1 / n)) + E2 * ep_c(i + 2)
591     If fc(i + 2) > fcc Then
592        fc(i + 2) = fcc
593     End If
594     Mc_temp = b * (h / 2 - c + (i + 1) * c / Delta) * (((2 * c) / Delta) * (fc(i) +
    4 * fc(i + 1) + fc(i + 2)) / 6)
595     Mc = Mc + Mc_temp
596 Next i
597
598 'Calculating strain in each layer of reinforcement.
599 ep_s1 = (c - h / 2 + ds1) * ep_ccu / c
600 If ep_s1 > ep_y Then
```

```
    ep_s1 = ep_y
End If
ep_s2 = (c - h / 2 + ds2) * ep_ccu / c
If ep_s2 > ep_y Then
    ep_s2 = ep_y
End If
ep_s3 = (c - h / 2 + ds3) * ep_ccu / c
If ep_s3 > ep_y Then
    ep_s3 = ep_y
End If
ep_s4 = (c - h / 2 + ds4) * ep_ccu / c
If ep_s4 > ep_y Then
    ep_s4 = ep_y
End If

''Calculate moment created for each layer of reinforcement-
''-with respect to the central horizontal axis of the section.
Ms1 = ep_s1 * Es * As1 * ds1
Ms2 = ep_s2 * Es * As2 * ds2
Ms3 = ep_s3 * Es * As3 * ds3
Ms4 = ep_s4 * Es * As4 * ds4

''Calculate sum of reinforcement moments.
''Calculate the flexural capacity of the section.
Ms = Ms1 + Ms2 + Ms3 + Ms4
Mbc_Faustino = (Ms + Mc) / 1000000

End Function
================================================================================
Function Pbc_Eid_Paultre(a_eq, b_eq, z_eq, fprime_cc, k1, k2, ep_y, ep_cu,
epprime_cc, E_cu, d, c, h, b, As1, As2, As3, As4, ds1, ds2, ds3, ds4)

'Calculating the axial capacity of the section for point "B" & "C" of the
interaction diagram.
'Based on Model by Eid and Paultre.

Dim Delta As Integer        'Number of iteration steps for integration.
Dim i As Integer            'Loop Counter.
Dim ep_c(101) As Double     'Array of concrete strains.
Dim fc(101) As Double       'Array of concrete stresses.
Dim Pc_temp As Double       'Compressive force due to concrete compression at each
level of depth.
Dim Pc As Double            'Sum of compressive force due to concrete compression.
Dim ep_s1 As Double         'Strain in reinforcement layer 1.
Dim ep_s2 As Double         'Strain in reinforcement layer 2.
Dim ep_s3 As Double         'Strain in reinforcement layer 3.
Dim ep_s4 As Double         'Strain in reinforcement layer 4.
Dim fs1 As Double           'Tension/compression in steel layer 1.
Dim fs2 As Double           'Tension/compression in steel layer 2.
Dim fs3 As Double           'Tension/compression in steel layer 3.
Dim fs4 As Double           'Tension/compression in steel layer 4.
Dim Ps As Double            'Sum of forces due to steel tension/compression.

''Calculating the force caused by concrete compression-
''-using numerical integration.
Delta = 100
Pc = 0
For i = 0 To 98 Step 2
```

```
656         ep_c(i) = (i * c / Delta) * (ep_cu / c)
657         ep_c(i + 1) = ((i + 1) * c / Delta) * (ep_cu / c)
658         ep_c(i + 2) = ((i + 2) * c / Delta) * (ep_cu / c)
659
660         If ep_c(i) <= epprime_cc Then
661             fc(i) = a_eq * ep_c(i) / (1 + b_eq * ep_c(i) + z_eq * (ep_c(i)) ^ 2)
662         Else
663             fc(i) = fprime_cc * Exp(k1 * (ep_c(i) - epprime_cc) ^ k2) + E_cu * (ep_c(i)
            - epprime_cc)
664         End If
665
666         If ep_c(i + 1) <= epprime_cc Then
667             fc(i + 1) = a_eq * ep_c(i + 1) / (1 + b_eq * ep_c(i + 1) + z_eq * (ep_c(i +
            1)) ^ 2)
668         Else
669             fc(i + 1) = fprime_cc * Exp(k1 * (ep_c(i + 1) - epprime_cc) ^ k2) + E_cu *
            (ep_c(i + 1) - epprime_cc)
670         End If
671
672         If ep_c(i + 2) <= epprime_cc Then
673             fc(i + 2) = a_eq * ep_c(i + 2) / (1 + b_eq * ep_c(i + 2) + z_eq * (ep_c(i +
            2)) ^ 2)
674         Else
675             fc(i + 2) = fprime_cc * Exp(k1 * (ep_c(i + 2) - epprime_cc) ^ k2) + E_cu *
            (ep_c(i + 2) - epprime_cc)
676         End If
677
678             Pc_temp = b * (((2 * c) / Delta) * (fc(i) + 4 * fc(i + 1) + fc(i + 2)) / 6)
679             Pc = Pc + Pc_temp
680     Next i
681
682     'Calculating strain in each layer of reinforcement.
683     ep_s1 = (c - h / 2 + ds1) * ep_ccu / c
684     If ep_s1 > ep_y Then
685         ep_s1 = ep_y
686     End If
687     ep_s2 = (c - h / 2 + ds2) * ep_ccu / c
688     If ep_s2 > ep_y Then
689         ep_s2 = ep_y
690     End If
691     ep_s3 = (c - h / 2 + ds3) * ep_ccu / c
692     If ep_s3 > ep_y Then
693         ep_s3 = ep_y
694     End If
695     ep_s4 = (c - h / 2 + ds4) * ep_ccu / c
696     If ep_s4 > ep_y Then
697         ep_s4 = ep_y
698     End If
699
700     ''Calculate force created in each layer of reinforcement.
701     fs1 = ep_s1 * Es * As1
702     fs2 = ep_s2 * Es * As2
703     fs3 = ep_s3 * Es * As3
704     fs4 = ep_s4 * Es * As4
705
706     ''Calculate sum of reinforcement forces.
707     ''Calculate the compressive capacity of the section.
708     Ps = fs1 + fs2 + fs3 + fs4
```

```
709   Pbc_Eid_Paultre = (Ps + Pc) / 1000
710
711   End Function
712   ========================================================================================
713   Function Mbc_Eid_Paultre(a_eq, b_eq, z_eq, fprime_cc, k1, k2, ep_y, ep_cu,
      epprime_cc, E_cu, d, c, h, b, As1, As2, As3, As4, ds1, ds2, ds3, ds4)
714
715   'Calculating the flexural capacity of the section for point "B" & "C" of the
      interaction diagram.
716   'Based on Model by Eid and Paultre.
717
718   Dim Delta As Integer          'Number of iteration steps for integration.
719   Dim i As Integer              'Loop Counter.
720   Dim ep_c(101) As Double       'Array of concrete strains.
721   Dim fc(101) As Double         'Array of concrete stresses.
722   Dim Mc_temp As Double         'Flexural moment due to concrete compression at each
      level of depth.
723   Dim Mc As Double              'Sum of flexural moment due to concrete compression.
724   Dim ep_s1 As Double           'Strain in reinforcement layer 1.
725   Dim ep_s2 As Double           'Strain in reinforcement layer 2.
726   Dim ep_s3 As Double           'Strain in reinforcement layer 3.
727   Dim ep_s4 As Double           'Strain in reinforcement layer 4.
728   Dim Ms1 As Double             'Moment created by tension/compression in steel layer 1.
729   Dim Ms2 As Double             'Moment created by tension/compression in steel layer 2.
730   Dim Ms3 As Double             'Moment created by tension/compression in steel layer 3.
731   Dim Ms4 As Double             'Moment created by tension/compression in steel layer 4.
732   Dim Ms As Double              'Sum of flexural moments due to steel tension/compression.
733
734   ''Calculating the moment caused by concrete compression with respect to-
735   ''-the central horizontal axis of the section using numerical integration.
736   Delta = 100
737   Pc = 0
738   For i = 0 To 98 Step 2
739       ep_c(i) = (i * c / Delta) * (ep_cu / c)
740       ep_c(i + 1) = ((i + 1) * c / Delta) * (ep_cu / c)
741       ep_c(i + 2) = ((i + 2) * c / Delta) * (ep_cu / c)
742
743       If ep_c(i) <= epprime_cc Then
744           fc(i) = a_eq * ep_c(i) / (1 + b_eq * ep_c(i) + z_eq * (ep_c(i)) ^ 2)
745       Else
746           fc(i) = fprime_cc * Exp(k1 * (ep_c(i) - epprime_cc) ^ k2) + E_cu * (ep_c(i)
          - epprime_cc)
747       End If
748
749       If ep_c(i + 1) <= epprime_cc Then
750           fc(i + 1) = a_eq * ep_c(i + 1) / (1 + b_eq * ep_c(i + 1) + z_eq * (ep_c(i +
          1)) ^ 2)
751       Else
752           fc(i + 1) = fprime_cc * Exp(k1 * (ep_c(i + 1) - epprime_cc) ^ k2) + E_cu *
          (ep_c(i + 1) - epprime_cc)
753       End If
754
755       If ep_c(i + 2) <= epprime_cc Then
756           fc(i + 2) = a_eq * ep_c(i + 2) / (1 + b_eq * ep_c(i + 2) + z_eq * (ep_c(i +
          2)) ^ 2)
757       Else
758           fc(i + 2) = fprime_cc * Exp(k1 * (ep_c(i + 2) - epprime_cc) ^ k2) + E_cu *
          (ep_c(i + 2) - epprime_cc)
```

```
759         End If
760
761             Mc_temp = b * (h / 2 - c + (i + 1) * c / Delta) * (((2 * c) / Delta) *
            (fc(i) + 4 * fc(i + 1) + fc(i + 2)) / 6)
762             Mc = Mc + Mc_temp
763     Next i
764
765     'Calculating strain in each layer of reinforcement.
766     ep_s1 = (c - h / 2 + ds1) * ep_cu / c
767     If ep_s1 > ep_y Then
768         ep_s1 = ep_y
769     End If
770     ep_s2 = (c - h / 2 + ds2) * ep_cu / c
771     If ep_s2 > ep_y Then
772         ep_s2 = ep_y
773     End If
774     ep_s3 = (c - h / 2 + ds3) * ep_cu / c
775     If ep_s3 > ep_y Then
776         ep_s3 = ep_y
777     End If
778     ep_s4 = (c - h / 2 + ds4) * ep_cu / c
779     If ep_s4 > ep_y Then
780         ep_s4 = ep_y
781     End If
782
783     ''Calculate moment created for each layer of reinforcement-
784     ''-with respect to the central horizontal axis of the section.
785     Ms1 = ep_s1 * Es * As1 * ds1
786     Ms2 = ep_s2 * Es * As2 * ds2
787     Ms3 = ep_s3 * Es * As3 * ds3
788     Ms4 = ep_s4 * Es * As4 * ds4
789
790     ''Calculate sum of reinforcement moments.
791     ''Calculate the flexural capacity of the section.
792     Ms = Ms1 + Ms2 + Ms3 + Ms4
793     Mbc_Eid_Paultre = (Ms + Mc) / 1000000
794
795     End Function
796     ================================================================================
797
798
```